THE UNIVERSITY OF MICHIGAN
INDUSTRY PROGRAM OF THE COLLEGE OF ENGINEERING

Absolute (d, α) Reaction Cross Sections and Excitation Functions

Oswald U. Anders

This dissertation was submitted in partial fulfillment of the requirements for the degree of Doctor of Philosophy in the University of Michigan.

April 1957

IP-216

ensm
UMR0096

ACKNOWLEDGMENTS

It is a great pleasure to thank Professor W. W. Meinke for his continued support, guidance and cooperation during the course of this work, his willing aid in procuring equipment and preparation of the manuscript.

The suggestions and advice of Professor L. O. Brockway, Professor K. Fajans, Professor J. Halford, Professor W. C. Parkinson, Professor C. Rulfs and Professor P. V. Hough are truly appreciated.

The willing assistance of Mrs. Rosemary Maddock, Mr. Morris Wahlgren, Mr. Ronald Shideler, Mr. George Grindahl, Miss Alice Burton and Miss Susan Holbrook in various phases of the problem is gratefully acknowledged.

Thanks also go to Mr. William Downer and other members of the University of Michigan cyclotron crew in arranging for the bombardments and to Mr. John Mannlein, Mr. Robert White and Mr. Hermann Roemer for the help in the construction of various equipment used in the research.

The aid given by the Engineering Industry Program in printing the thesis is appreciated.

The author is indebted to the U. S. Atomic Energy Commission for partial support of this research. Thanks be extended to Mr. B. Falk and the Arnold Engineering Company for providing thin metallic foils for the targets.

Last but not least the author wishes to express his sincere gratitude to his wife, Edith, who assisted in the reading of the counters during many small hours following the bombardments, in the calibration of the integrator, in many calculations and in the typing of the final manuscript.

Isotopic tracers were obtained from the Isotopes Division of the Oak Ridge National Laboratory and by several bombardments obtained at the Argonne National Laboratory.

TABLE OF CONTENTS

LIST OF TABLES

LIST OF FIGURES

ABSOLUTE (d, α) REACTION CROSS SECTIONS AND EXCITATION FUNCTIONS

ABSTRACT

The purpose of this research was the determination of the cross sections of various (d, α) reactions induced by the 7.78 ± 0.05 Mev deuterons from the University of Michigan cyclotron. Special emphasis was given to reactions involving closed shell nuclei as target isotopes. Experimental techniques were refined to permit precision measurement of the cross section values.

The investigation involved the bombardment of thin targets of metallic zirconium, molybdenum and titanium as well as of zinc sulfide, subsequent chemical separation of the product nuclei, identification of the products by x-ray and γ-spectroscopy and determination of the absolute disintegration rates of β- and x-ray emitting isotopes.

The instruments constructed during this research included: a current integrator permitting measurement of the intensity of the cyclotron beam with 1% error; two 4π β-ray proportional counters, a four-inch diameter x-ray proportional counter filled with krypton at two atmospheres pressure and a beta thickness gauge for thin films.

Procedures were developed to calibrate the current integrator, to determine, with an accuracy of 1%, the evenness of target foils by a non-destructive method, to prepare cyclotron targets of materials sublimating below 1500° C by high vacuum evaporation, to purify various reaction products by using carrier-free chemical separations with decontamination factors of 10^5 and better. Methods were devised to determine the yield of the chemical separations with radioactive tracers, to identify various isotopes by their γ- and x-ray spectra, to count absolutely x-rays and β-rays with proportional counters as well as with coincidence set-up, and to prepare thin films used for mounting the 4π counter samples.

The absolute cross sections σ, in millibarns, were measured for the following (d, α) reactions at the deuteron energy V $\pm$ 0.05 Mev.

Reaction	σ	V
Zr^{90}(d, α)Y^{88} *	2.34 $\pm$ 0.28	7.56
Zr^{92}(d, α)Y^{90} *	3.79 $\pm$ 0.26	7.56
Zr^{94}(d, α)Y^{92} *	4.01 $\pm$ 0.28	7.56
Mo^{92}(d, α)Nb^{90}	2.95 $\pm$ 0.14	7.71
Mo^{97}(d, α)Nb^{95} *	2.35 $\pm$ 0.14	7.71
Mo^{97}(d, α)Nb^{95m}	0.98 $\pm$ 0.09	7.71
Mo^{98}(d, α)Nb^{96}	2.53 $\pm$ 0.12	7.71
Ti^{46}(d, α)Sc^{44}	52.4 $\pm$ 2.6	7.71

Reaction	σ	V
$Ti^{48}(d, \alpha)Sc^{46}$	28.5 ± 1.7	7.71
$S^{34}(d, \alpha)P^{32}$ *	330.3 ± 23.1	7.73

Excitation functions were determined for the reactions with asterisk. The decay scheme of Y^{88} was investigated and a metastable intermediary state discovered. Similar metastable states were found for the decay of Mn^{54} and Sn^{113}.

Absorption curves in beryllium were experimentally determined for x-rays emitted by Y^{88} and Mn^{54}.

Part 1

INTRODUCTION

The study of nuclear reactions is one of the approaches to the knowledge of the properties of atomic nuclei. The quantity most significant for such investigations is the nuclear reaction cross section. It is a measure of the yield of the reaction and gives an estimate of the ability of the target nuclei to undergo a particular kind of transition.

In recent years many articles have appeared dealing with the study of nuclear reactions and the measurement of the corresponding cross sections. A distinction is made in this connection between the so called "absolute" cross sections and the "relative" cross sections. Relative cross sections are values giving the yield of a certain reaction with respect to another standard or reference reaction. The two reactions may involve different elements or isotopes or vary only in the interaction energies. Absolute cross sections, on the other hand, do not require such reference standards and are given in the absolute units of an area.

Many workers in the past were interested only in cross section values sufficient for rough theoretical treatment and spent much of their effort on the measurement of relative cross sections, using the few previously determined absolute values as their reference standards. Although sufficiently good relative data can be accumulated in this

way, large errors of the normalized values cannot be avoided without sufficient attention to details.

Many of the measured values have inherent errors much larger than estimated by the investigators. Neglect of the losses of reaction product due to recoiling and the uncertainties introduced by bulky counting samples emitting β-rays contributed to these optimistic error estimates. In some work carried out with "standardized" Geiger-Müller counters no correction was applied for the sensitivity of the counters to γ-rays emitted in coincidence with the β-particles or to the effect of backscattering from the supports of the counting sample. For some studies the side reactions that may have produced the same product as the reaction under investigation were neglected.

Some workers based their measurements on relatively thick targets for which they had no criterion as to their uniformity. Others encountered difficulties with the energy definition of the thresholds of charged particle reactions. This was due largely to uncertainties of the energy of the accelerator beam used. In some work the measurement of the bombarding particles proved difficult and yielded erroneous results due to the neglect of charge losses from secondary electrons emerging from the target and detecting device during bombardment.

Some investigators were very successful in minimizing one type of error, but neglected others completely.

It is in the light of these facts that previously reported reaction cross-section values have to be seen. Some authors aware of them may have quoted errors of the order of 100% or more, and their values are still to be considered good. There are very few authors, however, reporting standard errors of less than 20% for their determinations of absolute cross sections.

The following few laborious attempts performed by whole groups of investigators to establish absolute reference standards are among the most successful:

Excellent work on the $C^{12}(p, pn)C^{11}$ reaction, used as primary standard by many investigators, has been reported by Aamodt, Peterson and Phillips (1) as well as McMillan and Miller (86) of the University of California Radiation Laboratory, furthermore by Hintz and Ramsey (63) of Harvard University. They quote a probable error of 14% and attribute more than half of it to the uncertainties in establishing the absolute decay rate of the C^{11} reaction product, by means of a calibrated Geiger-Müller counter.

Self-absorption is again the major source of error in the work by Crandall, Millburn, Pyle and Birnham (25), who investigated the $C^{12}(x, xn)C^{11}$ and $Al^{27}(x, x\ 2p\ n)Na^{24}$ reactions (x = p, d or α). With foil thicknesses of polystyrene up to 0.015 inch and aluminum up to 0.010 inch

one cannot overcome the self-absorption difficulties even using a 4π counter. Errors up to 10% standard deviation were inherent in this work.

Some very good determinations of relative cross sections and their dependence on energy were reported by Ghoshal (44, 45) for silver and copper for the medium energy range and by Meinke, Wick and Seaborg (90) for thorium and uranium for bombarding energies of several hundred Mev. Errors of approximately 20% for the relative values were quoted for this latter work.

The present research attempted to avoid many of these difficulties as far as possible. New techniques were developed and various electronic equipment constructed and acquired to aid in this attempt.

Some of the investigations reported in the literature try to correlate measurements of cross sections for a certain type of reaction covering a wide range of atomic numbers. Measurements of this kind were published by Cohen for the (n, 2n) and (n, p) reactions (22), by Hughes and Sherman (66) for the (n, γ) reaction, by Harvey (58) for the (d, p) reaction, and by Blaser, Boehm, Marmier and Scherrer (13) for the (p, n) reaction.

Insight into certain structural properties of the nuclides can be gained from these articles.

No such systematic treatment has been given thus far to the (d, α) reaction. The relatively low yields of this reaction prohibited extensive investigation. The few

absolute cross sections reported thus far were insufficient in number to permit a meaningful correlation.

The purpose of this research was thus, to study the (d, α) reaction of various nuclides by determining the reaction cross sections for 7.7 Mev deuterons and measuring their energy dependence for lower deuteron energies where possible. The excellent resolution of the deuteron beam available at the University of Michigan Cyclotron, having a known energy of 7.77 ± 0.02 Mev, was of great help in this respect.

Particular attention was given to the so called "magic number nuclei" to investigate possible effects of nuclear structure on the (d, α) reaction yields.

I. Nuclear Reaction Cross Section

A. Definition

If a beam of particles is directed at a layer of matter, the effect of this layer is additively composed of the effects of the individual units (nuclei) in this layer. These act as individual scattering centers. The Cross Section of a nuclear reaction is thus defined by:

$$\sigma = \frac{\text{Number of events of a given type per unit time per nucleus}}{\text{Number of incident particles per unit area per unit time}} \qquad (1)$$

For charged particle reactions of the type:

$$a + X \longrightarrow C^* \longrightarrow Y + b$$

where an intermediate "complex nucleus" is formed, there exists a threshold dependent on the Coulomb repulsion between target nucleus and projectile. In this case reactions will require a minimum energy of the bombarding particle, since no compound nucleus can be formed unless the entering particle makes contact with the target nucleus.

The cross section defined by equation (1) is dependent on the interaction energy. The resulting "excitation" function is a characteristic of the reaction. The interaction or excitation energy is the energy of the bombarding deuterons and is measured in million electron volts.

B. Derivation

The cross section of a deuteron induced nuclear reaction can be written in the form:

$$\sigma = \frac{\text{Number of Nuclei formed by the Reaction}}{(\text{Number of Parent Nuclei/area})(\text{Number of Deuterons})} \quad (2)$$

The dimension of the cross section is then an area measured in $\frac{cm^2}{\text{nucleus}}$ or better in millibarns $= \frac{10^{-27}\ cm^2}{\text{nucleus}}$.

The number N_p of nuclei produced by a particular reaction per second is thus:

$$N_p = I \sigma \frac{n}{A} \tag{3}$$

where n is the number of parent nuclei, A is the target area and I is the beam strength in deuterons per second. If N is the number of product nuclei produced only by the reaction with cross section σ and lost only by decay, and t is the time during which the amount of the product changes:

$$\frac{dN}{dt} = I \sigma \frac{n}{A} - \lambda N \tag{4}$$

where λ is the decay constant related to the half-life by $\lambda = (\log_e 2)(t\frac{1}{2})^{-1}$. If the bombardment is constant during t, and if the transformation of parent atoms is small so that I, n and σ are essentially constant, the number of product atoms present at any time during the bombardment is given by the solution of above equation (cf. appendix)

$$N = \frac{1}{\lambda} (I \frac{\sigma n}{A}) (1 - e^{-\lambda t}) \tag{5}$$

At the end of a constant bombardment of time T

$$N = \frac{I \sigma (n/A)}{\lambda} (1 - e^{-\lambda T}) = N_o \tag{6}$$

and at any time after the end of the bombardment:

$$N = \frac{I \sigma (n/A)}{\lambda} (1 - e^{-\lambda T}) e^{-\lambda t} = N_o e^{-\lambda t} \tag{7}$$

The total number of product nuclei formed by the reaction considered is then:

$$N_T = N_p T = I\ \sigma\ n/A\ \ x\ T \tag{8}$$

If N_T is known the cross section can be calculated from

$$\sigma = \frac{N_T}{(n/A)\ I\ T} \tag{9}$$

If IT is obtained from the number of micro-ampere hours, Q, and the number of elementary charges on the bombarding nucleus, one obtains

$$I\ T = (Q/Z)\ \frac{3600 \times 10^{-6}}{1.60 \times 10^{-19}} \tag{10}$$

and

$$\sigma = 4.44 \times 10^{-17}\ \frac{N_T Z}{Q\ (n/A)} \tag{11}$$

N_T can be obtained by solving equation (6) for $I\sigma(n/A)$ and writing

$$N_T = I\ \sigma\ (n/A)\ T = \frac{N_o\ \lambda T}{1-e^{-\lambda T}} \tag{12}$$

If the bombardment is not constant, it can at least be divided into intervals of equal length during which I can be considered constant. In this case

$$N_o = \sum_{i=1}^{m} \frac{I_i\ \sigma\ \frac{n}{A}}{\lambda}\ (1 - e^{-\lambda\ \Delta\ t})\ e^{-\lambda t_i} \tag{13}$$

or

$$N_o = \frac{\sigma \frac{n}{A}}{\lambda} (1 - e^{-\lambda \Delta t}) \sum_{i=1}^{m} I_i \, e^{-\lambda t_i} \qquad (14)$$

where m is the number of intervals and t_i is the time from end of the i th intervals to the end of the bombardment. from equation (10) follows for this case:

$$I_i = \frac{Q_i}{Z \Delta t} \left(\frac{3600 \times 10^{-6}}{1.60 \times 10^{-19}} \right) \qquad (15)$$

Q_i being the number of micro-ampere hours in the i th interval.

Equation (14) can then be written:

$$N_o = \left(\frac{3600 \times 10^{-6}}{1.60 \times 10^{-19}} \right) \frac{\sigma \frac{n}{A}}{\lambda Z \Delta t} (1 - e^{-\lambda \Delta t}) \sum_{i=1}^{m} Q_i e^{-\lambda t_i} \qquad (16)$$

Substituting C_i/K for Q_i where K = counts per micro-ampere-hour, the calibration constant of the Current Integrator, and C_i the Current Integrator counts collected in interval i, we obtain:

$$\sigma = 4.44 \times 10^{-17} \frac{N_o \, \Delta t \, \lambda \, K}{\left(\frac{n}{A}\right) (1 - e^{-\lambda \Delta t}) \left(\sum_{i=1}^{m} C_i \, e^{-\lambda t_i} \right)} \qquad (17)$$

II. Experimental Approach

The cross section, defined by equation (2) can serve as a guide for the quantitative experimental approach to nuclear reactions. The efforts of this research may thus be classified under three main headings:

1. Measurement of the energy and number of deuterons
2. Determination of the number of parent nuclei
3. Identification and determination of the number of product nuclei.

The determination of the bombardment energies involved mainly calculations using the range-energy data in the literature (6, 102) while the determination of the number of deuterons entering the reaction was reduced to the measurement of the charge collected in a Faraday cup positioned behind the target.

The problem of determining the number of parent nuclei included the preparation of targets suitable for bombardment and the collection of dependable data on size, weight, and evenness of the targets. Values for the isotopic relative abundance were taken from the literature (65).

Most of the necessary experimental techniques, however, had to be developed for the identification and measurement of decay rates of the radioactive reaction products. Several new instruments were designed and built and new methods developed for chemical purification and counting of the reaction products.

Part 2

INSTRUMENTATION AND TECHNIQUES

In this chapter the instruments and techniques employed for measuring the (d, α) cross sections are described in detail. Design and performance data are given for the instruments and the principles of the procedures are discussed. Some findings made when testing the equipment are reported.

I. Determination of the Energy and Number of Deuterons

A. Cyclotron

The deuterons for the research were obtained from the 42-inch, fixed-frequency cyclotron of the Physics Department of the University of Michigan.

1. Layout:

A diagram of the topography of the cyclotron and its associated equipment is given in Fig. 1. Deuterons are produced in the tank of the cyclotron by an electric arc and accelerated to a maximum energy of approximately 7.8 Mev. When the maximum energy is reached the beam is deflected out of the tank by the deflector plate at B and conducted inside the pipe E to the Focusing Magnet F. Particles of 7.778 Mev are selected and magnetically focused to the target plane in the scattering chamber M. The bombardments for this research were carried out at the position R in front of the Faraday cage T. This is inside the

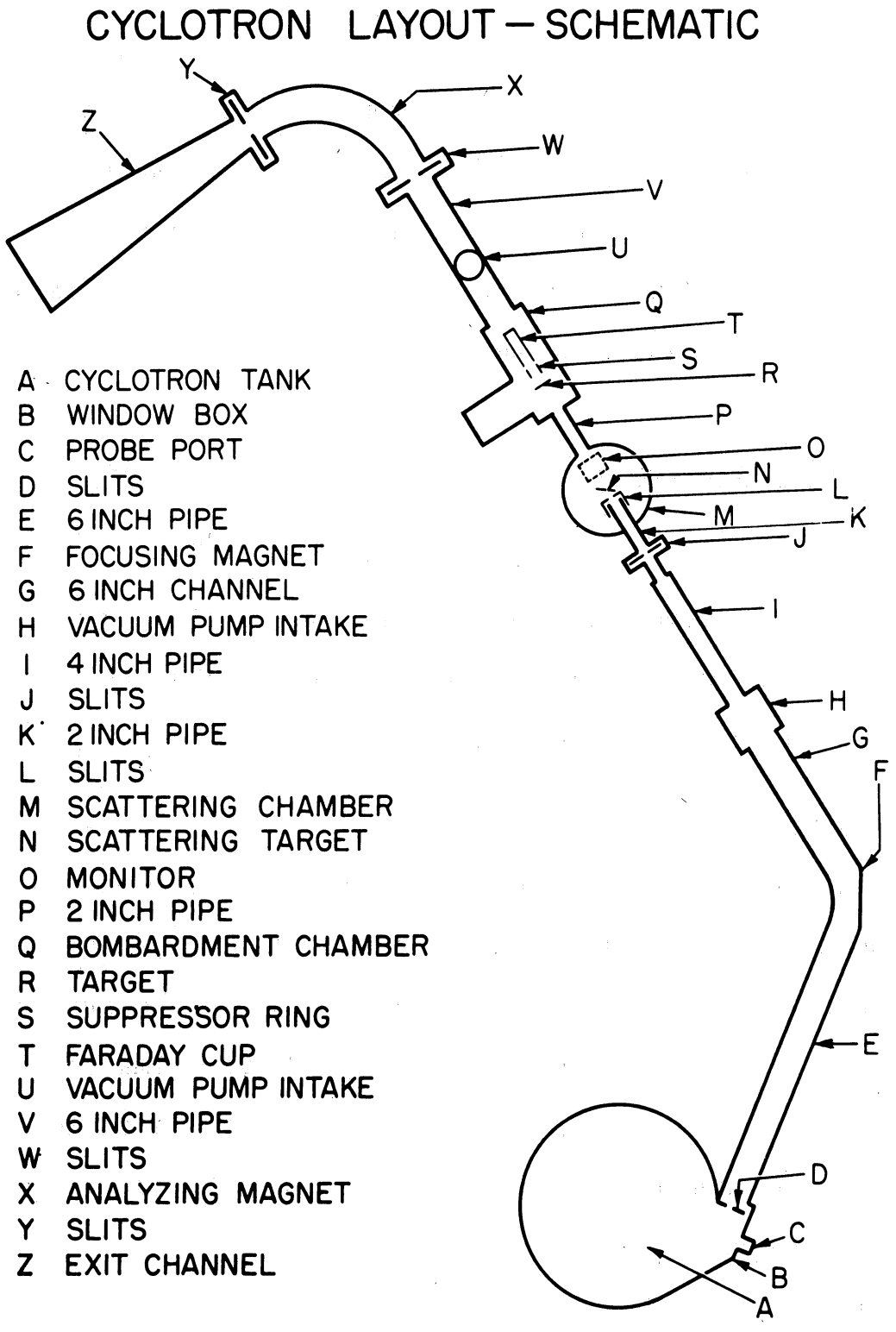

Fig. 1 Schematic representation of the layout of the cyclotron vacuum system

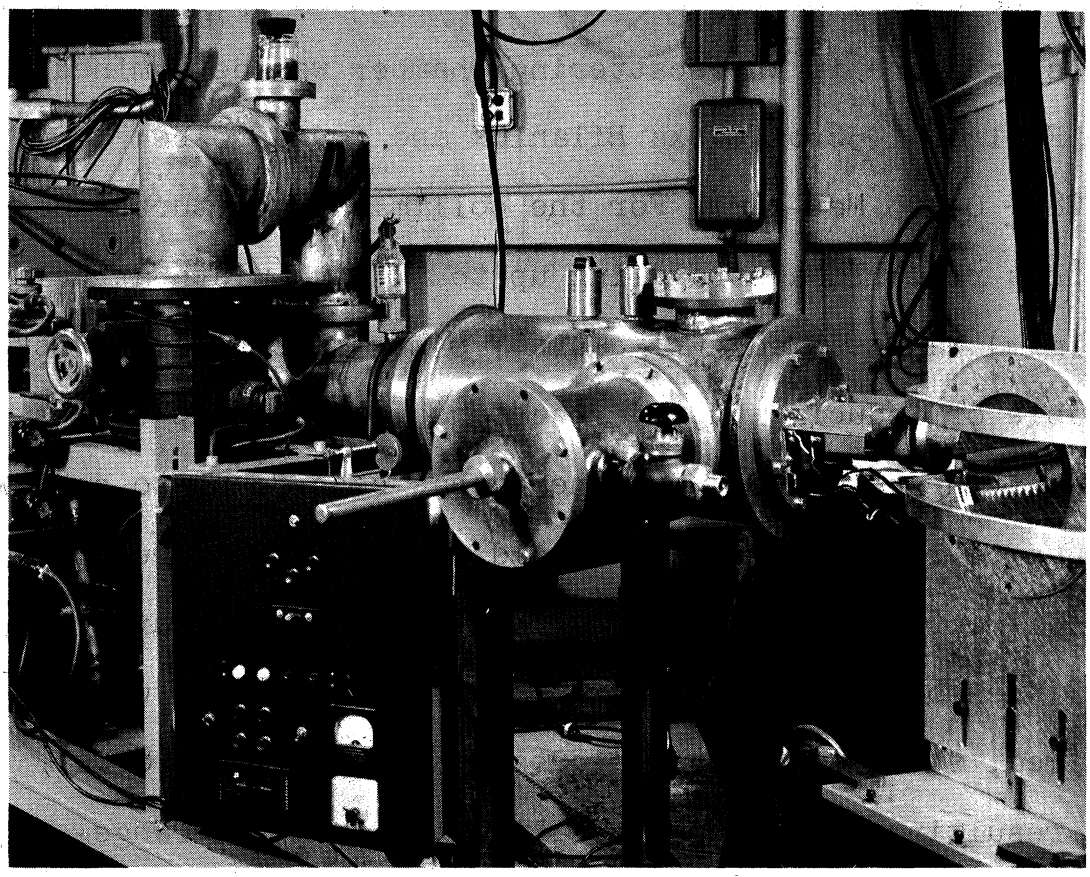

Fig. 2. Bombardment Chamber

Bombardment Chamber Q (Fig. 2), and situated approximately 2 ft behind the focusing plane. At the position R in the bombardment chamber the diverging beam covers an area of approximately 2 - 3 cm^2 and has a maximum strength of 1 - 2 micro-amperes under standard operating conditions. Behind the target position is the suppressor ring S, the Faraday Cup T and other equipment not related to this research.

2. Beam Energy:

The energy of the deuteron beam of the cyclotron at the focusing plane in the scattering chamber was determined in the Fall of 1956 by Olexa Bilaniuk and found to be 7.778 ± 0.005 Mev (12). For the collimator apertures used in this research a straggling up to 50 Kev (width at half maximum) was assumed (7). This 7.8-Mev deuteron beam is capable of inducing (d, α) reactions in nuclei up to the rare-earth region, but its energy has been found to be low enough to lie below the threshold of the (d, αn) reaction for elements as low in the periodic table as sulfur.

When bombardment energies lower than 7.8 Mev were desired, stacked-foil techniques were employed (88). The resulting energies were calculated from the range-energy curves of deuterons in the anteposed absorbers. The range-energy relationship for Mylar, aluminum, titanium, copper, zirconium and molybdenum used for this calculation are given in Table I. The values for aluminum and copper were taken from the literature (6, 102). The values for Mylar were obtained from Prof. W. C. Parkinson (94) and the values for titanium, zirconium and molybdenum were obtained by interpolation.*

This interpolation was done by the following method:

---

* The proton range-energy relations for molybdenum have recently been published in a Russian journal (107) but were inaccessible to the author.

Table I. Range–Energy Relationships for Deuterons in Various Materials

Energy of Deuterons (Mev)	Range					
	Aluminum (mg/cm^2)	Titanium (mg/cm^2)	Copper (mg/cm^2)	Zirconium (mg/cm^2)	Molybdenum (mg/cm^2)	MYLAR (mg/cm^2)
2	6.899	7.618	8.995	12.764	13.699	5.12
3	13.340	15.17	17.6	23.95	25.396	
4	21.59	24.89	28.58	37.58	39.69	15.52
5	31.18	36.53	41.8	53.42	56.01	
6	41.98	50.07	56.77	70.79	73.85	30.26
7		65.50	74.1	90.62	94.25	
8	68.96	82.73	93.27	112.57	116.49	49.66

The values of $\frac{\text{deuteron range}}{\text{at. wt.}}$ were calculated and plotted vs. the atomic number for aluminum, copper and silver. Slightly curved lines were obtained for the points of corresponding energies. The ratio

$$R = \frac{(\text{range/at. wt.})\ \text{element}}{(\text{range/at. wt.})\ \text{copper}}$$

was calculated and a plot of this ratio vs. the deuteron energy prepared. A smooth curve was fitted to the points of this plot and the value of this curve at a particular energy taken as the interpolated R. Multiplication by the $\frac{\text{range}}{\text{at.wt.}}$ value for copper and the atomic weight of the element yielded the range values of deuterons of the given energy in the element as reported in Table I.

$$(\text{range in element})_E = R\ (\text{range in copper})_E\ \text{at. wt.}$$

The uncertainties incurred by application of the extrapolations being of the order of $\pm$ 5% are smaller than the beam energy attenuation in the targets used.

B. Techniques and Instruments Used to Induce and Control the Nuclear Reactions

1. Bombardment Chamber.

The Bombardment Chamber (Fig. 2) contains the Faraday cage mounted on Teflon insulators (Fig. 3). A Suppressor Ring is mounted immediately before the mouth of the Faraday cage. The entire unit is mounted on a small wagon

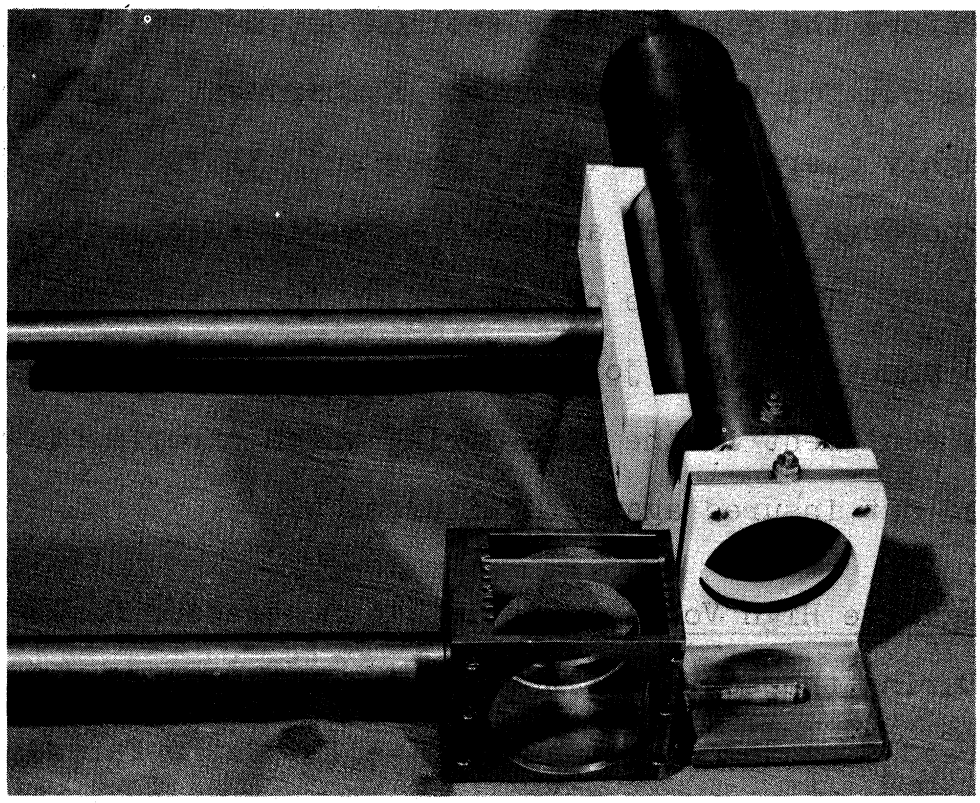

Fig. 3. Faraday Cage and Target Probe Assembly

by which it can be removed from the path of the cyclotron beam, when not in use. The cage as well as the suppressor ring are connected via shielded flexible cables to two Kovar-glass seals and Teflon insulated high voltage connectors on top of the Bombardment Chamber (Fig. 2).

The target, mounted on an aluminum frame fits into the target probe assembly, which is placed in front of the suppressor ring.

For introduction of the target probe into the evacuated bombardment chamber a vacuum lock is provided as can be seen in Fig. 2.

Before the actual cross section determinations were carried out for this research the bombardment chamber was thoroughly overhauled. The chamber and all its contents were thoroughly cleaned and new, more-flexible cables installed. The surface of the Teflon insulators was shaved and the solder joints rechecked. Intermittent check of the equipment in the time during which experiments were carried out insured against failures.

2. Negative High Voltage Supply and Suppressor Ring.

During the course of the bombardment secondary electrons are freed from the target and the walls of the Faraday cage by the impact of the deuterons. When electrons from the target are permitted to reach the Faraday cage or those produced in the Faraday cage permitted to escape it, wrong beam-current readings are obtained. It has been reported by Hall (49) that current readings as much as 27% too low are obtained in this case.

A suppressor ring placed between the target and the Faraday cage and charged with a negative potential exceeding 200 volt prevents secondary electrons from entering or leaving the Faraday cage. For the experiments carried out during this research a negative potential of 1000 volt was applied to the suppressor ring during the bombardments.

A special negative power supply was designed and built to supply this negative potential. Fig. 4 gives the circuit diagram of this unit. In Fig. 5 it can be

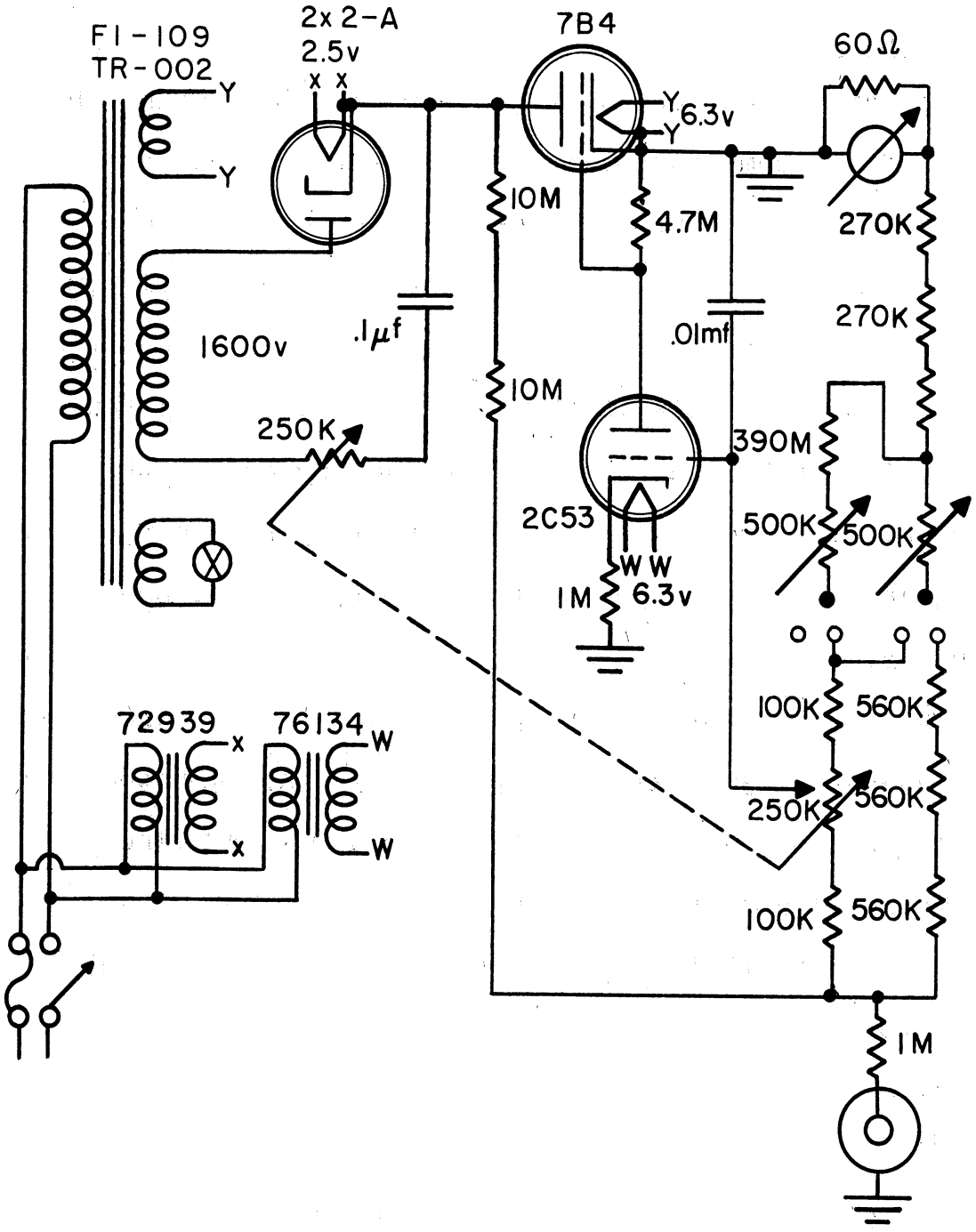

Fig. 4. Circuit Diagram of Negative High Voltage Supply

seen as the second panel from the top. The unit proved very dependable and no difficulties were experienced with it.

3. Current Integrator.

The charge collected by the Faraday cage during the course of the bombardment is measured by the current integrator. This charge divided by the charge of one deuteron ($+4.802 \cdot 10^{-10}$ esu.) represents the total number of deuterons which penetrate the target, with an error of less than 0.01%. This is the case since only very few interactions take place between the deuterons and the target nuclei, and almost the entire beam will emerge from the target attenuated somewhat in its energy but not in intensity.

The current integrator is connected to the Faraday cage by a low-capacity coaxial cable (UG 62/U) and mounted in a cabinet together with a Sorensen type 1000 S AC line voltage regulator and other auxiliary equipment. (Fig. 5)

a. The principle of operation of the current integrator is best described using the block diagram of Fig. 7.

If S is closed one has a conventional feedback amplifier on the left with an output load consisting of R_m plus the resistance of the meter. The voltage developed across this load is: $e_3 = A\, e_1\, i_1 - e_1$, but $A\, e_1 + e_1 = R_1\, i_1$ or $e_1(A + 1) = R_1\, i_1$ thus: $e_3 = Ae_1 = \frac{A}{A + 1} \times R_1\, i_1$, where A is the gain of the

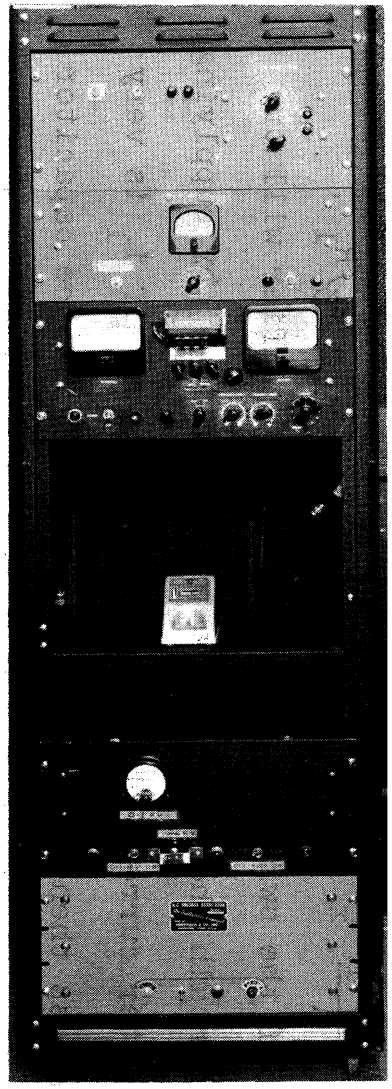

Fig. 5. Current Integrator Rack

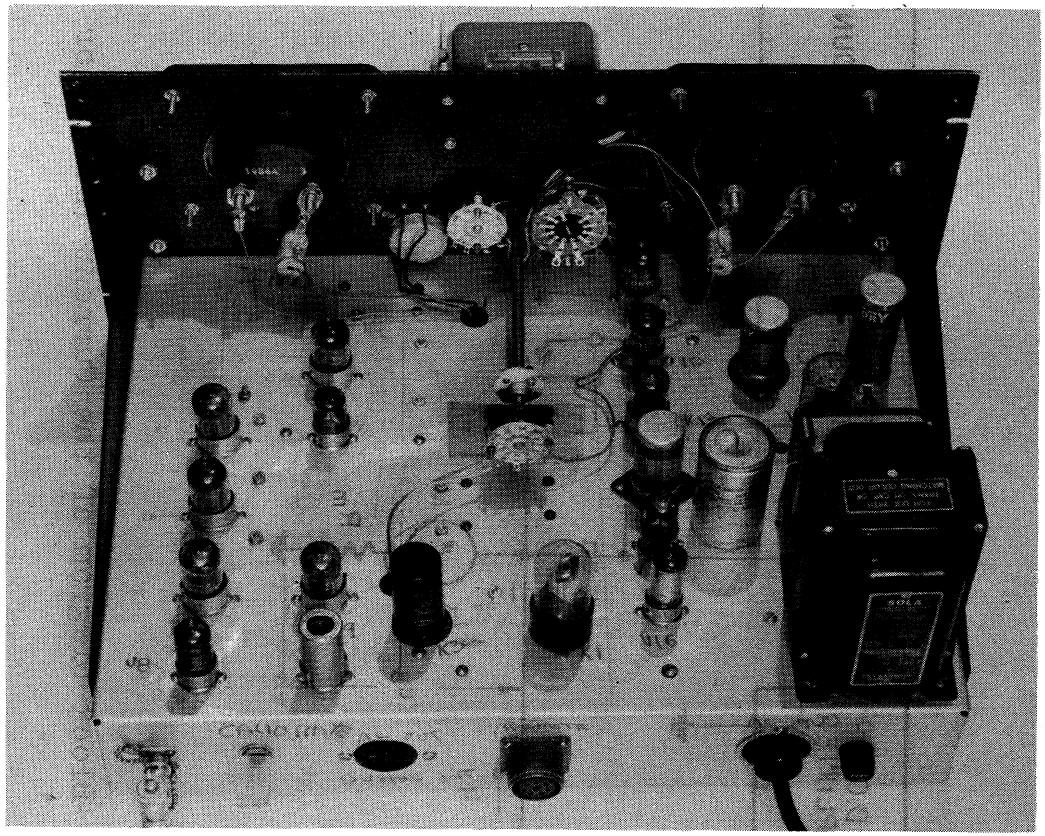

Fig. 6. Current Integrator Top

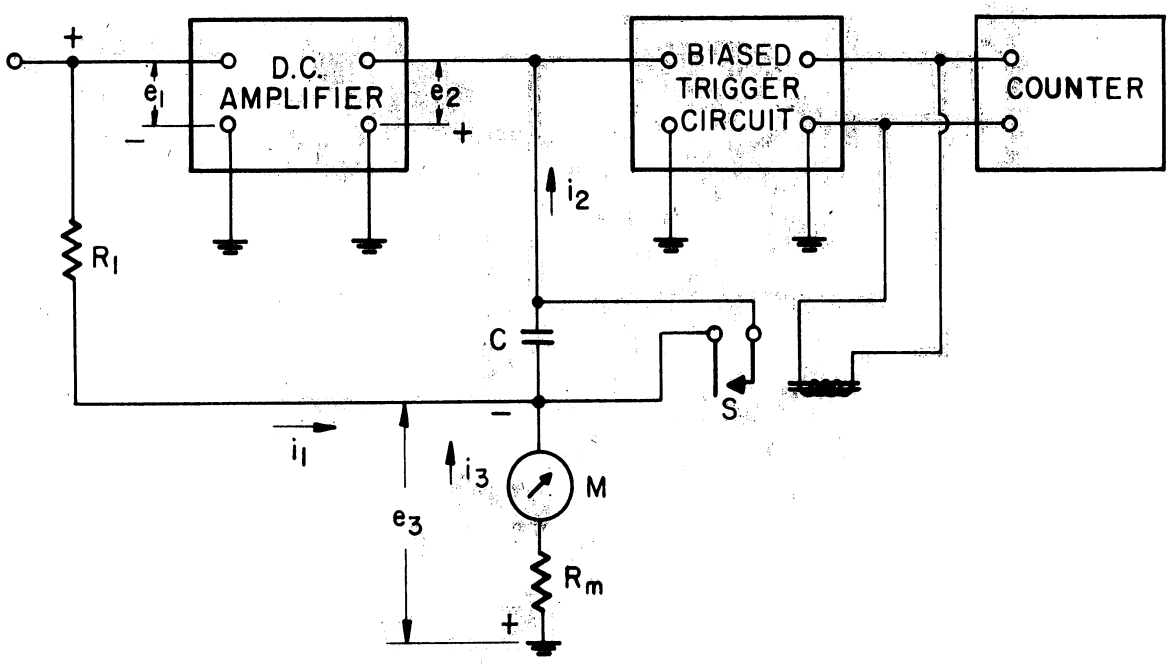

Fig. 7. Block Diagram of the Current Integrator

amplifier without feedback. If A is sufficiently large, then e_1 is small. In this case, the input terminal is held approximately at ground and the input current is $i_1 = \frac{A+1}{A} \times \frac{e_3}{R_1}$ or approximately $i_1 \simeq e_3/R_1$.

If the switch S is opened, the amplifier will try to maintain the appropriate potential at e_3 by supplying the meter current through the capacitor. If i_1 is very much less then i_3 than the voltage across the capacitor will be $Vc = (1/C)\int i_3 dt$. Since $e_3 = i_3 R_m$ and $i_1 \simeq i_3 (R_m/R_1)$ then $V_c = (1/C)(R_1/R_m)\int i_1 dt$.

Thus in effect the input current is amplified by a known factor R_1/R_m and integrated by the capacitor C.

b. Layout and Construction. The unit was layed out to accomodate the original version of the circuitry as obtained from S. Rankowitz (100) at Brookhaven National Laboratory (Fig. 6). The instrument has 10 ranges and is able to integrate currents as low as 0.01 micro-ampere and as high as 100 micro-amperes at full deflection of the "Current Indicate"meter (Fig. 8).

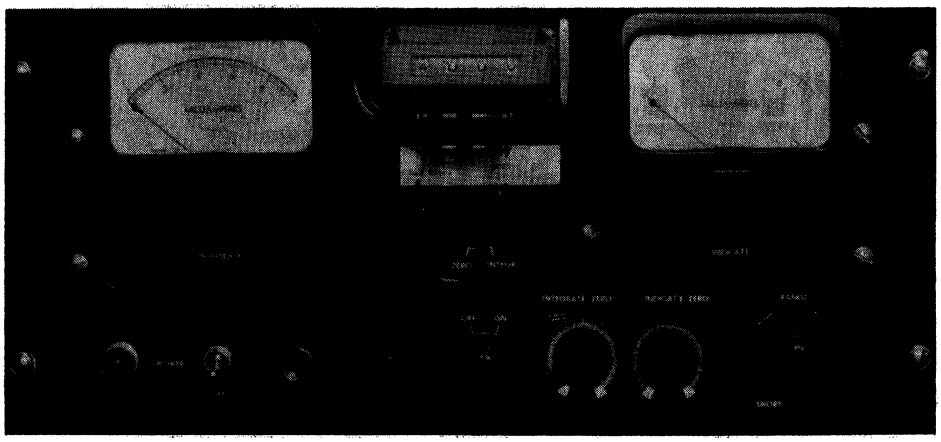

Fig. 8. Current Integrator Panel

When the instrument was first tested it was impossible to adjust it to indicate "no current". The wiring was thoroughly checked but with no avail. As precision parts were used throughout, component failure was quite unlikely. Introduction of a feedback loop, changing the values of several resistors and addition of a 75 ohm potentiometer for fine control adjustment of the "zero integrate" potenti-

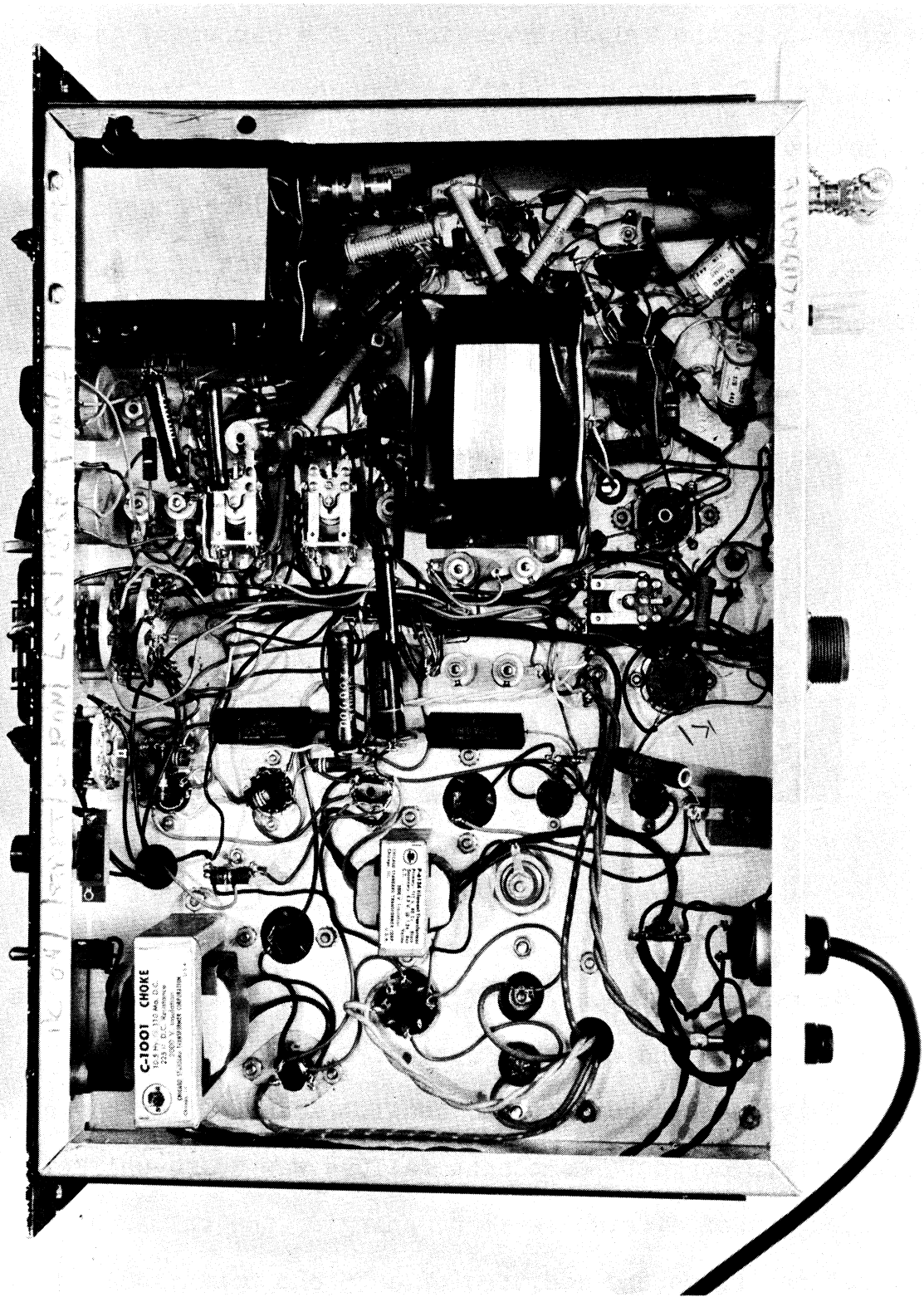

Fig. 9. Current Integrator Bottom

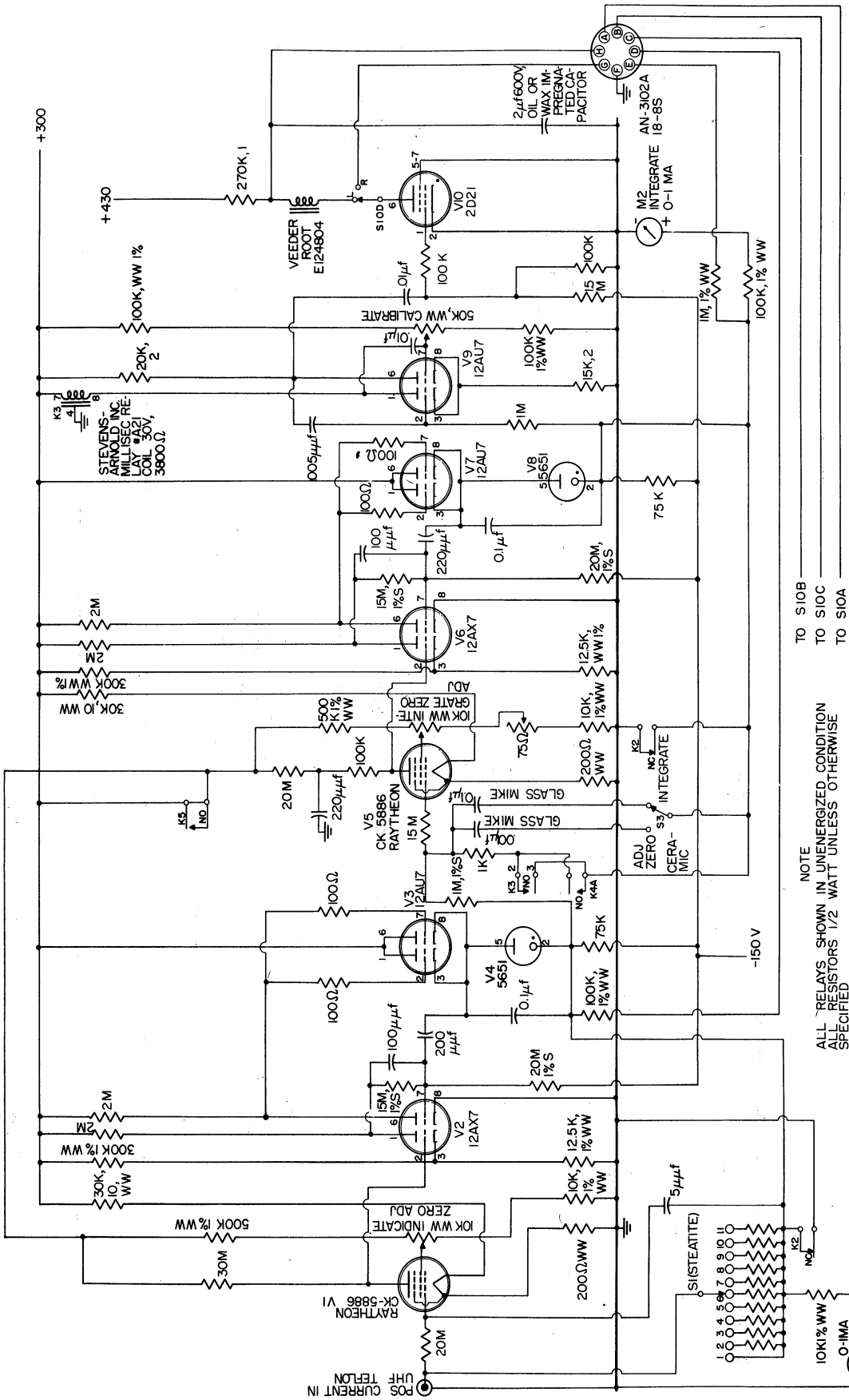

Fig. 10. Current Integrator, Circuit Diagram

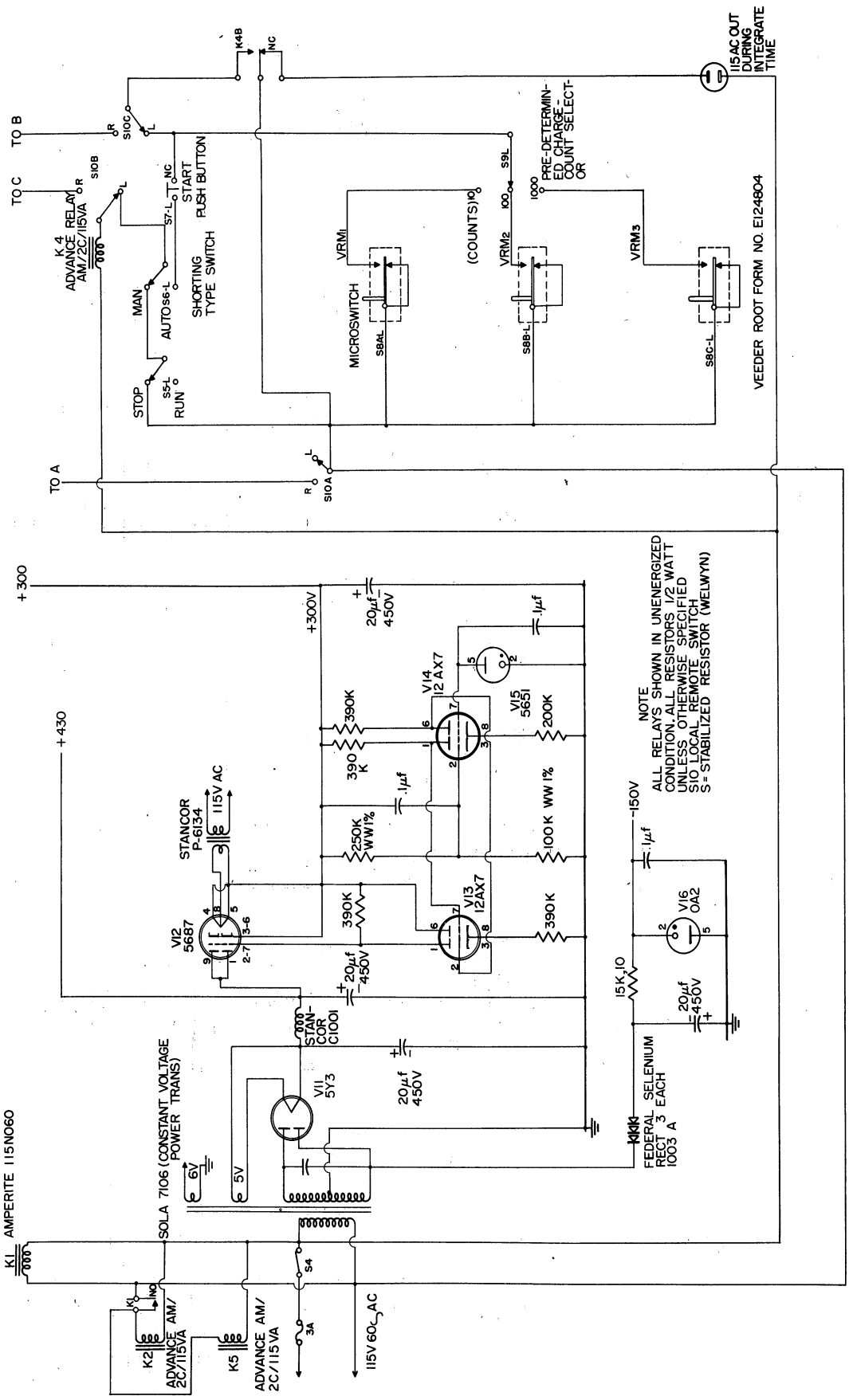

Fig. 11. Current Integrator Power Supply, Circuit Diagram

ometer, resolved the initial difficulties. A view of the chassis wiring is given in Fig. 9 and a close-up of the panel in Fig. 8. Fig. 10 and 11 give the diagram of the corrected circuits as used in the present unit.

c. Calibration of Current Integrator: The Current Integrator built in the Fall of 1955 was calibrated against a known current. The method employed is best seen from the block diagram of the calibration circuitry shown in Fig. 12. The Weston standard cell was compared with a wall

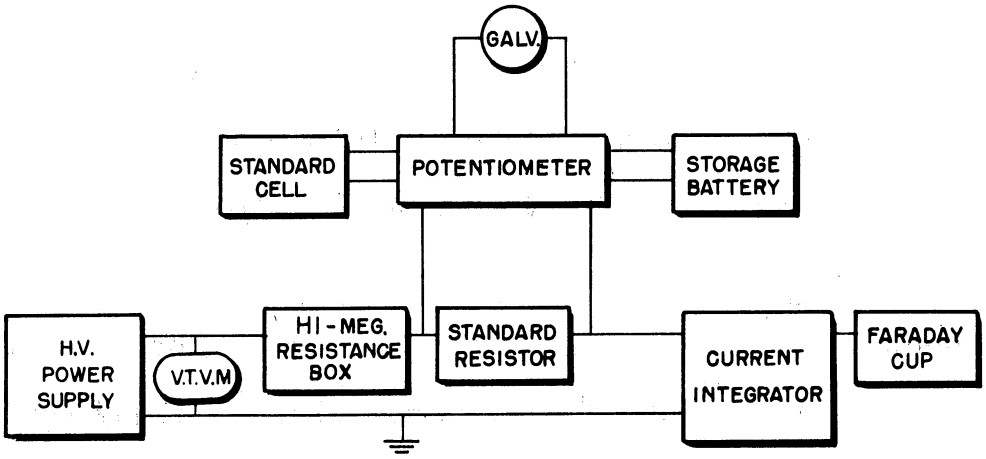

Fig. 12. Block Diagram of Apparatus Used to Calibrate the Current Integrator.

mounted standard to within $\pm$ 0.001%. The latter had been calibrated by the National Bureau of Standards. The Potentiometer was a Rubicon type B, operated with a Leeds and Northrup type R — 2500 galvanometer. This combination

was found to be able to measure a 1 millivolt drop of potential across a 10,000-ohm standard resistor with an accuracy of 0.02% standard error. A Leeds and Northrup type 4040 resistor was used for the standard. Its resistance had been measured in 1954 by the National Bureau of Standards and found to be 10,005.2 ohm $\pm$ 0.1 ohm.

Six drycells connected in series and parallel were used to drive the potentiometer. The High-Meg resistance box contained 13 glass-sealed high meg ohm resistors ranging from 10×10^6 to 104×10^9 ohms (Victoreen Instrument Co., Cleveland, Ohio) mounted on Steatite selector switches and enclosed in an airtight desiccated copper box with two (UG 496/U) cable connectors as output (Fig. 5, top panel).

A very stable high-voltage power supply was used for supplying the calibration current. This unit had been built in this laboratory by W. Cassatt (17) in 1953.

During the calibration procedure the Faraday cage was connected to the same input connector on the current integrator as the standard resistor. Excellent linear relation between current integrator counting rate and calibration current was found for all ranges of the unit. Fig. 13 is the calibration curve for the range used exclusively during this research, representing a slope of 64.79 counts per minute per micro-ampere.

The factor K of equation (17) is thus:

$$K = 64.79 \pm 0.6\% \text{ counts per micro-ampere hour.}$$

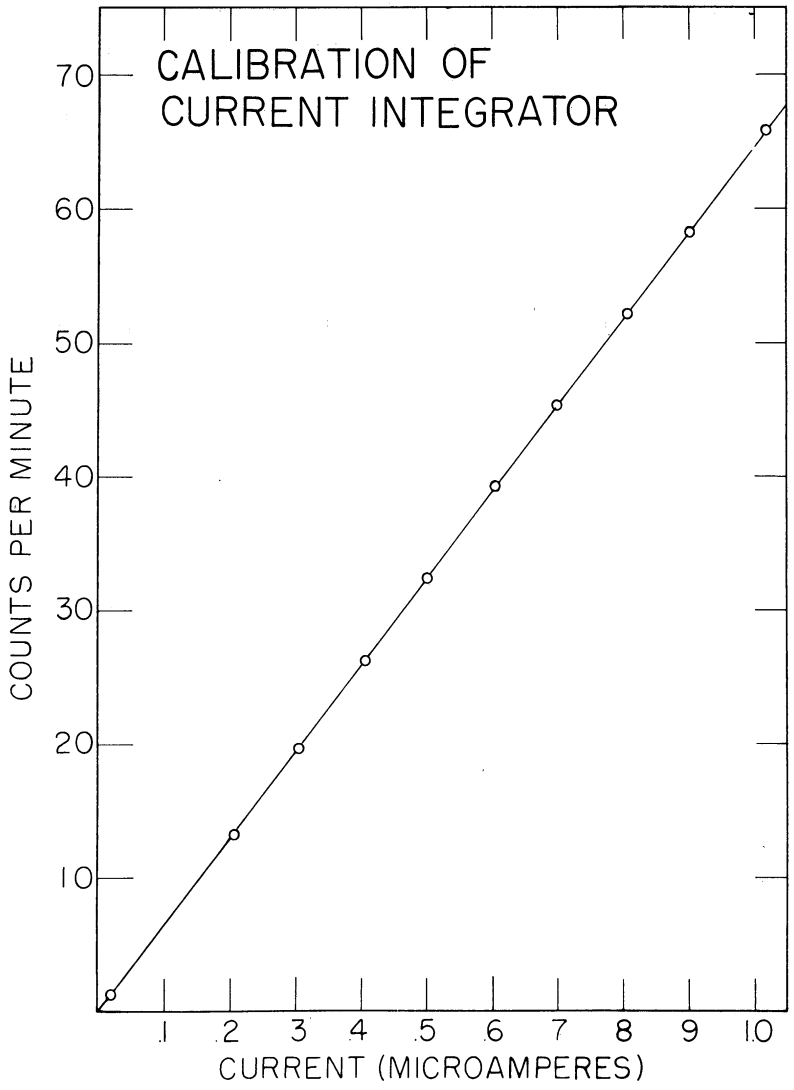

Fig. 13. Calibration Curve of Current Integrator

A least-squares analysis of the ten calibration points gave a standard deviation of 0.6% from perfect linearity. Since the deviation was found to be random, currents up to 1 micro-ampere could be integrated during the course of this research with standard errors of less than 1%. With

a half hour warm-up period before each bombardment run the drift characteristics were found to remain well within this 1% error for bombardments of two hours and more.

The performance of the instrument was very satisfactory after an initial failure of the millisecond relay due to exceedingly strong surge currents had been corrected.

II. Determination of the Number of Parent Nuclei in the Target

The second factor entering into the cross section equation (2) is the concentration of the number of parent nuclei in the target. This value depends largely on the dimensions of the targets whose measurements are facilitated by the use of carefully prepared targets.

A. Targets

Two factors enter into the considerations for preparing targets for the cross section measurements: When penetrating the target the deuterons are slowed down. For good energy definition of the cross sections it is, however, important that nuclei lying on the bottom of the target should undergo nuclear reactions with deuterons of more or less the same energy as those lying on the top. Thus, the target used for experiments intended to measure cross sections should be thin. Too few nuclei exposed to the beam in extremely thin targets, however, will result in too few interactions and too little reaction product for measurement. The optimum target thickness must thus be a compromise and was found for this research to be approximately 0.0001 inch or 2 - 5 mg/cm^2.

During the nuclear reaction the momentum of the bombarding deuteron is transferred to the compound nucleus

and part of it to the reaction product nucleus. This momentum might be strong enough to make the products leave the target itself. It was found (56) that such recoils emerge primarily from the back of the target and are stopped completely by a $\frac{1}{2}$-mil Mylar film placed immediately behind the target itself. For the present research 1-mil Mylar substrates were used for this purpose.

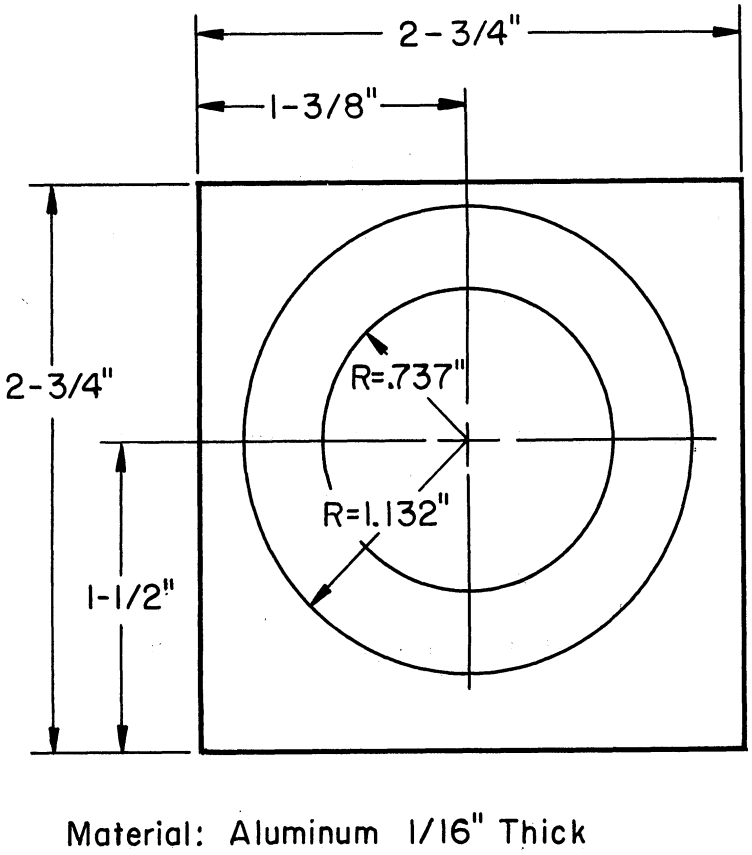

Fig. 14. Dimensions of Aluminum Target Frames

1. Target Preparation.

There are essentially two ways of preparing thin and even targets: the use of thin metal foils and the deposition of the target substance onto a substrate by high vacuum evaporation.

a. Metal Foils. Refractory metals like zirconium, titanium and molybdenum could not be evaporated in the metal evaporator available in this laboratory. With the help of various industrial firms it was, however, possible to obtain thin foils of these materials which could be used for targets. Disks were cut from the foils with a 1.474 $\pm$ 0.002-inch diameter punch die. These disks were glued onto a 1-mil Mylar film serving as the substrate and mounted on aluminum target frames.

Mounting the targets on 1/16-inch-thick aluminum frames prevented deuterons which did not penetrate the target from reaching the Faraday cage. To minimize interaction of target nuclei with any neutrons produced by the Al(d, n)Si reaction in the frame, targets were cut to just fill but not overlap the aperture of the target frame and mounted on the beam-exposed side of the frame. The dimensions of the target frames can be seen in Fig. 14.

b. High Vacuum Evaporation. Targets for the S(d, α)P reaction were made by high vacuum evaporation. Their preparation posed considerable difficulties. Materials to consider for these evaporations were: elemental sulfur,

Fig. 15. High Vacuum Evaporator

lithium sulfate, cadmium sulfide and zinc sulfide.

Only very uneven targets could be prepared with elemental sulfur, they were also found to evaporate during the bombardment with deuterons (54). Efforts to evaporate lithium sulfate, a substance producing no long-lived radioactive side products on deuteron bombardment, failed after repeated attempts. Reasonably good target deposits were obtained, however, with cadmium sulfide.

A technique was evolved at last for preparing targets for the study of the S(d, α)P reaction by evaporating zinc sulfide onto the roughened surface of a Mylar film.

The zinc sulfide did not stick to the smooth Mylar film. Proper roughening of the Mylar surface was accomplished in the following way. A 0.001-inch-thick sheet of Mylar was stretched over a glass plate with the aid of masking tape. The Mylar was then rubbed with a cotton wad dipped into a paste of fine pumice to produce an evenly roughened surface. Squares fitting the target frames were cut out of the roughened Mylar and mounted onto the frames with the roughened side facing away from the frame. For the evaporation a collimator mask consisting of an identical target frame with leveled edges was placed over the Mylar and this assembly mounted, mask down, onto the frame of the high-vacuum evaporator (Fig. 15). An aluminum block having a raised circular surface was placed onto the target frame so that the polished surface touched the smooth surface of the Mylar to serve as a heat dissipator during the evaporations.

Chemically pure zinc sulfide was placed in the tungsten boat serving as filament and evaporated unto the Mylar in high vacuum. Eight consecutive evaporations with intermediate rotation of the target were necessary to deposit approximately 1.5 mg/cm^2 of zinc sulfide on the Mylar, suitable for bombardment targets.

The weight of the deposit was determined by weighing the target frame before and after the deposition of the zinc sulfide. It was thus necessary to prove that during

the evaporations the target frame with the Mylar substrate did not change its weight. This was done by exposing an empty target frame with Mylar substrate to the same process, but with no zinc sulfide in the tungsten boat. The weight before and after this procedure remained the same within 0.006%, thus proving the suitability of the method.

c. Substrates and Absorbers. Mylar film 0.001-inch thick was chosen as substrate for most of the targets. The primary reasons for its choice were its relatively great durability toward radiation and its easy destructability during the chemical separations. The radioactive products due to the deuteron bombardment of Mylar (F^{18} and N^{13}) could be easily separated during the purification of the reaction products.

Aluminum foils of various thicknesses were used as substrate for the excitation function runs. This was advantageous, since aluminum could serve simultaneously as beam energy attenuator and catcher of the recoils. It was found able to withstand the greater beam intensities employed for these experiments. Some interference from aluminum in the chemical separations could be tolerated for these runs.

2. Target Measurements

a. Weight. The average thickness of the targets was determined from their weight and area. The weights of the foil disks were found by direct weighing with a semi-micro

balance, which permitted weighing within 0.02 mg, representing an error of less than 0.1% for the targets.

The weight of the zinc sulfide deposits was determined with a regular chainomatic analytical balance. The empty target frame with Mylar substrate was weighed before the evaporation and then reweighed after the ZnS was deposited. The difference in weight represented the weight of the ZnS deposit with a standard error of approximately 0.5%.

b. Area. The area of the metal foil disks was determined by the dimensions of the stamp die used for cutting the disks. The area of the target deposits prepared by high vacuum evaporation was determined by the dimensions of the collimating mask used. The area of the targets was thus known with an error of less than 0.1% standard deviation.

c. Evenness. Erroneous results may be obtained for the reaction cross section, if uneven targets are used with a non-homogeneous beam. The cross-section value would be too large, if the center of the beam struck a part of the target which is thicker than the calculated average. It was thus necessary for this research to prepare even targets and obtain an estimate of the thickness variation for each individual target.

Several methods are available to determine the evenness of target films of the type described above. The more accessible ones are less reliable and usually destructive. A crude way would be direct measurement of the

thickness at different parts of the target with a good micrometer. A destructive method consists of cutting a prototype target into several small sections and determining the weight and area of each (50). The variation in the thicknesses of the sections will serve for an estimate of the thickness variation in the destroyed sample. The same variation is assumed to occur in the other targets made from the same batch.

For the present research a reliable, sensitive, and nondestructive method was sought. The search for such a method resulted in the design of the beta gauge, shown in Fig. 16, for localized measurements of thin films (4). The instrument employs the weak 0.23-Mev β-rays of Pm^{147} and allows an estimate of the evenness of films a few mg/cm^2 thick by reproducibly scanning the sample with a collimated parallel β-ray beam 3/32-inch in diameter.

The β-ray point source of Pm^{147} was prepared by a method reported previously (3). Approximately 5 millicuries of carrier-free promethium chloride were deposited in a circle about 0.05 inch in diameter on a 0.04-inch-thick Lucite disk. The source was covered with Cellophane tape and mounted in a 7/8-inch-thick Lucite collimator with a smooth-walled hole of 3/32-inch diameter. The details of the source and collimator assembly are given in Fig. 16. A microscope-type movable stage mounted on the source assembly allows reproducible scanning of the

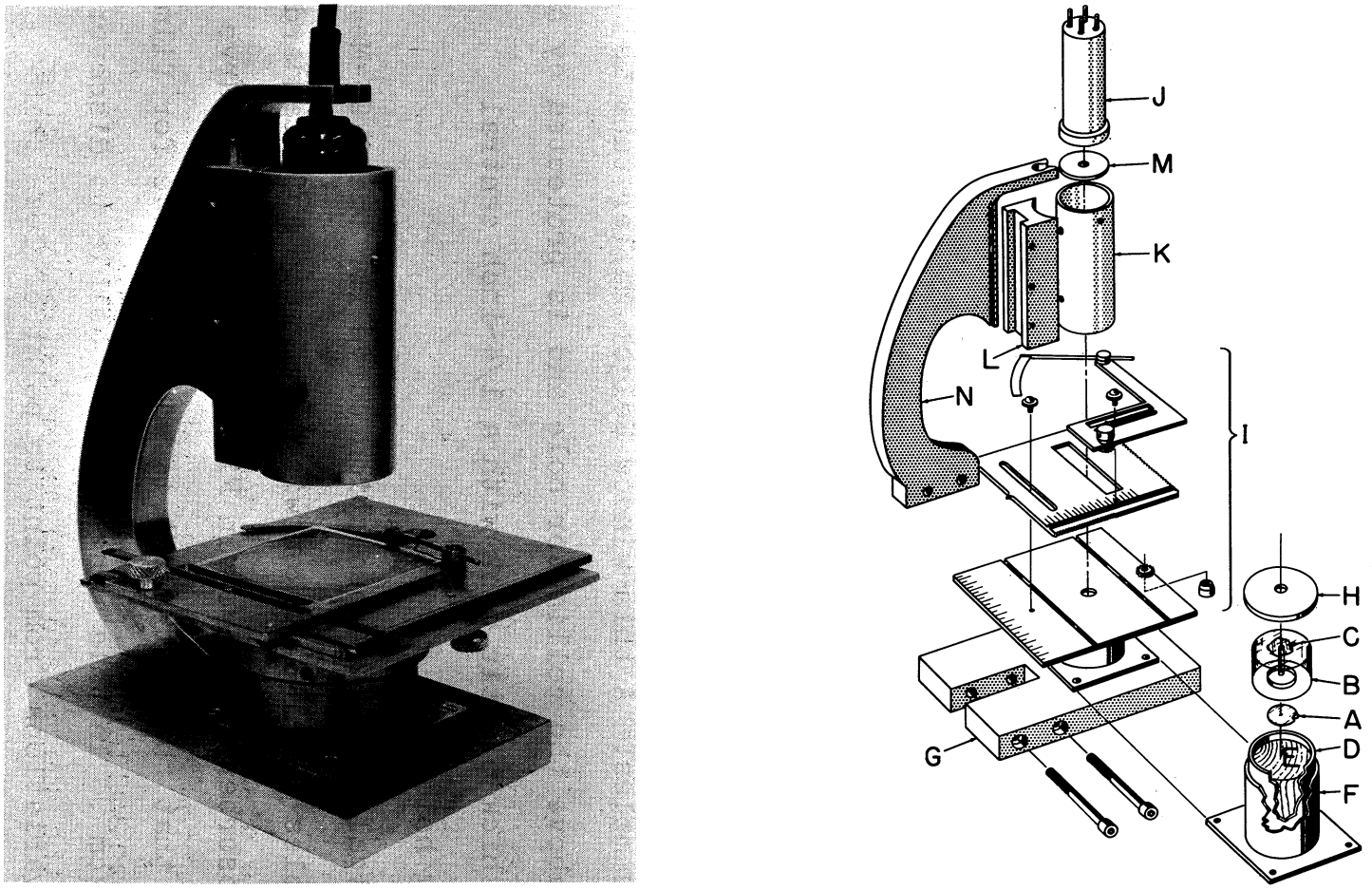

Fig. 16. Beta gauge. (A) 5 mc Pm^{147} point source; (B) Lucite collimator; (C) 20- g/cm^2 zapon film as dust guard; (D) 1/2-in. lead shielding; (E) wood support; (F) brass mount; (G) base plate; (H) 1/2-in. lead collimator; (I) movable stage; (J) G-M tube; (K) G-M tube mount; (L) guide; (M) plastic disk; (N) G-M tube support arm.

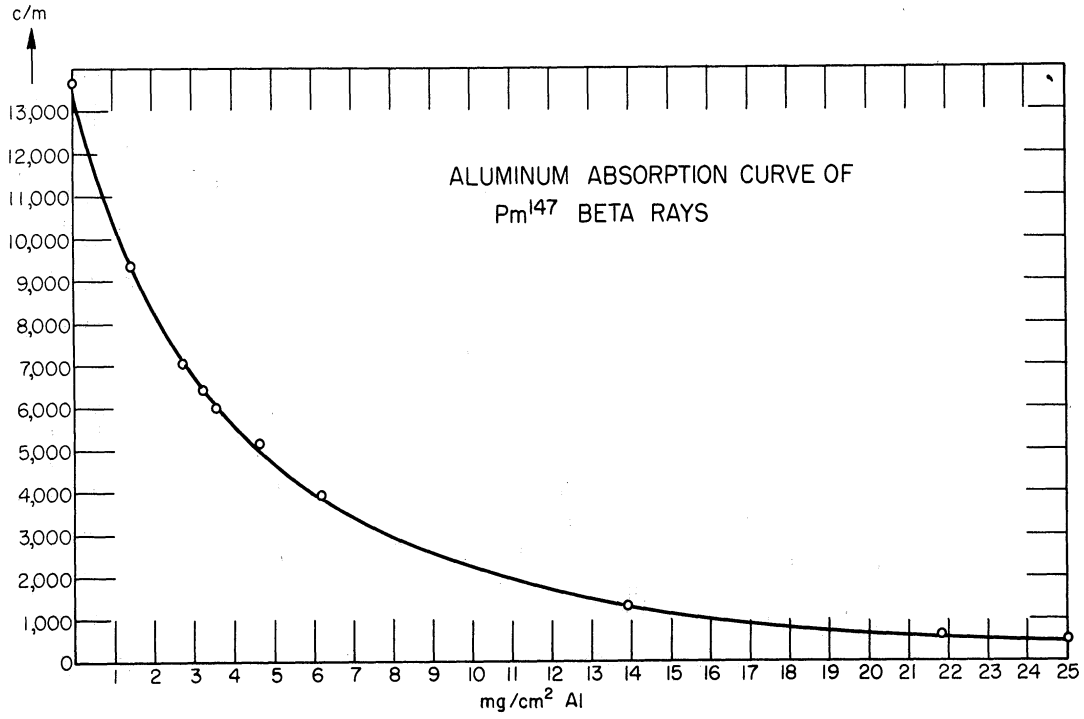

Fig. 17. Aluminum Absorption Curve of Pm^{147} β-rays

thin-film samples. A thin-window Geiger-Müller tube is suspended above the collimator hole and is protected by a 0.04-inch-thick plastic disk with a 1/4-inch central collimating hole.

A typical aluminum absorption curve for the 0.23-Mev β - particles of Pm^{147} taken with the gauge and standard aluminum absorbers is given in Fig. 17. From this curve it is seen that the instrument is most sensitive for films up to 6 mg/cm^2. In this range it is possible to discover thickness variations from point to point of less than 0.1 mg/cm^2. Fig. 18 shows the performance of the gauge

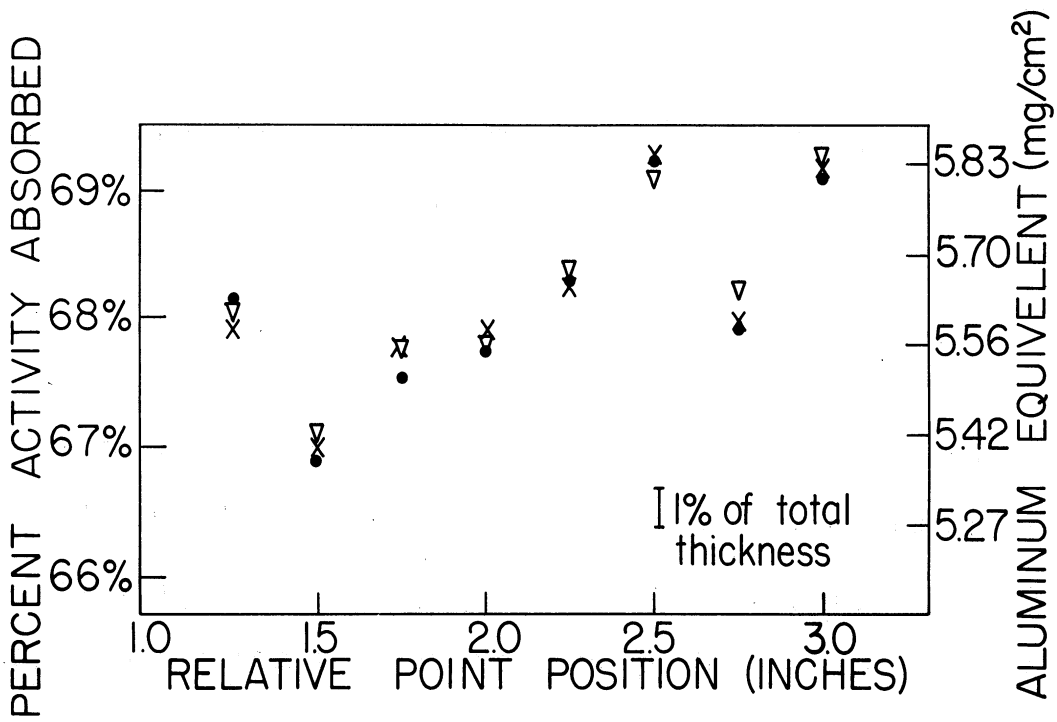

Fig. 18. Typical Scanning Data Obtained with a Relatively Uneven Sulfur Target. Nine points 1/4 inch apart were scanned three times in random order. (X) Scan No. 1; (▽) Scan No. 2; (•) Scan No. 3. Counting time was 10 min per point giving a reliable error of 1% per count.

with a relatively uneven target of elemental sulfur deposited on Mylar.

The thickness variation of all cyclotron targets used in this research was determined with the Pm^{147} gauge. The metal foils could be measured directly, the variations in the ZnS deposits were determined by difference. For the latter, fifteen measurements were taken on the Mylar substrate at points distributed over a 25 cm^2 area. Zinc sulfide was then evaporated onto the film and counts again

taken at the identical 15 positions. The difference of the counting rates was calculated for each position and the data evaluated by the least-squares method. A standard deviation from perfect evenness of less than 1% was obtained for several ZnS deposits by this procedure.

B. Calculations

The total number of nuclei in the target given by the chemical atomic weight and Avogadro's number, the weight and area of the target, as well as the isotopic abundance of the nuclei of the parent species in the naturally occurring element enter into the calculation of the parent isotope concentration for a nuclear reaction.

Data for weight and area were obtained experimentally as described above. The chemical atomic weights were taken from the International Table of Atomic Weights (125), the isotopic abundances from the Brookhaven National Laboratory Report on Neutron Cross Sections of July 1955 (65).

The concentration of the parent nuclei in the target was then calculated by:

$$n/A = \frac{(\text{weight})\ (\text{isotopic abundance})\ (6.02 \cdot 10^{23})}{(\text{atomic weight})\ (\text{area})\ (\text{chemical atomic weight})}$$

III. Determination of the Number of ProductNuclei

The third factor entering the cross-section equation is the number of nuclei produced by the reaction. From the development of the cross-section formula as given in section I-B of the Introduction, it is seen that this amounted to the determination of the absolute disintegration rate of the product nuclei at the end of the bombardment. The methods and instruments used for purifying, identifying and counting the nuclei produced by the (d, α) reactions are described below.

A. Radiations from Product Nuclei

An excess of either protons or neutrons in a nucleus can, according to Fajans' and Soddy's "Displacement Law" of 1913 (35, 118) be corrected by the emission of an appropriate β-particle. Nuclei with neutron excess emit negatrons (β^-), nuclei with proton excess emit positrons (β^+). The energies of the β-rays emitted by a particular nucleus vary from very small values to a certain maximum energy characteristic of the emitter. The distribution of these energies (β-spectrum) can explain certain nuclear characteristics, and is at the present the subject of extensive studies carried out by many authors (e.g. see 68 and 71).

For the positron emitters there exists an alternate path of decay. The nucleus can capture an electron

from the electronic shell of the atom and by this process achieve the same effect as by positron emission. As the hole in the electronic shell is filled, a characteristic x-ray is emitted indicating the capture process.

In case the product nucleus from a β - decay or electron capture process is left in an excited state, it will lose energy by γ-ray emission to go to a less excited, more stable form of the same isotope. The three types of radioactivity encountered in the middle of the periodic table are thus: β-rays, x-rays and γ-rays.

To count the absolute disintegration rates of β-ray emitting reaction products the self-absorption of β-particles in the source material has to be considered. Electrons and positrons emitted as β-rays strongly interact with matter and have relatively short ranges in solids and liquids. When counting β-rays emitted by a source containing much solid matter, many of the β-particles will never even leave the source and enter the sensitive area of the counter. It is thus of great importance to use only weightless or "carrier-free" β-ray sources, when their absolute disintegration rates are to be determined.

X-rays and γ-rays are more penetrating kinds of radiation. Self-absorption in the source is of minor importance when counting them. The very fact of their greater penetration through matter, however, requires

special techniques for their measurement. Much more detector material has to be used to bring them to interact, posing problems of large background rates of the counters, partial interaction of the radiation with the counter material, etc.

B. Chemical Separation

The product nuclei of the (d, α) reaction are chemically different from the target element and any other nuclear species produced by the interaction of 7.8-Mev deuterons with the target nuclei. It is thus possible to separate the (d, α) reaction product from the target material and radioactive impurities by chemical means.

The determination of absolute disintegration rates in a sample of β-ray emitting reaction product can only be carried out on bulk-free counting samples. The chemical separation steps must thus form a "carrier-free" procedure and yield the (d, α) reaction product in pure and bulk-less form. In addition it is necessary to know the yield of the chemical separations employed.

1. Methods for Carrier-free Chemical Separations

Primarily four methods are available for the chemist to separate a small amount of activity from macro amounts of impurities by carrier-free procedures: recoil methods, solvent extractions, simultaneous precipitation and ion exchange.

a. Recoil Methods. Recoil methods were employed already in the early stages of nuclear chemistry and seem to gain increasing interest in the recent literature (91, 120). They are based on the principle that upon the emission of radiation (in particular α radiation) or after the impact of an accelerated particle, the recoiling daughter nucleus has enough momentum to escape from the sample. This carrier-free product may be collected in some catcher material. In another case, recoiling nuclei might break their bonds in insoluble substances and form soluble ions which can be eluted from the original molecular substance (24, 121).

These methods are extremely suitable for the characterization of short lived isotopes. They cannot be used, however, for absolute yield determination of nuclear reactions, since not all reacting nuclei will recoil in the right direction to escape the original sample and be collected by the catcher.

b. Solvent Extraction. Solvent extraction methods are relatively common for carrier-free separation procedures.

They make use of the different solubility of certain species in various solvents. As this behavior is the same for micro and macro amounts, rather good chemical separations can be effected (73). For the present research solvent extraction procedures were avoided. They seemed to offer too few real advantages to offset the risks of spills when performing them in a hurry and under pressure.

c. Simultaneous Precipitation or Scavenging. Micro-amounts of radioactive species will precipitate from a medium in which they are insoluble together with an added carrier of different chemical nature which is equally insoluble in the medium (33,34). The latter forms the bulk of the precipitate which can be centrifuged and filtered. When employing such a method it is well to keep in mind that every precipitation from a radioactive solution will carry some adsorbed traces even of soluble radioactive materials (coprecipitation). The amount of these impurities may vary greatly, however, depending on the physical form of the precipitate. The latter often depends on the way the precipitation was carried out. Gelatinous precipitates are usually good carriers, micro-crystalline precipitates not (103).

In working with small amounts of a desired species when losses cannot be afforded, precipitates intended to carry the desired activity should be the only ones formed in a solution. In the case that this is not possible, it was found that homogeneous precipitations as pioneered by Willard (126, 127) carry least of a desired activity kept in solution. Homogeneous precipitations have the additional advantage of being able to precipitate only one of two species, where both would be precipitated, if any excess of reagent were added.

d. Ion Exchange. Ion-exchange techniques have found wide application during the past decade as they opened up an entirely new field of separation chemistry. They permit dependable and easy separation of species virtually inseparable by classical methods (61, 74, 75, 93). For the present research ion exchange procedures had the additional advantage of equal applicability to macro and trace amounts. When overloading of the resin bed was avoided, very clean separation could be achieved. Ion exchange steps were mainly used for the final purification of the reaction product rendering it in carrier-free form suitable for absolute β-ray counting. It was necessary to use conductivity water when preparing the eluents.

Many of the ion exchange steps carried out employed Dowex-2 resin in the hydrochloride form. This anion exchange resin, obtained from the Dow Chemical Company, Midland, Michigan, was purified by washing with various solutions in the following sequence:
Water, conc. HCl, water, 2 M HCl, water, 2 M $HClO_4$, water, 2 M NH_4OH, water, 2 M NaOH, water, conc. HCl.*

The resin thus purified was stored in 6 M HCl and used in small portions over a period of more than two years, giving very satisfactory performance. For each

---

* The resin purified by a similar procedure is now available commercially from the Bio·Rad Laboratories of Berkeley, California.

separation step the resin was packed into small columns and washed again with distilled water and conc. HCl. Fig. 20 gives the dimensions of the columns used with Dowex 2. Table II indicates the ion exchange behavior of many metals in such Dowex-2 columns (61). Fig. 19 shows the experimental apparatus to study the elution rate of P^{32} from a Dowex-50-$Fe(OH)_3$ column as described in the procedure for the separation of phosphorus from zinc sulfide.

2. Determination of the Chemical Yields.

When the product of the (d, α) reaction is obtained in carrier-free form, the question remains: How much of the original amount of reaction product was lost during the chemical purification and how much was actually incorporated into the sample ready for counting?

An excellent method to determine the yield of a carrier-free separation is the isotope dilution technique. A known amount of a carrier-free isotope of the reaction product is added to the undissolved target. Complete isotopic exchange between this tracer and the bombardment product is effected in a homogeneous solution under rigorous chemical conditions. The amount of tracer isotope mounted with the purified reaction product on the counting sample is determined. The amount of tracer lost in the separation process will then be proportional to the amount of reaction product lost in the separation procedure.

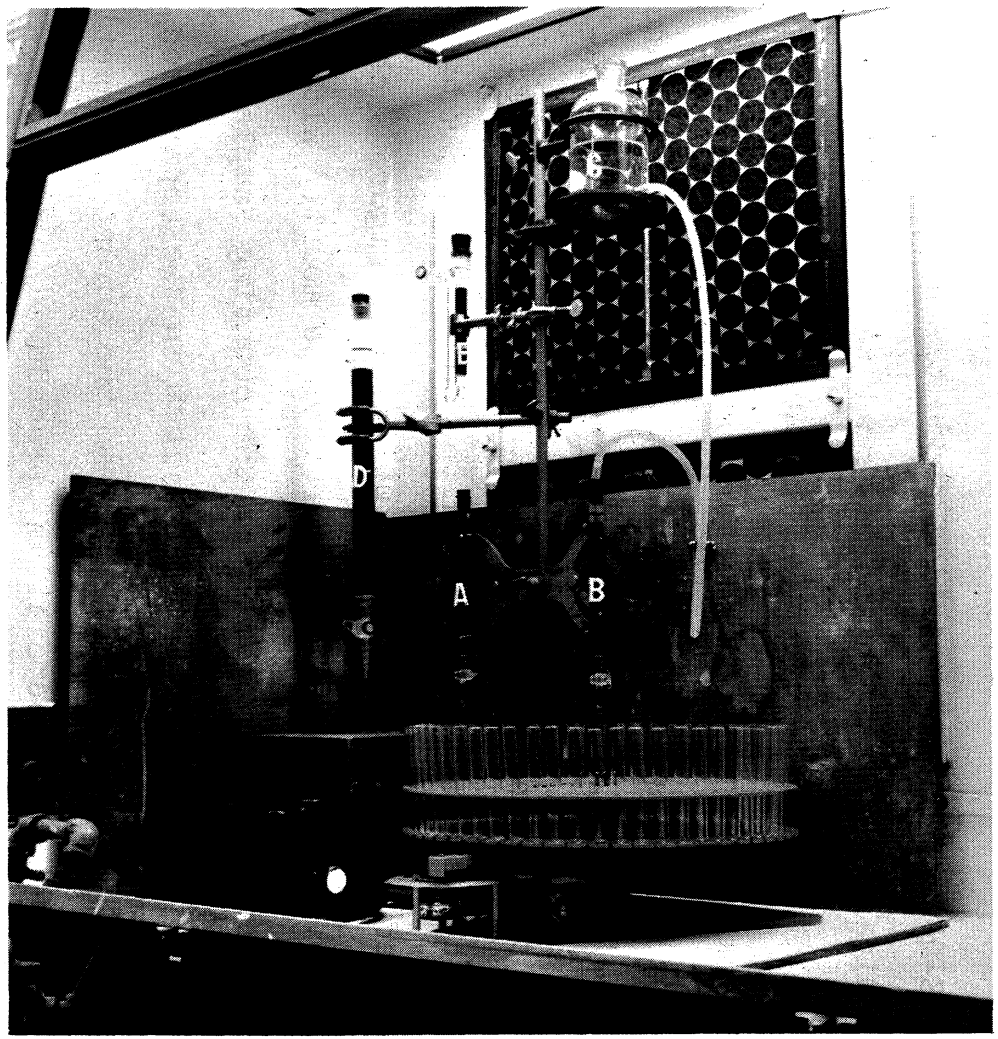

Fig. 19. Hood with P^{32} Separation Equipment

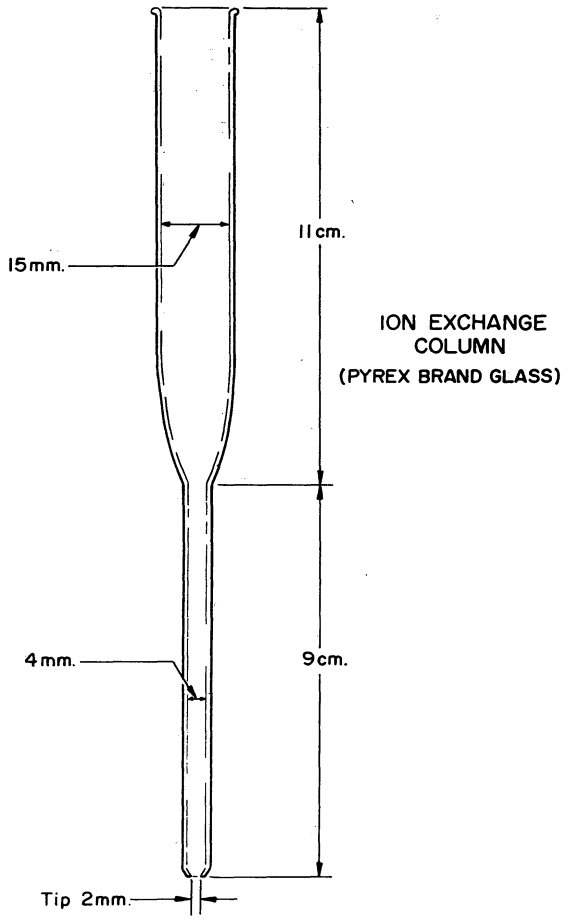

Fig. 20. Small Ion Exchange Column

Table II. Elution Properties of Various Elements from a Small Column Charged with Dowex 2 (200 - 400 mesh) (61).

Eluting Agent	Elements Eluted by ~5 ml. Eluting Agent
12 M HCl	Alkali Metals, Alkaline Earths, Rare Earths, Sc, Y, Ti^{III}, $V^{II\ III\ IV}$, Ni, As^{III}, As^{V}, Se^{III}, Se^{IV}, Tl^{I}, Pb^{II}, Bi^{III}, Cu^{II} slowly, Al, Cr^{III}, Fe^{II}, Mn^{II}
6 - 9 M HCl	Ti^{IV}, V^{V}, Ag*, Ta*, Pt^{II}, Zr, Hf
3 - 6 M HCl	Fe^{III}, Co, Ge, Nb*
1 - 3 M HCl	Zn, Ga, Mo^{VI}, In, Sn^{IV}, Te^{IV}, Te^{VI}, Au (as $AuCl_2$), Pb^{II}
Below 0.01 M HCl	Sn^{II}, Hg^{II}, Bi^{III}, Sb^{V} slowly
3 M $HClO_4$	Po, Cd, Sb^{III}, Sb^{V} slowly
1 M NH_4OH	Pd, Ag, Sb^{III}, Sb^{V}
1 M NaOH	W
Not eluted	Tc*, Ru, Rh, Re, Os, Ir, Pt^{IV}, Au^{III}, Tl^{III}

* In trace concentrations only

It may be pointed out that complete isotopic exchange is a stringent requirement for the successful application of this method. It can be achieved only in homogeneous liquids under severe chemical conditions such as strong acids and oxidizing media. Radioactive isotopes to be used for yield determination of the separations of this research had to meet the following specifications. The half-life of the tracer must be either considerably longer or shorter than that of the reaction product to permit easy resolution of the decay curves. If there is only one reaction product, the tracer must not be identical with it. The tracer must be chemically pure, free of contaminating activity and available in carrier-free or partially carrier-free form.

If the tracer used is identical to one of several reaction products, at least two bombardments will be necessary for the cross-section determination. The first bombardment will establish the ratio of the components in the reaction product at the end of the bombardment without addition of tracer. The second experiment, with tracer, will determine the ratio of the components as if the tracer had also been produced by the bombardment. The amount of isotope identical with the tracer, but produced during the second bombardment can then be calculated from the count rate of the other component and the ratio determined by the first bombardment. The chemical yield is established by comparing the amount of tracer

carried through the separations with the amount of tracer isotope initially added.

It is unneccessary to determine the count rate of the tracer absolutely or with the same counter with which the reaction product is counted; as long as it is possible to establish the ratio of tracer material carried through the chemical procedure to the amount originally added, the chemical yield can be determined.

The various tracer methods employed during this research as well as the identification of the tracers used will be described with the individual bombardments in the experimental part.

C. Identification and Measurement of Radioactive Reaction Products

Various counters were employed in this research to identify the reaction products and determine their decay rates. The operation and design of these counters as well as their use is described below.

1. Beta-ray Counting.

Most of the reaction products encountered were β-ray emitters. Particular emphasis was thus given to counting this type of radiation. Relative β-ray counting was carried out with a Los Alamos type thin window proportional counter; absolute beta counting with two Borkowski-type 4π pro-

portional counters. For aliquoting and estimations of β-ray activities Geiger-Müller counters were used.

a. Proportional Counting. The proportional counter consists of a cylindrical or rectangular chamber whose walls are made of conducting material. A thin wire serving as anode forms the axis of the chamber. This center wire is insulated from the conducting wall and can be charged to a potential of several thousand volts. As counter gas very pure methane or mixtures of argon and methane are used. The design of todays proportional counters is essentially the same as was developed by Geiger and Müller in 1928 (42). The ionization-amplification in the counter procedes by the following steps:

A particle enters the chamber and produces primary ionization of the counter gas in the vicinity of its trajectory. The "secondary" electrons thus produced are attracted to the anode wire and accelerated by the electric field. When their kinetic energy reaches a value great enough to ionize another gas molecule on collision, a second generation of electrons is produced. Both electrons travel now towards the anode, colliding with new gas molecules as they gain momentum. This avalanching continues until all electrons are collected by the anode, resulting in a sudden drop of the potential of the wire and producing an electric pulse to the number electrons collected.

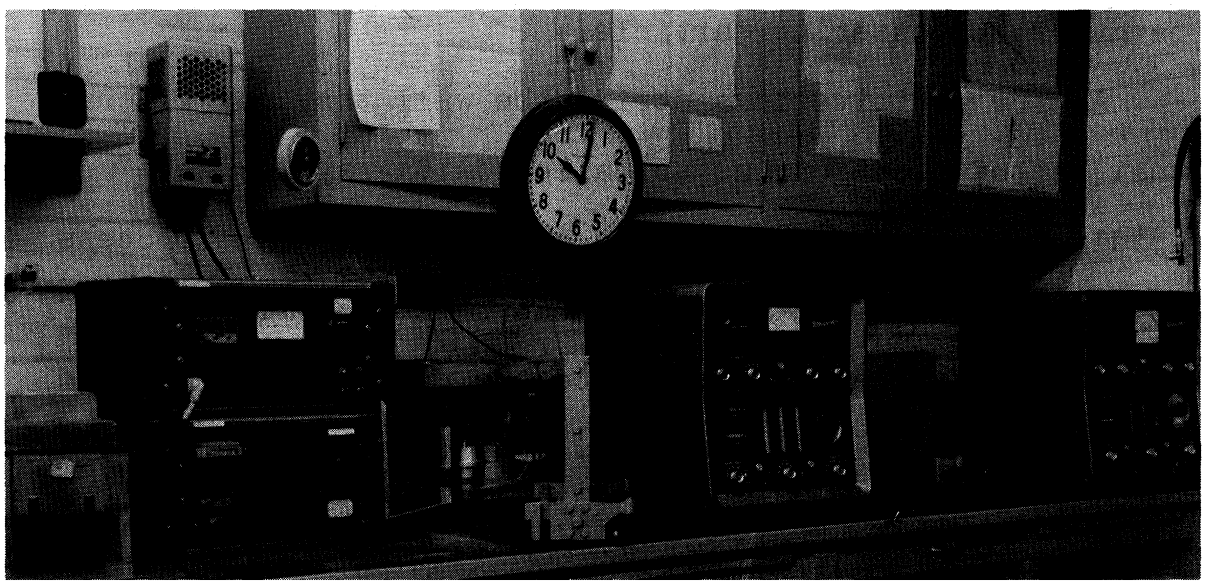

Fig. 21. Counting Room. Left: thin window proportional counter housing and PA-2 amplifier etc. Center: Borkowski-type 4π proportional counter in lead housing with Nuclear Chicago Ultrascaler. Right: same as center. Counter shielding closed.

The field gradient around the anode is very large. Most of the avalanche thus takes place in the direct vicinity of the wire. This results in an excess of positive ions in the vicinity of the wire which are repelled from it with great violence. As the positive ions recede from the wire and travel toward the wall, the negative pulse is further increased by induction. The second part of the process requires approximately hundred times as much time as the collection of the electrons, so that the total pulse has a steep initial rise turning into a slower further rise until the positive ions reach the walls and the potential at the anode is restored. The

size of the pulse is "proportional" to the number of secondary electrons which again is proportional to the energy of the entering particle.

As the positive ions strike the wall they may liberate a new set of electrons as so called delta-rays. These move rapidly towards the center wire and thus renew the process previously terminated. To suppress this "double pulse" effect organic substances are admixed to the counting gas or used themselves for the counting gas. The organic molecules exchange electrons with the positive ions so that virtually only ions of the organic molecules reach the counter walls. The energy which would otherwise be used for liberating electrons from the wall is now used to decompose the molecule of the "quencher". The probability of producing delta rays despite the quench gas is increased with the size of the avalanche which in turn is dependent on the anode potential. Double pulsing will thus determine the upper limit of the potential with which the chamber can be operated.

One characteristic of every counter is its voltage plateau. This plateau is the range of anode voltages for which the counter is able to produce distinguishable pulses for every particle entering the counter during its sensitive time. The limits of the plateau are voltages too weak to permit the formation of a distinguishable pulse for some of the particles, and potentials for which the quenching

gas becomes unable to successfully control the formation of delta-rays.

As the polarization potential of a proportional counter is increased, the field will first reach the strength to produce avalanches. This voltage is the "threshold of the counter". As the potential is increased further, the pulse height is approximately doubled for every 200 volts until Geiger region is reached and very large amplifications due to multi-avalanche production are obtained.

At some potential along the way the counter will be producing pulses large enough to be recognized by the electronic circuitry connected to it. This potential will depend on the sensitivity of the amplifier and shall be called the "threshold of the counter-amplifier combination". As the potential is increased further the "plateau" is reached, i.e., the counter produces recognizable pulses for every particle entering its sensitive volume and the count rate does not vary with the increase of the potential. The upper limit of the usable plateau of a counter-amplifier combination is generally the overloading of the amplifier which is unable to handle an excessive range of pulse heights and will block or double trigger the scaler. (Note: this double triggering of the amplifier is due to the differentiation of overloading pulses and is not the same as the double pulsing due to failure of the quenching process in the counter.)

The insensitive time of the counter-amplifier combination, i.e., the time during which a pulse occurs, is amplified and the counter potential restored, is of the order of a few microseconds.

The dead time for a counter-amplifier combination is dependent on the pulse height. The results of an experiment carried out with one of our 4π-proportional counter to prove this effect can be seen in Fig. 22 and Table III. The cause for the effect is the size of the pulse which has a length somewhat related to its height.

The advantages of proportional counting over Geiger-counting are manyfold. Longer plateaus can be obtained, and higher counting rates accomodated; the energies of the ionizing particles can be measured by the height of the proportional pulses and less quenching material is required for very dependable performance.

Certain requirements on the electronic circuitry, however, made the use of the proportional counter practically impossible until recent years. The sensitivity of the amplifier must be great enough to recognize the smallest pulses from the counter produced by a single ion in the counting gas. As the smallest practical proportional pulses are of the order of a few millivolts and the trigger pulse of the scaler of the order of one volt, a minimum amplification of about 1000 is required. Electronic noise in the amplifier must be kept well below this one millivolt level so as not to be confused with true pulses.

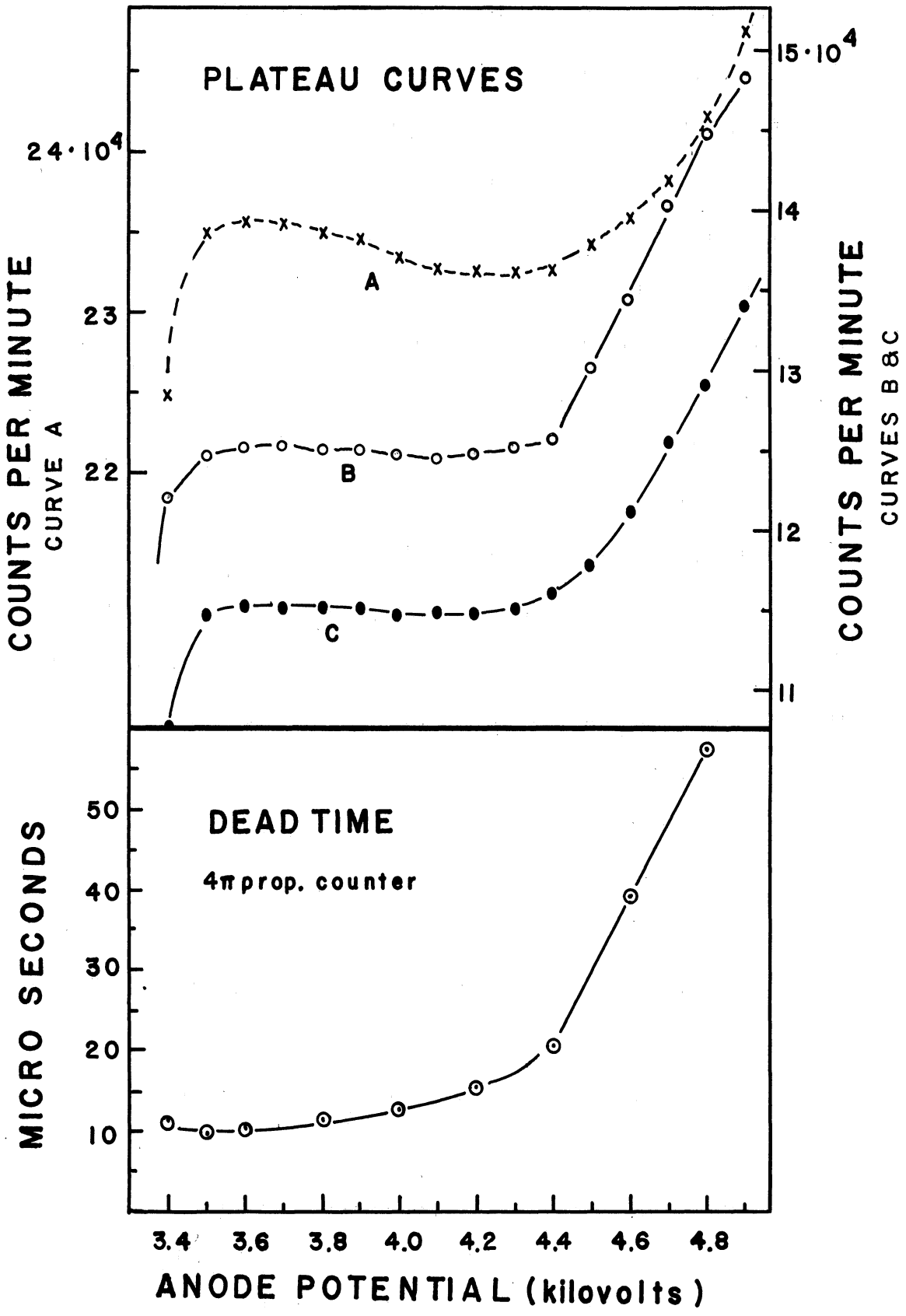

Fig. 22. Pulse Height Dependence of Dead Time for Proportional Counters.

Table III. Data for the Investigation of the Dead Time vs. Voltage Relationships for Proportional Counters

HV	Dead Time (10^{-6} sec)	R_1	Correction to R_1	R_2	Correction to R_2	$R_{1,2}$	Correction to $R_{1,2}$
3400	11.04	107,659	2,175	122,042	2,803	224,960	9,713
3500	9.84	114,757	2,201	124,844	2,609	234,996	9,420
3600	10.20	115,301	2,305	125,153	2,720	235,659	9,834
3800	11.04	115,240	2,497	125,016	2,944	235,062	10,626
4000	12.72	114,830	2,865	124,600	3,381	233,513	12,163
4200	15.24	114,764	3,445	124,840	4,088	232,535	14,598
4400	20.52	116,316	4,818	125,892	5,664	232,577	20,098
4600	39.18	121,301	10,435	134,429	12,935	236,060	43,020
4800	57.54	129,136	18,253	144,761	23,336	242,199	73,274

The primary ionization of the counter gas when counting β-particles may vary by a factor of 100 and more. The range of pulse heights presented to the amplifier will be of the same magnitude. If plateaus of the order of 800 v are to be obtained and the pulse height is approximately doubled by a 200 volt increase of the counter potential, the amplifier will be required to recognize separate pulses varying in size by factors of 2000 or more. For the largest pulses, the amplifier must not overload and double trigger the scaler. The dead time of the amplifier must be small to make best use of the properties of the proportional counter. The scaler unit must be fast enough to handle count rates up to 500,000 counts per minute without appreciable loss.

These requirements could not be met until the advance of the electronic age, but even today the cost of the highly refined equipment prohibits the use of the method in many cases.

b. Los Alamos-type Thin Window Proportional Counter.

Most of the relative β-ray counting carried out during these investigations made use of a Los Alamos-type thin window proportional chamber (76). A diagram of this counter is given in Fig.23. The instrument was set up in the Fall of 1955 and is being operated in conjunction with a modified Los Alamos type PA-2 amplifier and S C-4 scaler (Fig. 21, left) custom built by Trott Electronics Company, Rochester,

Explanation of Fig. 23

1. High voltage connector UG - 560/u
2. Connector support
3. Left shelf rack
4. Counter body
5. Right shelf rack
6. Polystyrene insulator
7. Cover
8. Aluminized 1/4 mil Mylar window
9. Window frame
10. Shelf stop
11. Polystyrene insulator

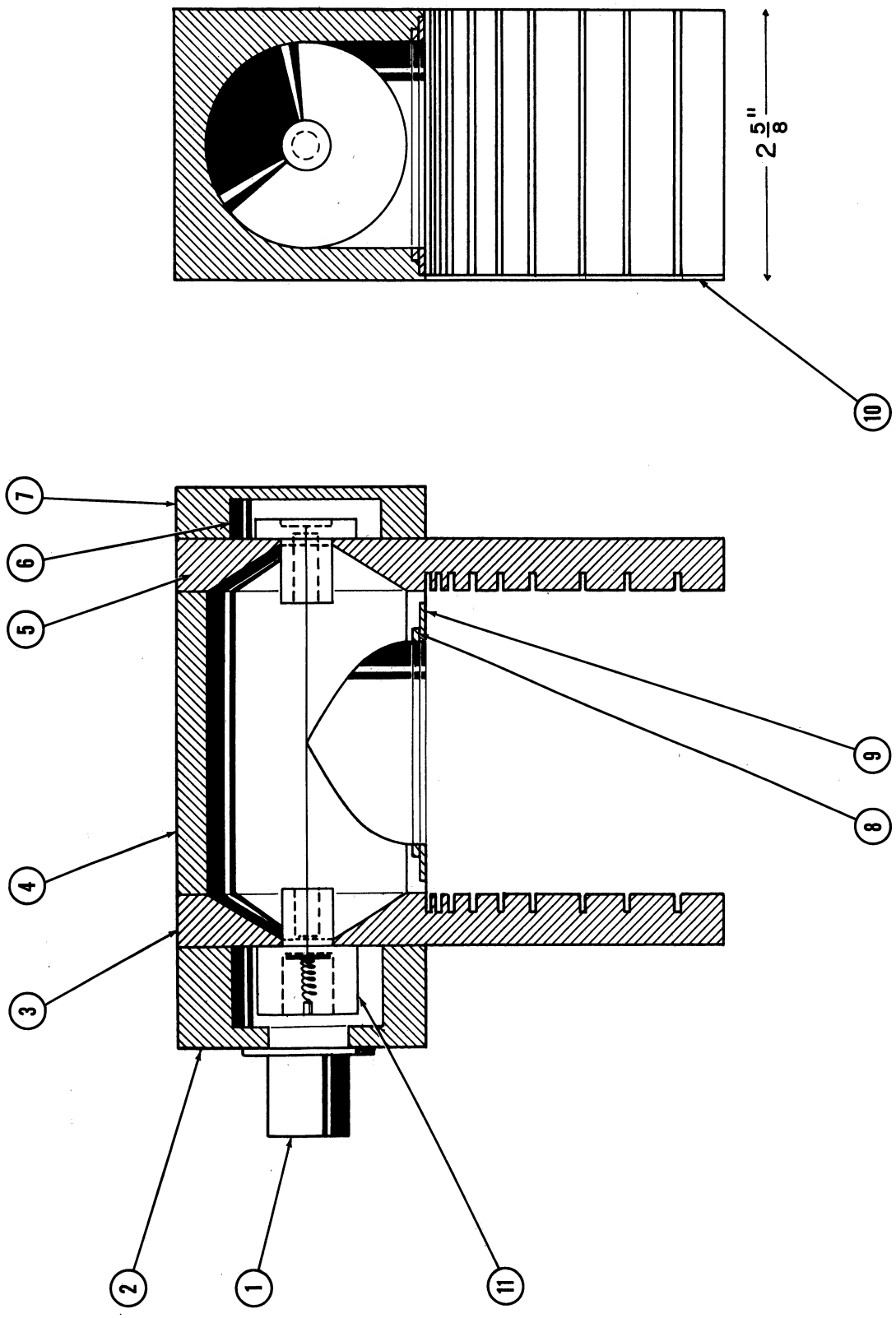

Fig. 23. Schematic Diagram of Thin Window Proportional Counter

New York. Plateaus obtained with this combination at two different settings of the amplifier are seen in Fig. 24. During this research the counter was operated at a 4400 volt anode potential employing 99-mol-percent methane (Phillips Petroleum Company, Bartlesville, Oklahoma) as the counting gas.

The counter was shielded by a two-inch lead housing to reduce the background to approximately 56 counts per minute. Very reliable performance was obtained with the counter-amplifier combination. It can be seen at the far left of Fig. 21.

c. 4π-Proportional Counters. Absolute counting of β-particles was carried out with two Borkowski-type 4π-proportional counters (122). An aluminum disk 0.010-inch thick with a 3/4-inch-diameter hole in the center covered with a thin film on which the source is mounted separates two identical halves of the counter. The resulting two chambers are connected in parallel to the same input of the amplifier so as to add their counting rates and register coincidences as single counts. They are thus able to detect practically every β-particle emitted by the sample in any direction. The loss of β-rays striking the 10-mil aluminum sample support is negligible if the radioactive sample is deposited in a small circle of approximately half the diameter of the sample plate aperture. Gamma rays emitted in coincidence with the

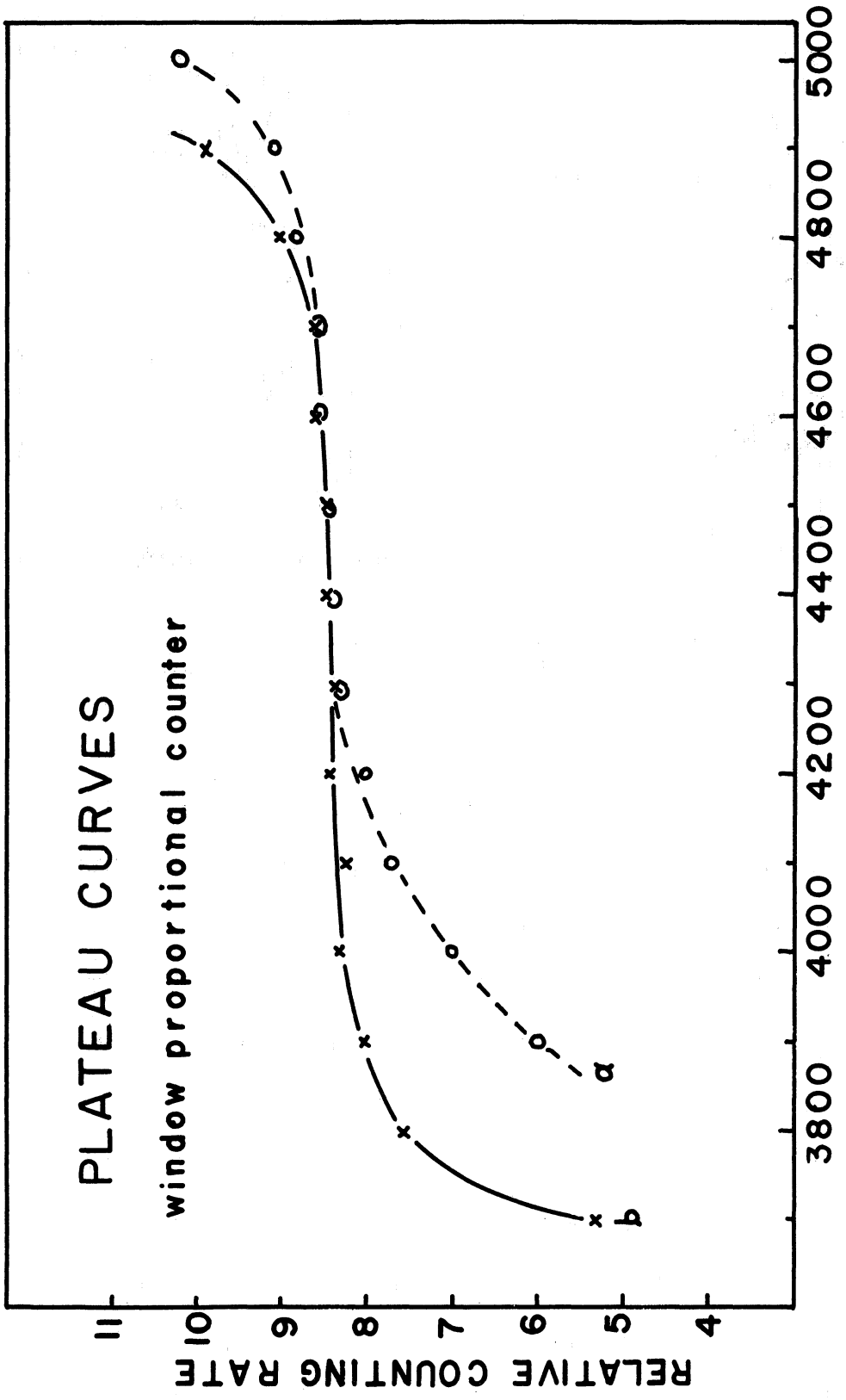

Fig. 24. Plateau Curve Obtained with Thin-Window Proportional Counter

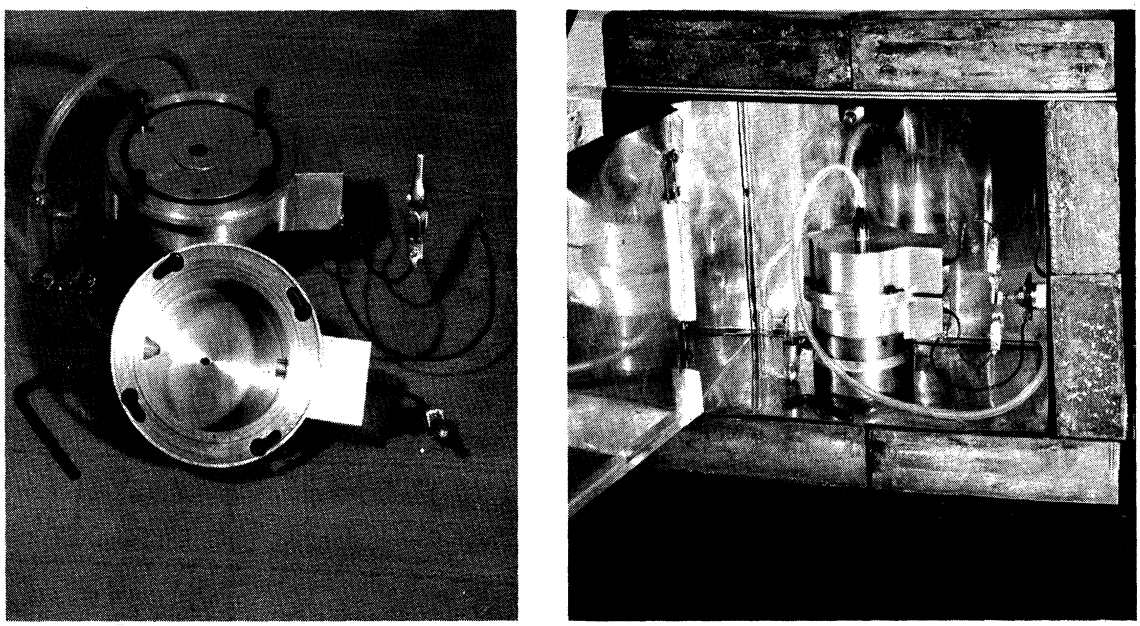

Fig. 25. 4π-Proportional Counter. Left: counter opened. Right: counter inside housing.

β-rays during the decay process will only increase the size of the β-ray pulse when interacting with the counter gas. The singularity of the pulse, indicating one disintegration will, however, be preserved. True 100% efficiency of the counter for detecting disintegrations by which β-rays are emitted is closely approximated in the case of relatively strong β-rays and if "weightless" samples are used. In the case of very weak β-rays self-absorption in the thin film sample mount has to be considered and the necessary corrections applied.

Fig. 25 shows two photographs of one of the 4π counters. The original design of the counters by Borkowski (122)

specified operation with a mixture of 90% argon and 10% methane at an anode potential of 1700 volts or methane counting gas at 2600 volts. For this purpose a 1-mil stainless-steel wire was used as anode and the counter evacuated and filled with gas for each count rate determination.

To make the counters more rugged and suitable for routine internal counting of many samples, the design was modified for this research. The counters operate now with 2-mil stainless steel wires at 4000 volts chamber potential. They are used as gas-flow counters using 99-mol-percent methane (Phillips Petroleum Company) as counting gas.

The design of the 4π counters is seen in Fig. 26. When operated with suitable amplifiers, plateaus of the type seen in Fig. 27 can be obtained with these counters.

The two units used were completely interchangeable so that exactly the same count rate was obtained when counting a sample of very long half-life in each of the two counters. This interchangeability together with the long plateaus obtained and the counting of long-lived secondary standards which had been compared with a P^{32} standard obtained by the National Bureau of Standards were the tests for proper operation of the counters and the basis for assuming absolute counting of β-particles in the counter.

Explanation of Fig. 26

1. Top chamber
2. Bottom chamber
3. Teflon insulators
4. Sample plate (10-mil aluminum disk with a central aperture of 3/4-inch diameter)
5. Seal insert
6. Brass nut
7. Hose connector
8. High voltage cable
9. Kovar seal
10. Cap screws, No. 10 - 24, Allen Head, 1/2 inch long
11. "O" ring 3/4 x 9/16, 3/32 cross section
12. "O" ring 3 1/4 x 3, 1/8 cross section
13. 0.002-inch stainless steel wire

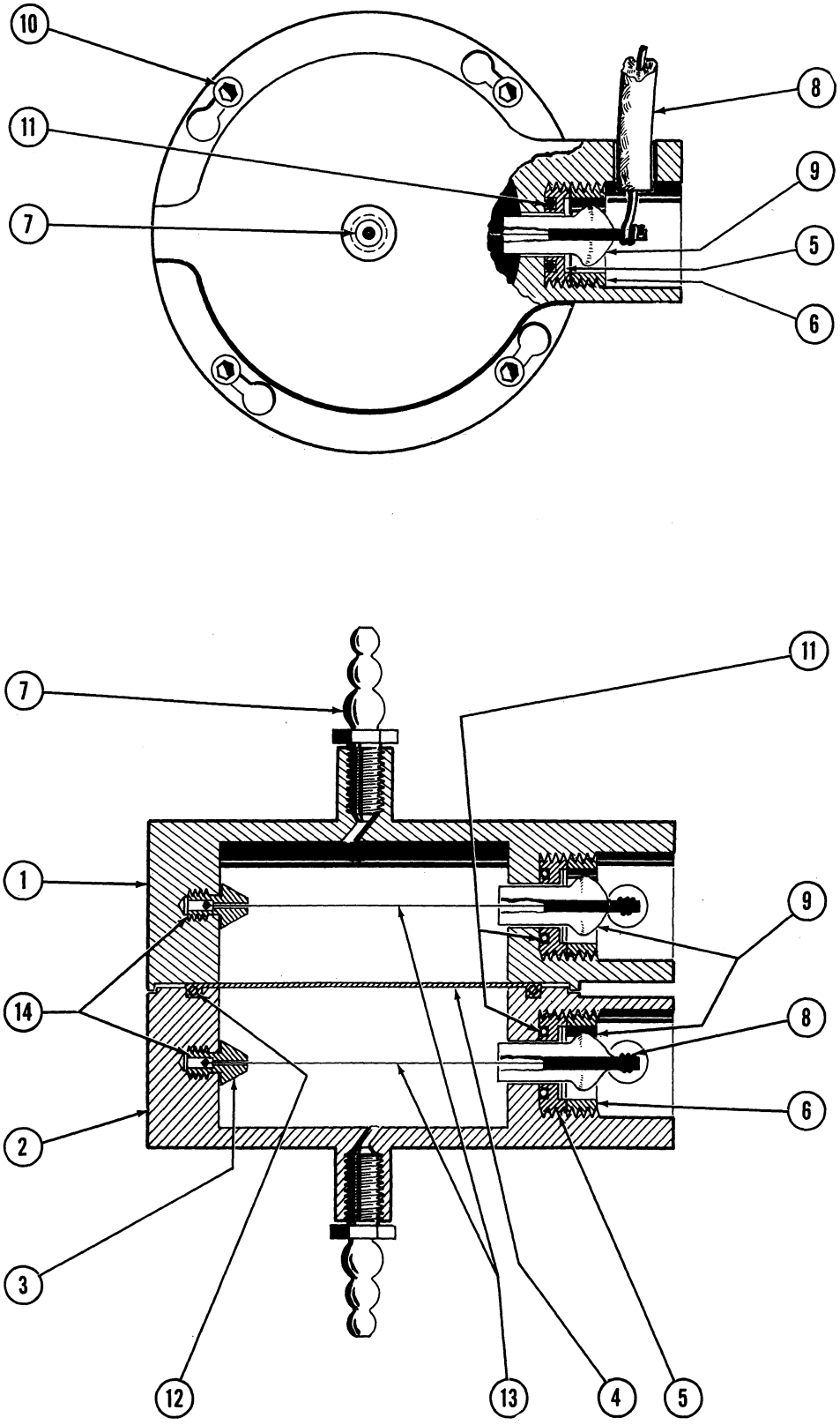

Fig. 26. Schematic Diagram of 4π-Proportional Counter

Explanation of Fig. 27

	Amplifier sensitivity	Correction to ordinate
×	1 millivolt	0
o	2 millivolt	+500
•	4 millivolt	+1000
▼	6 millivolt	+1500
◘	8 millivolt	+2000

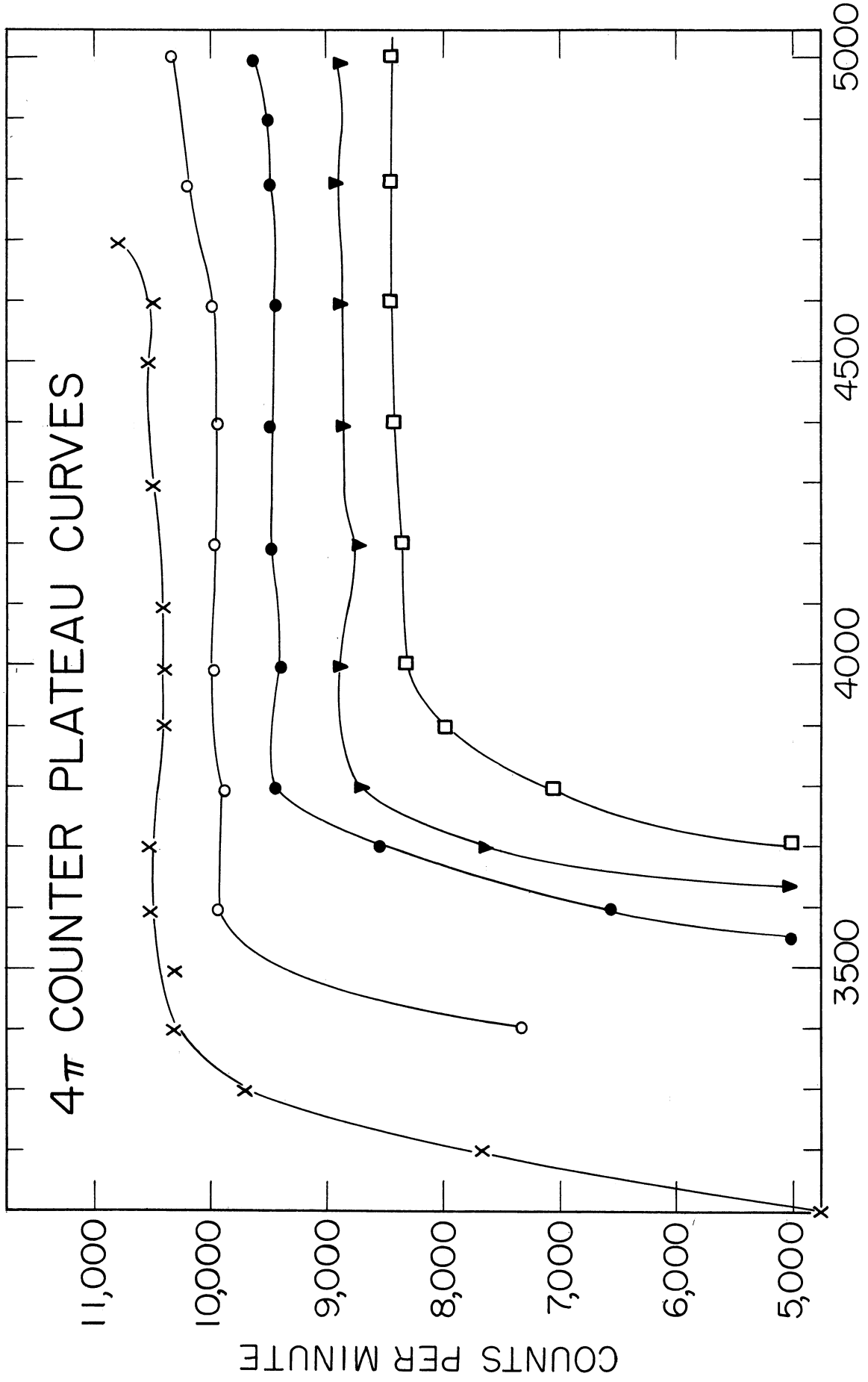

Fig. 27. 4π Counter Plateau Curves with Gold-Plated Sample

d. 4π-Counting Methods. Considerable time and effort was spent in the present research to develop optimum procedures for 4π counting. These ensured fool-proof and reliable routine operation of the counters over the long periods of time required for following the decay curves of the samples.

Thin Films Used as "Weightless" Source Mounts for 4π Counting. Absolute β-ray counting is only possible if the self absorption is negligible. When bulk-free sources are used it is important to mount them on "weightless" films or foils to make best use of the 4π counter. Various materials are being used for this purpose and are listed in Table IV together with their supplier, minimum thickness and method of preparation.

During the present research only Zapon films and VYNS films were used for 4π counting, the former for tracers, the latter for reaction products. The advantage of the Zapon is its relative resistance toward acids and bases but easy destructability by conc. H_2SO_4. The advantage of the VYNS is its complete inertness toward practically all inorganic chemicals, and its great strength and durability.

The method used for preparing the Zapon films is desribed in great detail by Hall (51). The method for preparing the VYNS films is given below. The latter is an adaptation of the method reported by Pate and Yaffe (95).

A pail is filled with water to the brim and the water surface cleaned by moving a metal bar across it. Two metal bars are placed parallel to each other close to one side of the pail. Approximately five drops of a 1/3-saturated solution of VYNS in cyclohexanone are then placed at equal distances between the two bars. The bar next to the open water surface is now moved lengthwise along the edge of the other bar to distribute the solution evenly in the channel between them. The bar is then momentarily lifted from the water and some of the solution permitted to spread across a part of the water surface. The bar is then lowered to touch the drying part of the moving film and pulled across the water surface drawing the film along at a desired rate. The rate of this motion determines the thickness of the film.

An even film area is selected by the color of reflected light and an aluminum frame slightly moistened with the film solution is placed on the film to cover this area (95). A woodsplint moistened with cyclohexanone serves as a knife to free the frame from the surrounding film. The excess film is removed and the frame with the film lifted from the water with a rolling motion.

Several layers of film can be built up in this way. Care must be taken that no water droplets and air bubbles are trappled between the layers as the frame is lowered onto a new film on the water.

Notes to Table IV

A. Casting drops on water as described by Brown, Felber, Richards and Saxon (15) and Hall (51).

B. Teflon-30 solution is painted on aluminum foil and baked at 350°. The aluminum is then dissolved away by dilute HCl.

C. Solution is pulled across clean water surface as reported in section the text.

D. Obtained from manufacturer.

Table IV. Thin Film Material Used for Sample Supports of β- and x-ray Emitters

Substance	Manufacturer	Thin Films Thickness	Method of Making Film	Reference	Solvent	Attacked by	Rigidity
Cellophane	Du Pont de Nemours	~1/4 mil	D			strong acids	medium
Formvar E (poly vinyl acetal)	Shawingingan Products Co.	2-3 gr/cm^2	A	113, 21	ethylene dichloride	acids and bases	strong
Collodion	Merck Co.	6 gr/cm^2	A	113, 21	alcohol amyl acetate	acids	medium-weak
Nylon No. 6501	Du Pont de Nemours	10 gr/cm^2	A	113, 21	butyl alcohol (not iso butyl alc.)		medium
Zapon	Atlas Powder Company	2-5 gr/cm^2	A	113, 21, 51	amyl acetate	strong acids in time hot conc. H_2SO_4	weak
Teflon-30	Du Pont de Nemours	0.1 mil	B	98	colloidal suspension	inert	medium
Teflon	Du Pont de Nemours	1/4 mil	D			inert	strong
Mylar	Du Pont de Nemours	1/4 mil	D		hot conc. H_2SO_4 + 30% H_2O_2 (Fuming HNO_3)		strong
VYNS (poly chloride acetate co-polymer	American Bakelite Company	2-5 g/cm^2	C	95, this research	cyclo hexanone	inert even to conc. H_2SO_4 + 30% H_2O_2	strong-medium
Aluminum oxide		300 m gr/cm^2		119			strong
Saran wrap	Dow Chem. Company	1/4 mil	D				

4π-Sample Preparation. Aluminum source disks with two layers of film giving a brown-yellow coloration in reflected light were used for 4π counting. The sources were deposited on the film by means of a micropipet. Several drops placed individually in the center of the film area could be deposited simultaneously to permit faster evaporation. Sufficient distance between the drops and the aluminum frame was kept to minimize the number of β-rays striking the aluminum.

The samples were dried with a warm air blower and heat lamp. The dry samples were covered with one layer of film prepared by the same method as described above but using a larger frame. Frosting the sample surface onto which the film was to be placed helped the film to stick better.

Similar one-layer films were prepared and gold plated. One of them was deposited on top and one on the bottom of each sample so that the gold layers formed the conducting outside surface. A "Q-tip" saturated with cyclohexanone served to remove excess film and ensured electrical contact between gold layer and aluminum disk.

Gold plating of the 4π-sample films was carried out either in the high vacuum evaporator mentioned above or a specially built gold evaporator described below. The mounted films were placed onto the frame of the evaporator and gold evaporated from the filament. The progress of

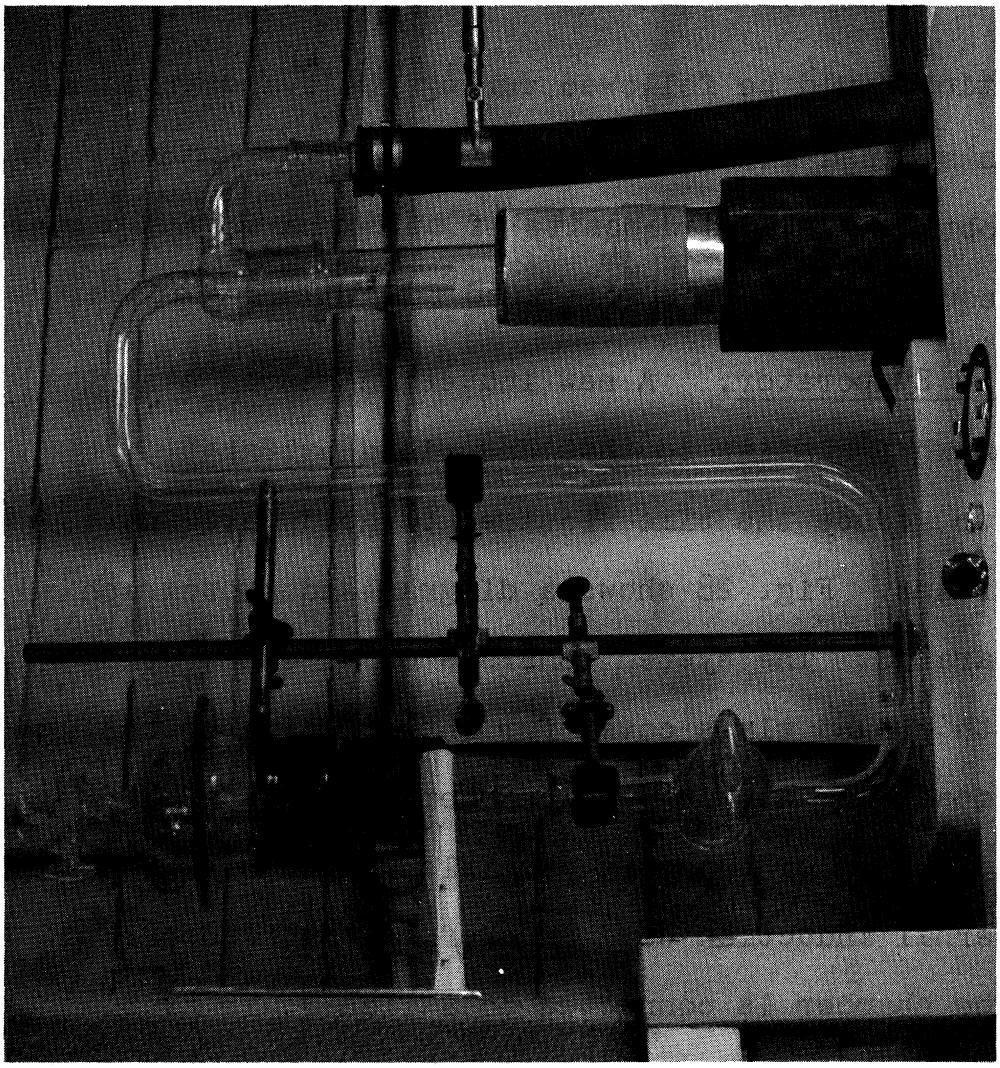

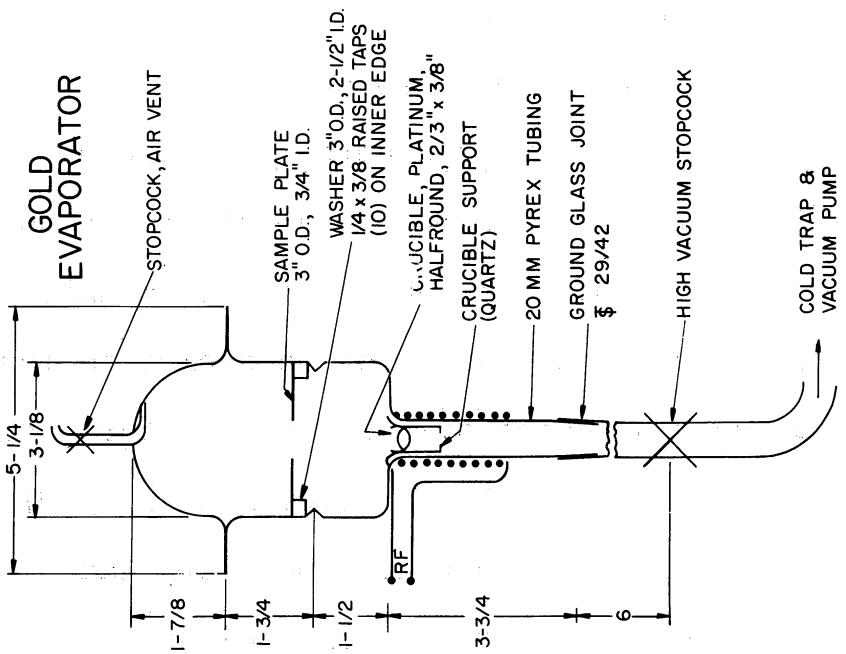

Fig. 28. Schematic Diagram and Photograph of Gold Evaporator

the deposition could be followed during the evaporation and the process stopped when a desired shade of blue transmitted light was obtained. Gold deposits of approximately 20 micrograms per square centimeter were used for the 4π samples.

Gold Evaporator. A new induction heated evaporator somewhat similar to that described by Pate* was built to reduce the time required to goldplate the 4π sample films. Fig. 28 shows a diagram and photograph of the apparatus. The system consists of an evaporation chamber with ground glass cover for introduction of the sample frames. The neck of the chamber receives a hemispherical platinum or tungsten crucible, which can be heated by the external induction coil made of 1/4-inch copper tubing. The chamber is connected to a liquid air trap. A Welch Duo-Seal High vacuum pump is able to pump the whole system down to 0.1 micron in two minutes. By using an all glass system no leak problems were encountered.

Need of Conductive Source Mounts. At the beginning of the investigations there was considerable uncertainty as to the need of a conductive source-mount.

Results from a number of laboratories seemed to indicate that much depends upon the size of the aperture across which the film bearing the sample is stretched (52, 59, 96, 122). Sample plates originally used in this laboratory had openings of 1/2-inch diameter, for which some experiments

---

* Pate, B. D., Disintegration Rate Determination by 4π Counting. Mc Gill University Ph. D. thesis, April 1955.

seemed to indicate that absolute counts could be obtained without conductive coating.

At sufficiently high anode potentials these samples would discharge, however. Sporadic discharge and scattering of data were observed occasionally even at plateau voltages. The effects seemed especially pronounced for weak beta- and x-ray emitters (48).

To investigate these phenomena a sample of Y^{88} (a long-lived emitter of x-rays and weak positrons) was prepared by depositing the isotope in carrier-free form on a non-conducting layer of Zapon film and covering it with a film of the same material. A sample plate with 1/2-inch aperture was used for this experiment. The sample was introduced into the counting chamber and the dependence of count rate vs. anode potential investigated. A plateau with a definite maximum was obtained and an abrupt uncontrolled rise in counting rate occurred at a relatively low applied potential.

To investigate this further, one-minute counts were taken in succession at 100-volt intervals indicating a maximum in the plateau region. When the same counts were taken without interruption and before the breakdown potential had been reached on the previous curve, a curve with a maximum was again obtained, but the count rates were consistently far below the corresponding ones of the first curve. A third curve taken without interruption again lay below the previous one and thus successive curves. A certain

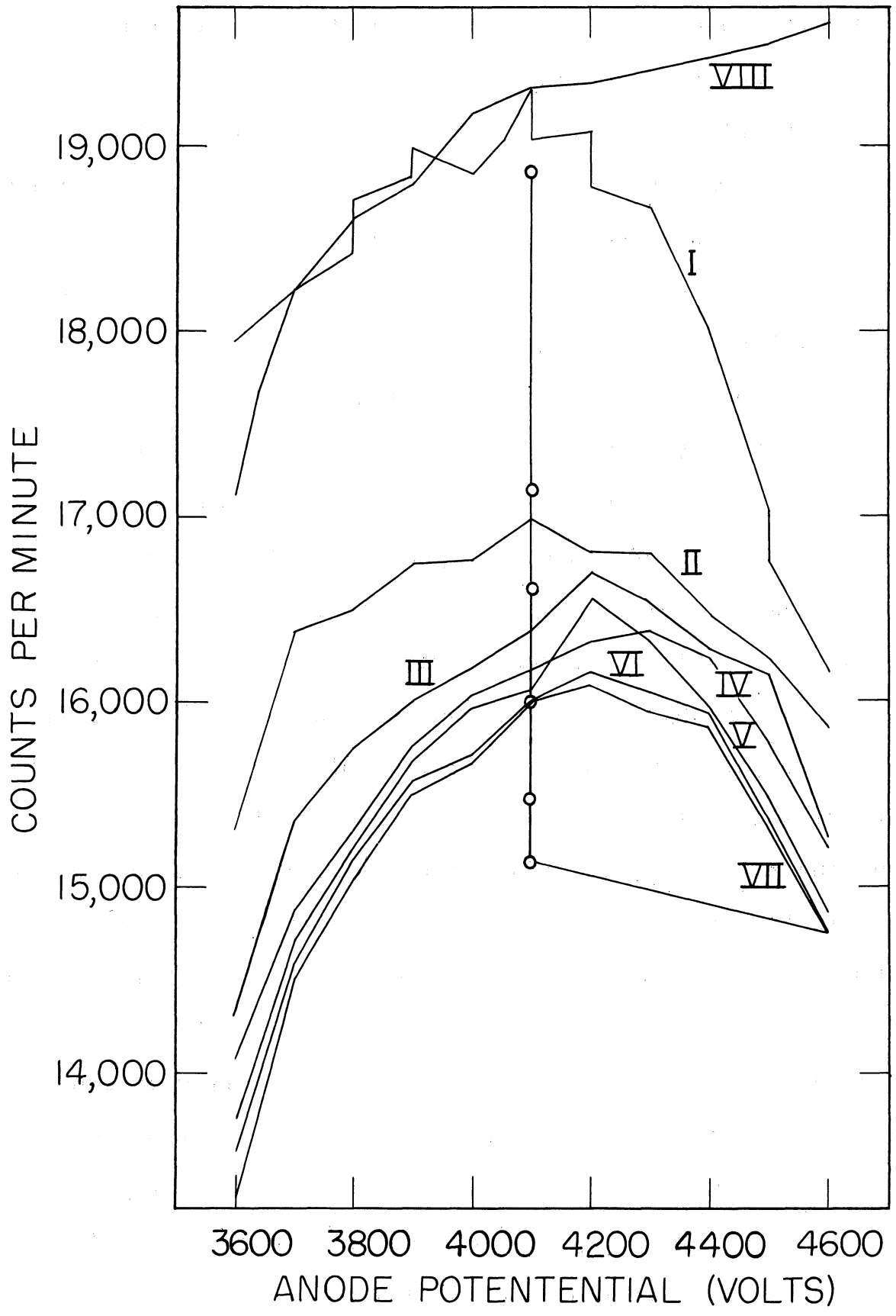

Fig. 29. 4π-Counter Plateau Curves with Non-Gold Plated Sample

limiting curve seemed to be approached after several curves were taken. This can be seen from Fig. 29. Interruption of the successive counts, when the anode potential was at the upper end of the range resulted in a much lower following curve, while hesitation at a lower voltage resulted in a higher plateau curve. When the voltage was turned off for several hours the original curve could be reproduced.

This time and voltage dependent hysteresis effect can be explained in the following way. Charge is building up on the sample by drifting positive ions striking the non-conductive film (122). The effective potential between source and anode is thus decreased below the edge of the plateau and the count rate decreased. As this effect is dependent on the rate of production of positive ions in the proportional counter which again depends on the size of the avalanche, a maximum in the plateau curve is to be expected.

Another phenomenon was traced to the same cause. When the voltage on the counter reached the breakdown potential, a discharge started, then accelerated until the scaler jammed. Reduction of the high voltage several hundred volts below the "breakdown" potential would not terminate the discharge. When the high voltage was turned off completely after a discharge and then turned on again, discharge started at a much lower potential than the first time. Longer waiting after the voltage was turned off raised the breakdown potential.

The same sample was next gold plated on one side without improving the above characteristics. When the other side was also gold plated, however, a reproducible plateau as seen in curve VIII, Fig. 29 was obtained. No maximum was observed in this plateau and no discharge occurred up to 5000 volts. (The relatively large slope of this curve is due to double triggering of an overloading amplifier and has since been rectified).

The result of this investigation proved the necessity of conducting source mounts for 4π samples. All samples used for the cross section experiments reported in the experimental part were goldplated and no scattering of data or sporadic discharges was experienced with them. As a result of these findings 3/4-inch-aperture sample mounts were used facilitating the sample preparation for the bombardment runs.

Amplifier. The amplifier is the most sensitive part of a proportional counter set-up. It must distinguish pulses from the proportional chamber varying in size by a factor of 2000 or more and introduce no spurious counts. Its dead time must be small and the amplifier responsive even at very high counting rates.

It took considerable effort to find the best amplifier scaler combination for the two 4π counters. The final choice fell on the Nuclear-Chicago Ultrascaler Model 192X which incorporates in one unit an excellent amplifier with

good overload characteristics, a very stable 5000-volt power supply, and a fast and dependable scaling unit. Several other features included in this unit made routine counting less tedious.

Difficulties were, however, experienced even with these amplifiers. It took several months to bring the two units to operate properly. Part of the difficulties may be ascribed to the higher humidity and temperature in the counting room during the summer months, part to tube failures and maladjustments of certain components. When replacing all 6AK5 tubes in both units with the more dependable type 5654, considerable improvement in reliability could be achieved. It was found advisable, however, to check the tubes of the amplifier every two months and make the necessary replacements.

It took the author considerable time and effort to set up the proper procedure for 4π counting and learn the remedies for the shortcomings enumerated in Table V. After this experience was gained, however, no more serious delays were encountered due to failure of the 4π-counting equipment which is now considered among the most dependable apparatus of the laboratory.

Table V. Difficulties Encountered with the Operation of a 4π Proportional Counter

Abnormal Indications	Probable Cause	Remedy Suggested
Maximum in the plateau curve and discharge of the counter	Sample is mounted on non-conducting film	Gold plating
Maximum in the plateau curve of a sample counting above 100,000 c/m	Dead time dependance on pulse size causes this	Count at the low end of the plateau, or better: make another, less active sample
Scatter of counts much above statistical variation; high background	Dirt or dust in the counting chamber	Brush out with soft brush
	Noise in the amplifier	Check tubes for microphonics
Short and sloping plateau	Amplifier is double-triggering for the larger pulses	Check and replace tubes
Counting rate increases for consecutive counts while settings remain the same	Some air is still in the counting chamber	Bubble at the rate of 3 / sec for about 30 minutes after introduction of the sample

Table V (continued)

Abnormal Indications	Probable Cause	Remedy Suggested
Scaler counts while high voltage is off	Noise in amplifier	Check tubes for microphonics
No high voltage	trouble in high voltage supply	Check tubes
Sample breaks after several weeks	An acid solution was deposited on Zapon film when making sample	Use gold plated VYNS film to cover both sides of broken sample and check thickness for self- absorption correction
	very high flushing rate used	

2. X-ray Proportional Counting.

In the course of these investigations various isotopes were studied which decayed by the electron-capture process. It was attempted to identify the radiations by their characteristic energies, as well as to count absolutely the x-rays emitted by a given sample (10, 39, 104, 105).

An x-ray proportional counter was built for this purpose and various electronic equipment was constructed or acquired to operate the counter in conjunction with a pulse spectrometer.

a. X-ray Proportional Counter: The operation of an x-ray proportional counter is very similar to the β-ray proportional counter described in section III-C-1 (26, 40). Some significant differences, however, shall be pointed out at this time.

Interaction of X-rays with the Counter Gas. X-rays do not cause primary ionization but produce in the gas of the counter ionizing particles by either of the following three processes:

1. Photoelectric Effect: The x-ray entering the counter collides with a gas atom and ejects an electron from one of the outer electron shells of the atom. This photo-electron having a kinetic energy practically equal to the energy of the x-ray now acts like the primary

particle starting the counting process described before. The counter pulse, proportional to the amount of primary ionization in the counter gas, will be proportional to the energy of the x-ray.

2. Compton Effect: The x-ray entering the counter collides with a gas atom and transfers its energy to the atom which uses the energy for the ejection of an orbital electron. This Compton electron will behave as in the case above. The rest of the energy of the original x-ray will be emitted as a so called scattered quantum. This quantum behaving similarly to the original x-ray may collide with another gas atom and repeat the Compton process or eject a photoelectron.

In the two cases mentioned so far the entire energy of the original x-ray is eventually transferred into ionization of the counter gas and a pulse proportional to the original x-ray energy produced. Pulses of this energy will fall in the so called "Photopeak" of the x-ray spectrum.

3. Photo-Effect with Escape-X-ray from Counter Gas: The third process by which primary electrons can be produced in the counter gas is primarily important for x-rays having a greater energy than the binding energy of the K-electrons of the counter gas. Such x-rays may transfer their energy to the tightly bound K-electrons of the counter gas atom on collision. The ejected photo-

electron will have a kinetic energy corresponding to the energy of the initial x-ray minus the binding energy of the K-electron. The ionization it will produce in the counter will be proportional to this energy difference and the counter pulse smaller than that produced by the other two processes mentioned above. As the position of the ejected K-electron is filled again a new x-ray characteristic to the counter gas will be emitted. This very penetrating x-ray may not react any further with other gas atoms and escape from the sensitive volume of the counter. The pulses created by this process will fall in the so called "escape-peak" of the x-ray spectrum corresponding to an energy equal to the energy difference between the initial x-ray and the characteristic x-ray of the counter gas.

Design Considerations: X-rays are more penetrating than β-particles. An x-ray proportional counter thus must

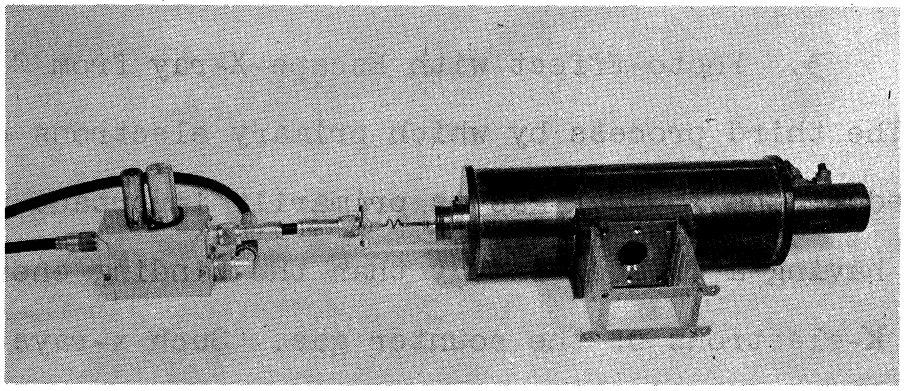

Fig. 30. X-ray Counter with Preamplifier

have a greater sensitive volume and contain more counting gas than a β-ray counter. The former can be realized by building a bigger counter, the latter by putting the counter gas under pressure. The use of a heavier counting gas will also increase the efficiency of the counter.

Construction Details. The design of the x-ray proportional counter built for this research is given in Fig. 31.

In the Fall of 1954 the original design obtained from the Brookhaven National Laboratories was modified so as to simplify the machining and soldering and the counter built by the Physics Shop of the University of Michigan. A photograph of the counter is seen in Fig. 30.

The counter was initially operated with a 90% argon, 10% methane mixture filling and connected to a commercially available scaler. Plateau curves obtained for different x-ray emitters by means of this combination are shown in Fig. 32.

The counter was tested for leaks with a filling of three atmospheres argon-methane mixture, by submerging the entire counter in water. While all solder joints were found tight the 0.010-inch beryllium window obtained from the Brush Beryllium Company of Cleveland, Ohio, was found to contain pinholes through which gas escaped. This had been suspected since the thresholds of the counter when operated with the scaler had dropped considerably during the previous weeks.

Explanation of Fig. 31

I. 4-inch brass tubing

II. 1 1/4-inch Kovar tubing

III. Beryllium window made leak-tight by spraying ~27 mg Glyptal lacquer on 2-inch Beryllium disk, 0.01 inch thick. Window cemented to surface with Apiezon W wax

IV. Stainless-steel plate to hold window in place

V. Rubber O-ring used for gasket

VI. UG 560/u H-V connector

VII. 3/32-inch Kovar tubing

VIII. This space machined to fit plastic counting shelves

IX. Edges rounded off with ball of hard solder

X. Glass to Kovar seals

XI. 0.004-inch stainless steel wire

XII. 0.04-inch Ni tubing spot connected to counting wire

XIII. Clean soft solder joints. Caution: avoid flux getting into counting chamber

XIV. Mill surface after all soldering is done

XV. Base soft-soldered to tube.

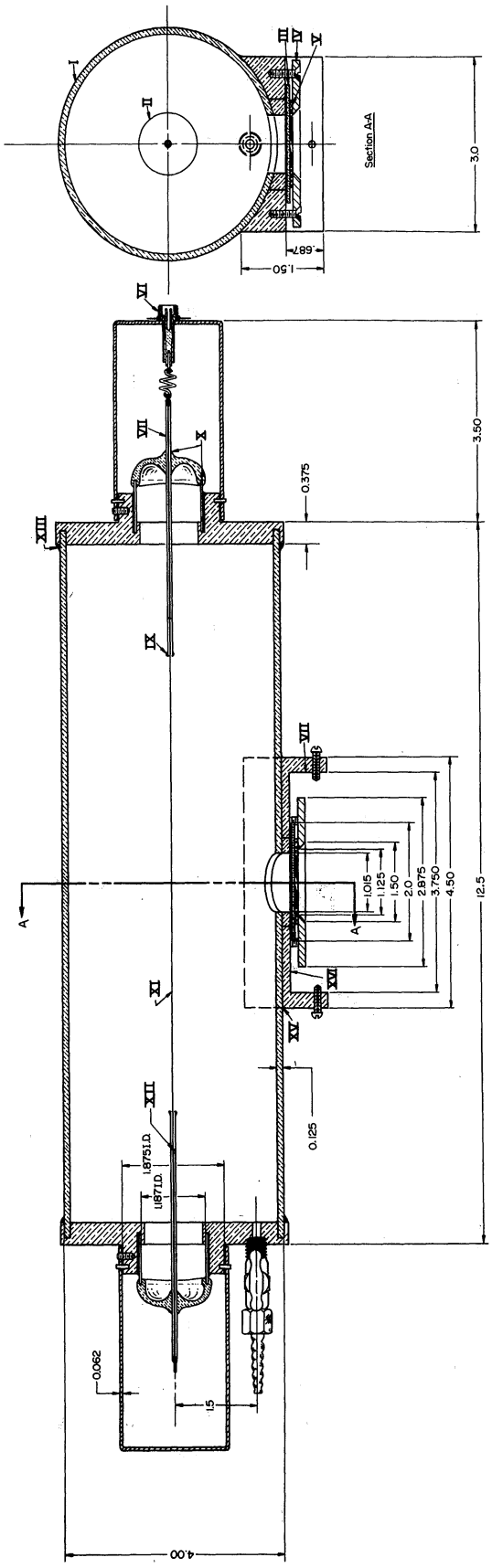

Fig. 31 Schematic Diagram of X-ray Proportional Counter

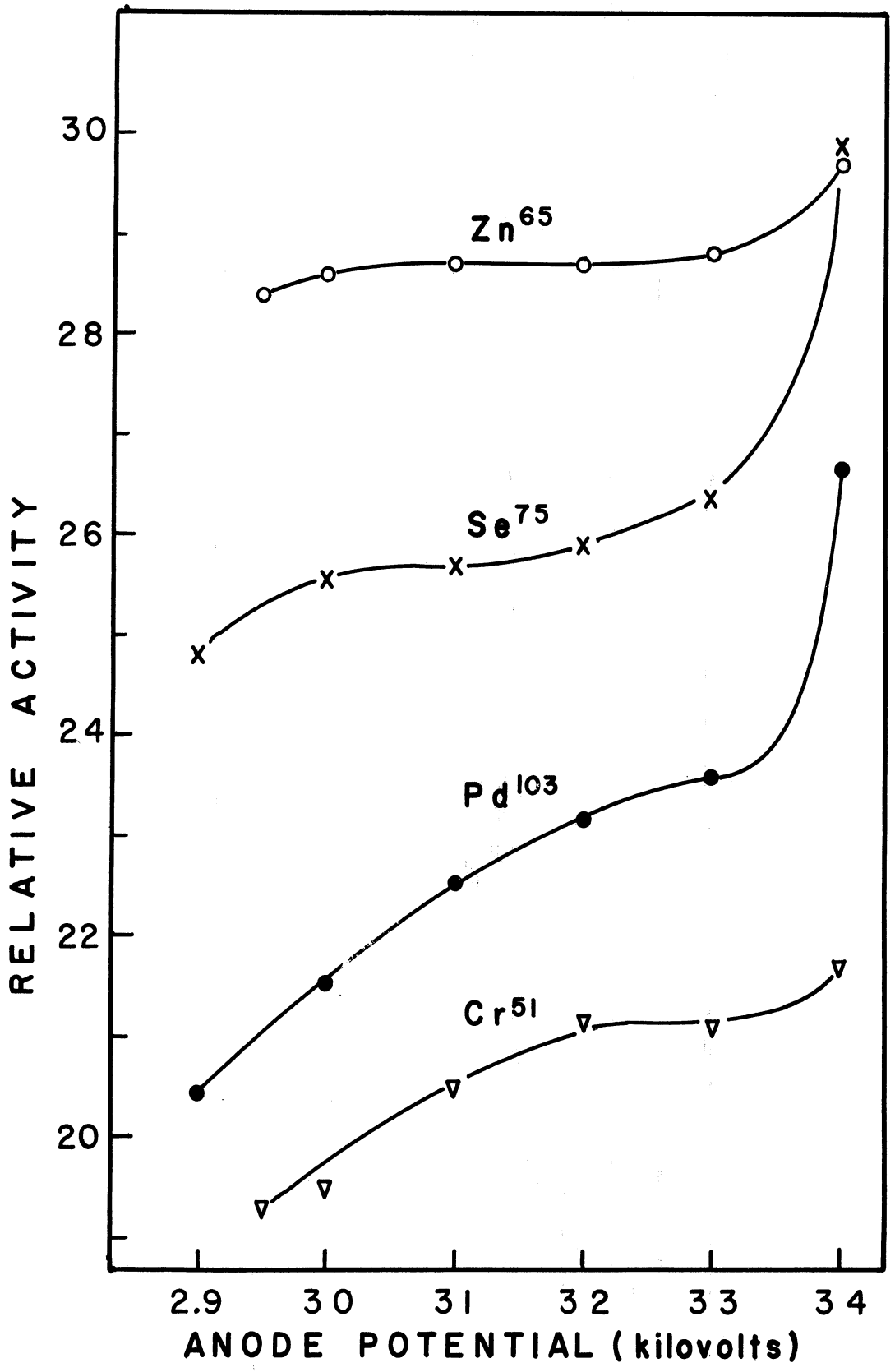

Fig. 32. Plateau Curves Obtained with Argon - Methane Filled X-ray Counter

To seal the pinholes of the beryllium window a solution of red Glyptal lacquer in acetone was sprayed onto the disk in several layers. Intermediate drying was effected with the use of a 1500-watt heat lamp. The gain of weight of the window disk due to the lacquer was found to be 1.35 mg/cm^2.

After replacement of the window, the counter was again tested for leaks. After several hours immersion no bubbles were observed either on the window or at any other point of the counter. Another test period of one month showed no change in threshold potential. The counter was then considered leak tight and ready for its permanent filling.

The linear absorption coefficients for various x-ray energies were calculated from the available literature data (Fig. 33). It was estimated that for a 4-inch diameter counter practically 100% counting efficiency could be obtained for x-rays below 25 kv, if a 2-atmosphere krypton filling was used.

A mercury pump and manometer assembly was then constructed according to the diagram of Fig. 34 and the counter filled with 151.15 mm Hg krypton and 15.2 mm Hg of 99% pure methane (Phillips Petroleum Company). Extreme care was taken not to contaminate the counter during the filling operation.

Tests of the 2-atmosphere krypton-filled x-ray counter proved inconclusive since the plateaus as obtained

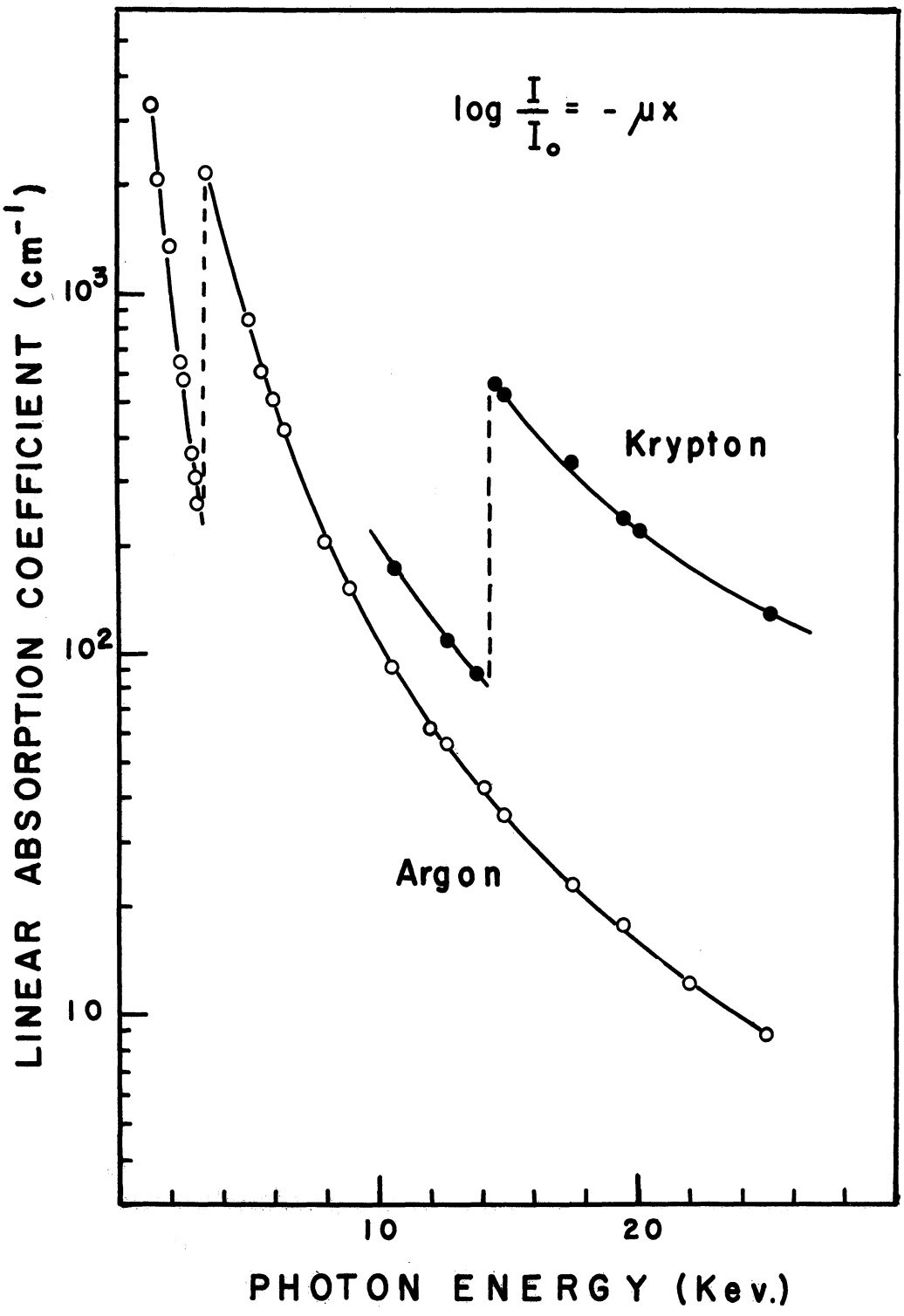

Fig. 33. Linear Absorption Coefficients for X-rays in Argon and Krypton under Atmospheric Pressure

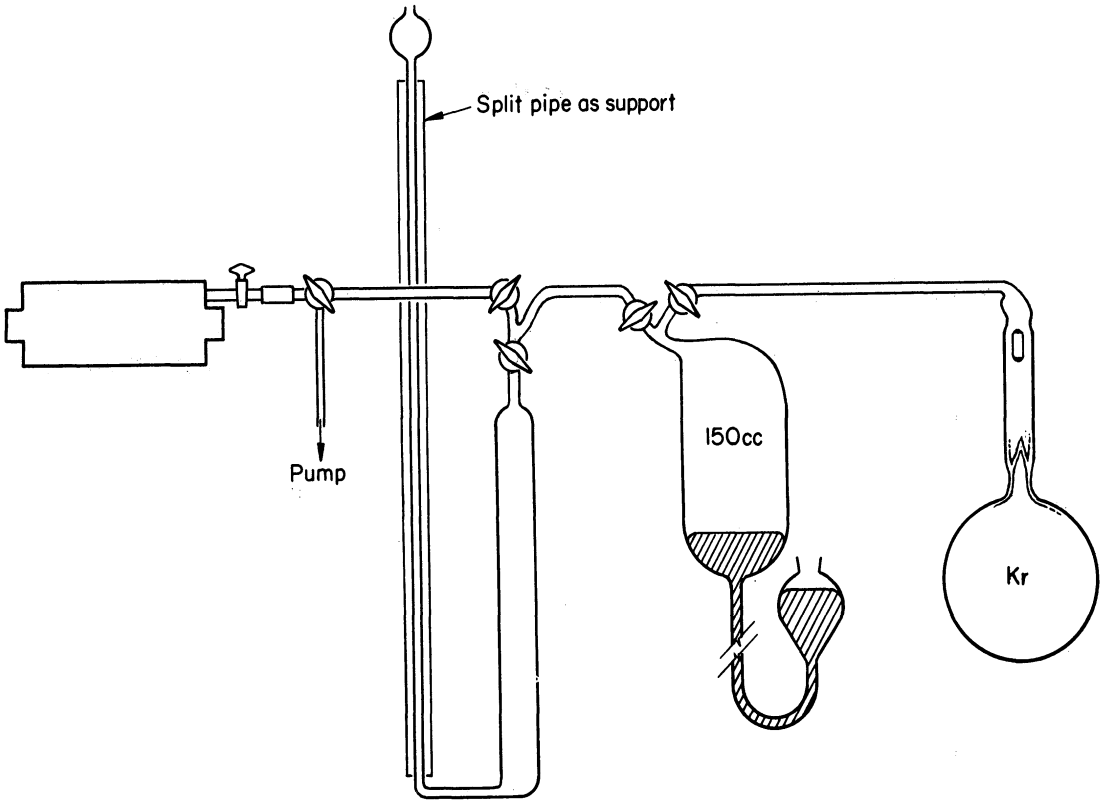

Fig. 34. Diagram of mercury pump and manometer for filling the x-ray proportional counter with 2 atmospheres of krypton.

with the commercial scaler seemed to lie above 4900 volts.

b. Electronics. Special electronic equipment to operate the x-ray counter and make best use of its potentialities was thus required. Particular emphasis had to be placed on the linearity and the overloading characteristics of the amplifiers.

The preamplifier was designed with the assistance of Prof. Hough of the Physics Department and built according

to the circuit diagram of Fig. 35. Fig. 30 gives a picture of the preamplifier connected to the x-ray counter. The preamplifier operates as a simple cathode follower of gain 1 with a large overload safety factor. The unit has shown very dependable performance for more than a year.

The purchase of a suitable non-overloading amplifier for the x-ray counter proved difficult. It was first intended to build a double delay-line amplifier according to the design of Francis and Bell (38). The construction of

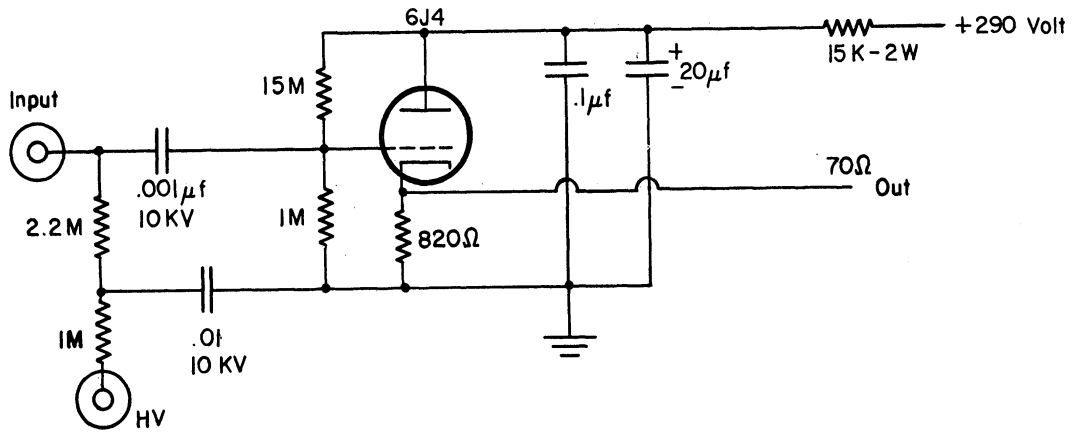

Fig. 35. Circuit Diagram of Preamplifier for X-ray Counter

this circuit was contracted to the Beva Laboratory of Trenton, New Jersey, in early Spring of 1955. When insurmountable difficulties appeared in obtaining the unit in August 1955 a commercially available non-overloading amplifier was purchased. The design of this unit followed

the layout of Chase and Higinbotham (20). The amplifier together with a highly regulated 5000-volt power supply was obtained from the Radiation Instrument Company of Silver Spring, Maryland, and put into operation at the end of 1955.

The amplifier as now available has a maximum gain of 40,000. The stability is excellent and the overload characteristics sufficient for obtaining good x-ray spectra with 14% half-width resolution for Sr K-x-rays. The linearity of the amplifier seems very good and distinction between the x-rays from Y^{88} and Nb^{92} is easily obtained (Fig. 55).

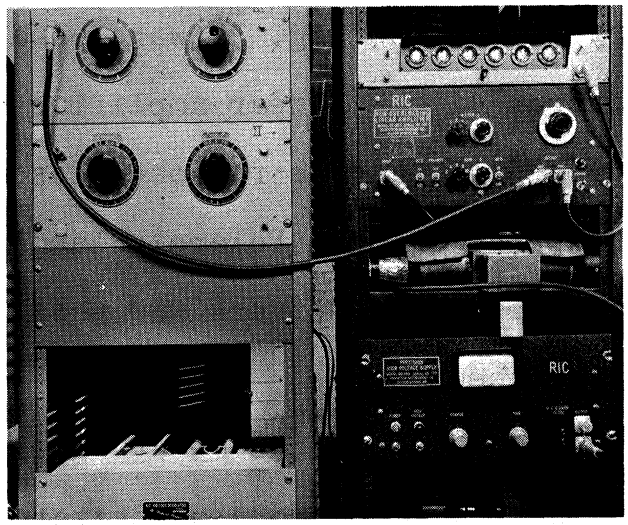

Fig. 36. X-ray Spectrometer Setup

One important feature of the RIC 107P non-overloading linear amplifier is a pulse-height selector permitting the introduction of a certain trigger bias. Pulses higher than this bias level are recognized and a square pulse

produced for direct counting in a scaler. The circuit of this pulse height selector was changed slightly to operate with the auxiliary equipment available. After these adjustments were made trouble-free operation was realized.

c. Performance.

X-ray Spectra. The x-ray spectra shown in Fig. 37 were obtained with the above equipment. The output pulse of the amplifier was analyzed by a single-channel pulse-height analyzer (Atomic Instrument Company No. 510, seen in Fig. 36) and recorded with a Leeds and Northrup Speedomax recorder. Spectra of the type shown in Fig. 38 were obtained by displaying the output of the linear amplifier on the screen of a Tektronix-type 514D cathode-ray oscilloscope and photographing the pulses with a Polaroid Land camera. Identification of the x-ray emitters was possible by either of the two procedures.

X-ray Counting. When the decay rate of an x-ray emitter was to be determined, a more quantitative method had to be found for counting the x-ray pulses. It was originally planned to scan the spectra by recording counts manually or semi-automatically with a step-sweep mechanism and to integrate the counts under the peaks at the desired energy. This was found to be an extremely laborious undertaking, especially for samples of low activity. Bad

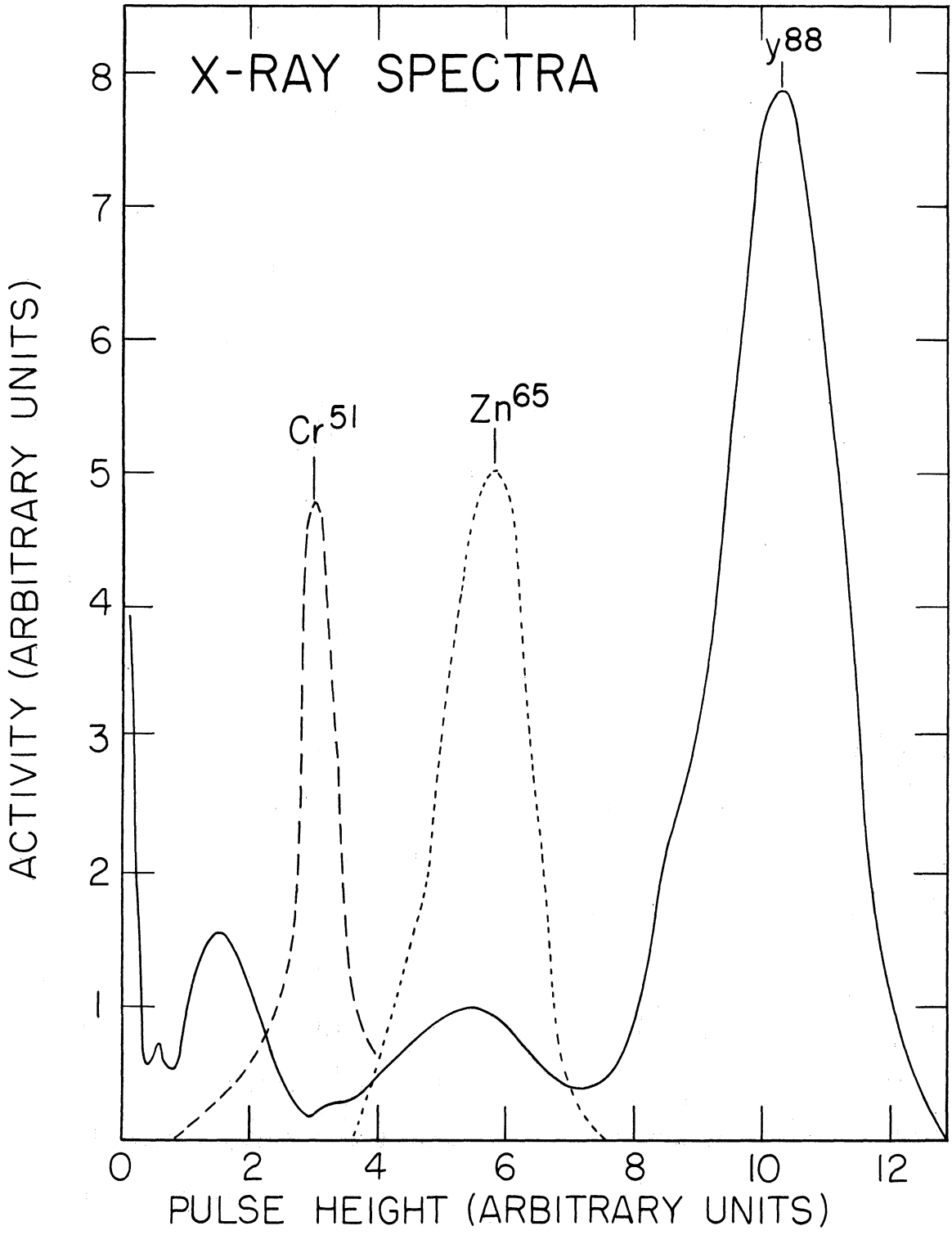

Fig. 37. Spectra of x-rays emitted by Cr^{51}, Zn^{65} and Y^{88} as obtained with the krypton filled x-ray counter.

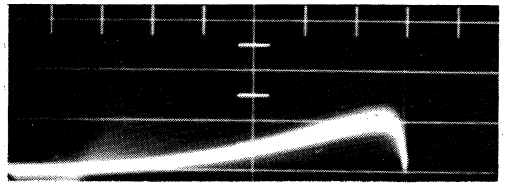

Mn^{54}

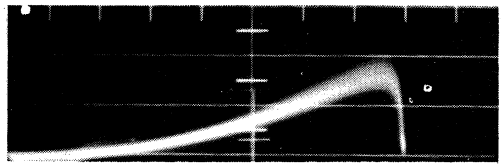

Zn^{65}

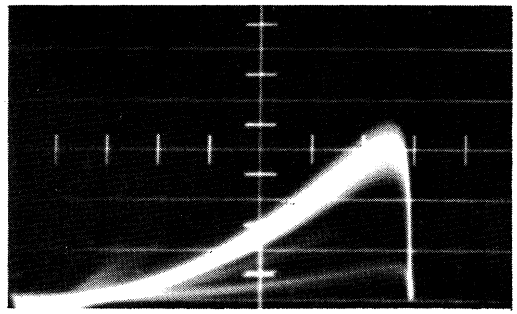

Y^{88}

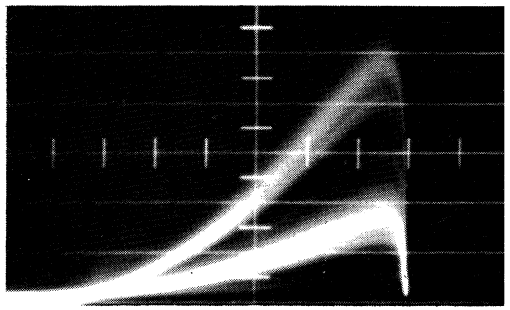

Cd^{109}

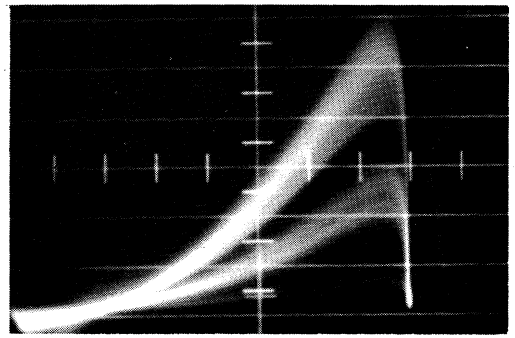

Sn^{113}

Fig. 38. Spectra of x-rays emitted by Mn^{54}, Zn^{65}, Y^{88}, Cd^{109} and Sn^{113}. Same settings were used to take spectra with krypton-filled x-ray counter

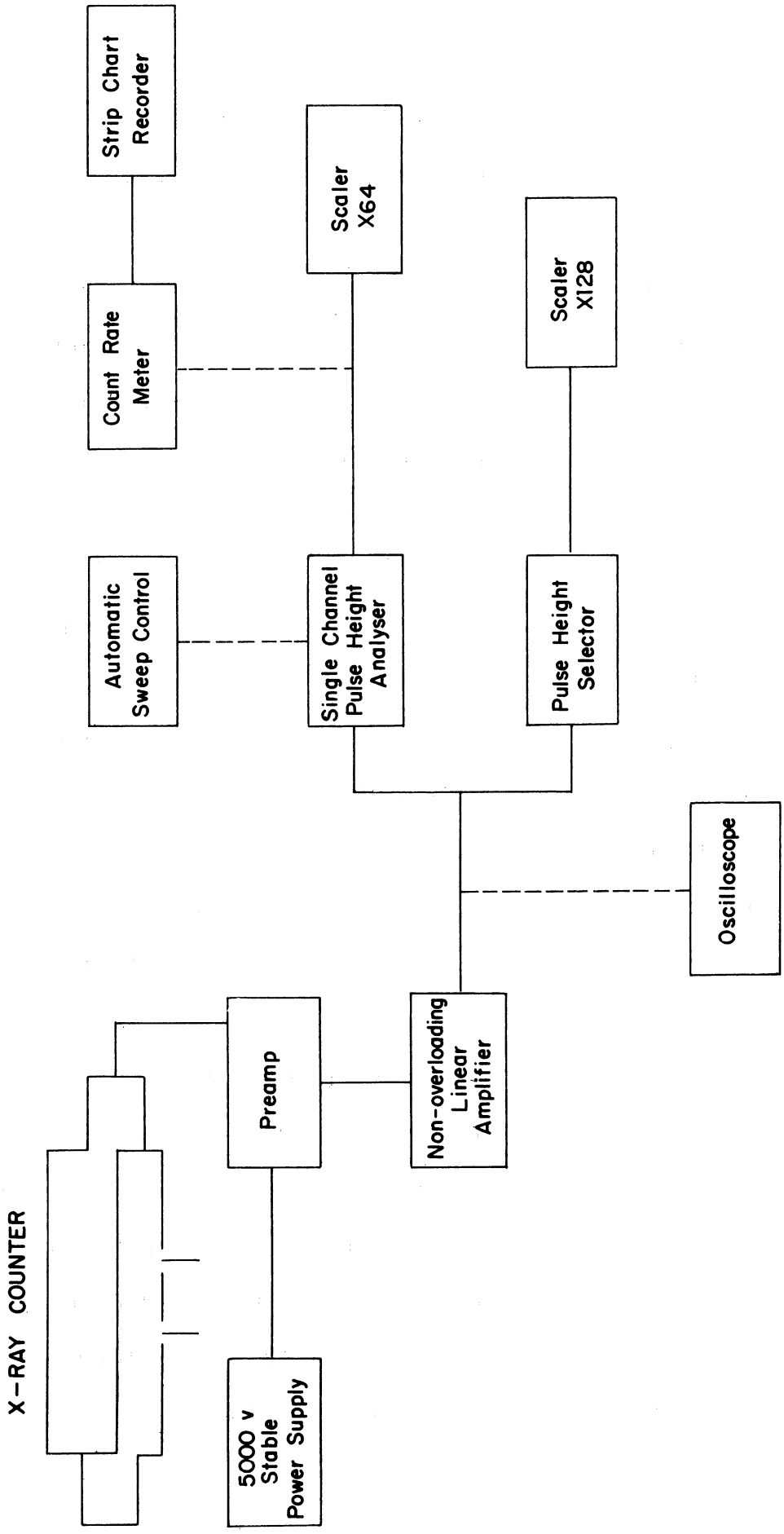

Fig. 39. Schematic Diagram of the X-ray Counting Setup

statistics caused by the small number of counts and small drifts in the equipment over the long time intervals necessary to count low levels of activity, limited this method.

To overcome these difficulties, a procedure was evolved whereby that part of the x-ray spectrum falling on the desired peak could be obtained in a single measurement. The peak was first located by a rapid sweep of the spectrum. By judicious setting of the pulse-height-analyzer base line on the high energy edge of the peak and the pulse-height selector on the low energy edge, it was possible to obtain two simultaneous counts, the difference of which gave the counting rate of the peak. A background count, with the same setting but without the sample, is also required since the background for a typical x-ray peak counted by the above method, is of the order of 300 counts per minute. This represented approximately 25% of the total background of the large counter. A schematic diagram of the x-ray counting setup is seen in Fig. 39.

When care is taken to keep the counting geometry constant, the counting rates obtained with this procedure are reproducible to within the statistical limits (cf. Fig. 48). Slight drifts in the equipment will introduce errors only in the valley regions of the spectrum, but these errors are generally much below the statistical error of the counts.

3. Gamma-ray Scintillation Counting

Gamma-ray counting served in this research for the identification of tracers and bombardment products. Relative count rates of tracers were determined and calibration of the x-ray counter carried out with γ-ray scintillation counters. Extensive work was performed with the scintillation spectrometer to verify certain decay schemes and follow the decay of γ-ray emitters.

a. Principle of Operation: Gamma-rays are a very penetrating type of radiation. Dense materials have to be employed for their detection and characterization. In addition to gas-counters, operating as proportional or Geiger counters (109) filled with krypton or xenon, most γ-ray counting today uses the scintillation process. Solid scintillators containing preferably a high atomic weight constituent are employed. The principle of interaction between the scintillator material and the γ-rays follows in its initial steps closely the types outlined in section III-C-2 for the x-ray counter. The essential difference is, however, that the energy of the ejected electrons or delta rays is not used to produce an avalanche, but is converted into fluorescent light which can be "seen" by a photomultiplier tube. The electric pulse from the photomultiplier is proportional to the intensity of the light radiation which in turn is proportional to the amount of energy spent by the γ ray inside the

scintillator. The probability of part of the γ-ray energy escaping after previous Compton scattering is great for small scintillators and hard γ rays. The spectra will thus contain a photopeak and a broad, more or less continuous plateau due to the Compton effect, cf. Fig. 54. This Compton plateau is separated from the photopeak by a valley representing the difference in energy between the total energy of the γ-ray and the minimum energy of the photon scattered backward by the Compton effect (110).

b. Design Considerations. Scintillation probes, including scintillation crystal, photomultiplier tube and preamplifier are now commercially available. Fig. 40 is a diagram of the generally used construction. The thallium-activated sodium-iodide crystal used as scintillator has to have one highly polished side which can be optically coupled with the face of the photomultiplier. The other sides reflect the light and concentrate it onto the polished side as diffused illumination. For obtaining the experience of packaging a large rather hygroscopic sodium-iodide crystal a scintillation probe was constructed during this research.

c. Construction. The cylindrical sodium-iodide crystal had a dimension of 1 1/2-inch diameter and 1-inch height. It was polished and packed by the following procedure:

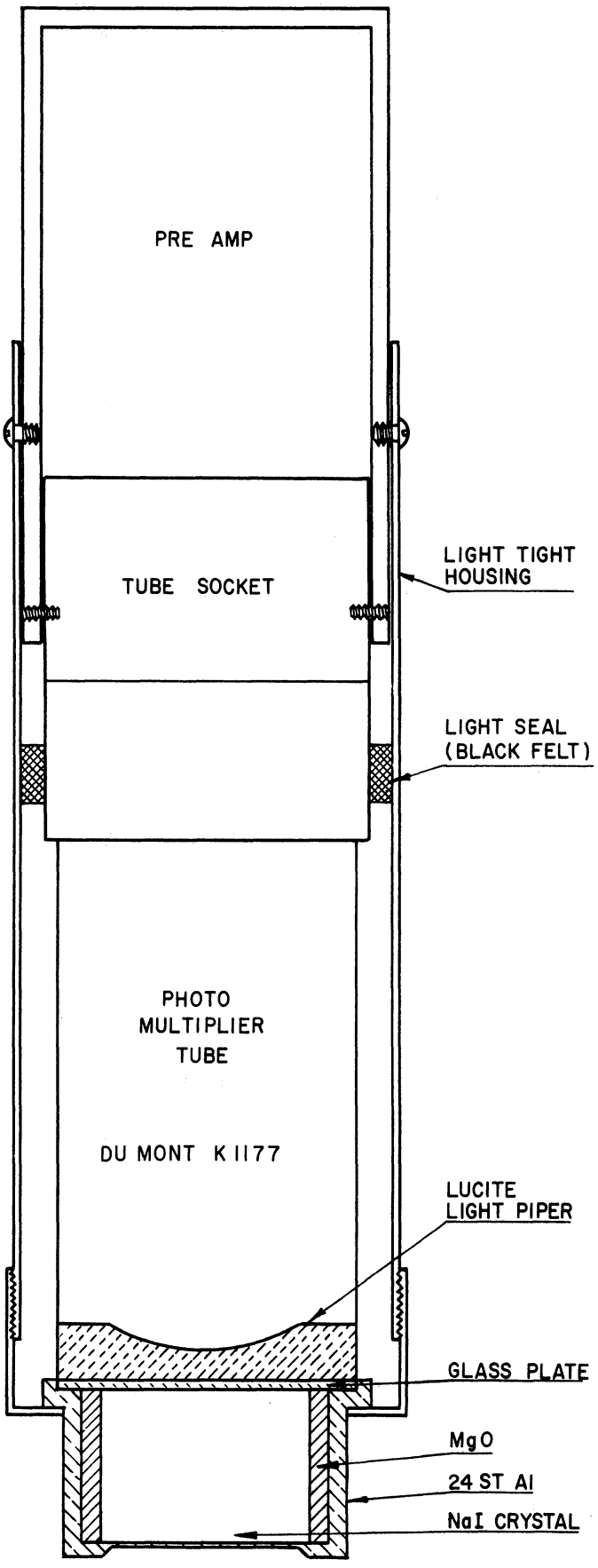

Fig. 40. Schematic Diagram of Scintillation Counter

A polished aluminum can, having a 0.005-inch-thick bottom was introduced in a drybox together with the crystal and other equipment. The crystal was freed of its saw-marks and roughened on all but one side with emery paper. This was followed by a rinse in xylene to remove grit and excess sodium iodide. The optical side was then polished with cloth saturated with n-butanol until an even highly polished surface was obtained. The crystal was again rinsed in xylene and mineral oil and finally wiped dry with lens paper.

The polished crystal was then mounted in the aluminum cup containing a thin layer of dry magnesium oxide as reflectant. More magnesium oxide was filled along the sides of the crystal and firmly packed into place. The surface of the crystal was cleared of magnesium oxide with a hair-brush and a drop of Dow-Corning Fluid 200 placed on its optical side. A 1/16-inch-thick soft glass window was then placed on top of the packed crystal making optical contact with its polished side and cemented in place with bonding agent type R-313. *

The packaged crystal could now be optically coupled with a Dumont 6292 photomultiplier tube by means of a Lucite "lightpiper" and Dow Corning 200 fluid. The light-piper was constructed from a cylindrical piece of Lucite whose one side was contoured to fit exactly the face of the photomultiplier.

---

* Carl A. Briggs Co., 11616 West Peko Boulevard, Los Angeles 64, California.

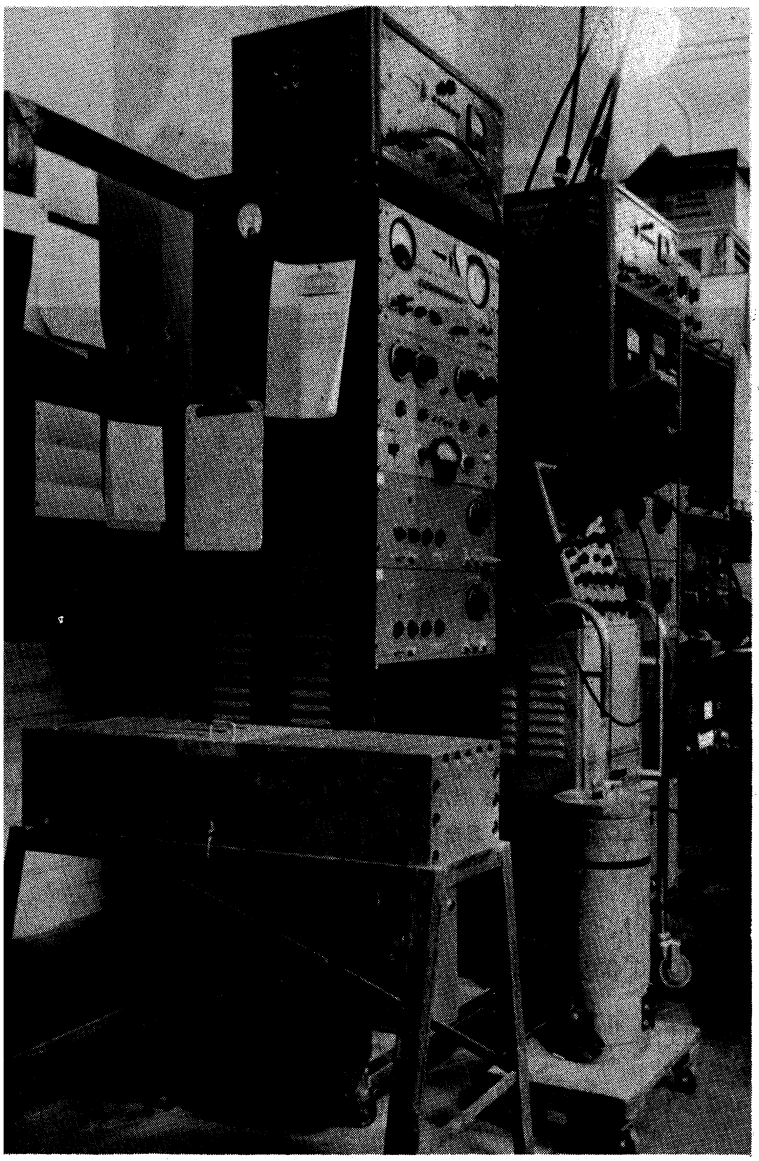

Fig. 41. Spectrometer Equipment

The photomultiplier with mounted crystal was introduced in a light-tight housing containing a

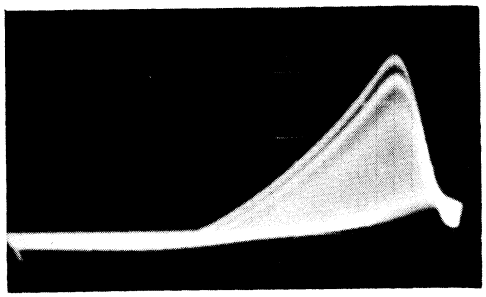

Co^{60}

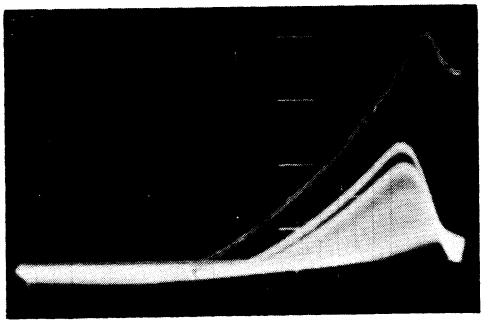

Nb^{92}

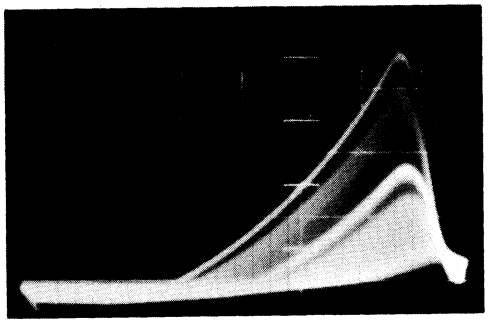

Y^{88}

Fig. 42. Gamma-ray spectra of Co^{60}, Y^{88} and Nb^{92} taken at the same time with the same amplifier and oscilloscope settings (cf. Fig. 51)

magnetic shield for the photomultiplier as well as a pre-amplifier. This "probe" was placed in a 2-inch-thick lead shield and used as a gamma counter (Fig. 41 foreground).

d. Gamma Counter Performance: Several additional γ-ray counters of the same design as described above were employed during this research giving generally very good performance and requiring a minimum of maintenance. Various spectra were taken with these counters in conjunction with the pulse spectrometer (Fig. 41) as can be seen from Figs. 42, 47 and 48. Whenever unknown γ spectra were investigated

a known standard was counted immediatly before or after the unknown to serve for the energy calibration.

D. Absolute Counting Methods

To determine absolute cross sections the total number of nuclei produced during the bombardment has to be known. This number can be calculated, if the bombardment product, or a known fraction of it, is counted "absolutely", i.e., if for every disintegration occurring in the counting sample a count is registered or otherwise indicated.

1. 4π Counting

From the earlier discussion of the 4π counters in section III-C-1 it was seen that absolute β-ray counting is achieved, if the self-absorption of the source is negligible. To realize this, only bulk-free sources were counted in the 4π chambers. It was thus possible to register all disintegrations by which a β particle of relatively high energy is emitted.

a. Self-absorption. No corrections for self-absorption were deemed necessary during these investigations for the counting of Y^{92}, Y^{90}, Nb^{90}, Sc^{44}, Sc^{47}, Sc^{48} and P^{32}. Self-absorption corrections were applied, however, for Sc^{46}, P^{33} and Nb^{95}. The corrections necessary for Sc^{46} were determined by Hall (55) for films of the type used in this research.

The self-absorption correction for the P^{33} radiation was approximated with the 0.23-Mev β-rays of Pm^{147}. The procedure was the following. The count rate of the Pm^{147} source of the thin-film gauge was measured for a certain setting of the Geiger-Müller tube (the window collimator was removed). A copper absorber was placed over the source and the P^{33} sample placed on top of the copper plate. The count rate of the P^{33} sample was then established with no interference of β rays from Pm^{147}. The copper absorber was now removed and the Pm^{147} plus P^{33} count rate determined. The difference represented the count rate due to Pm^{147} alone. From this and the count rate of the Pm^{147} source without absorber, the fraction absorbed by the P^{33} sample was established.

It was assumed that half of this fraction would have been absorbed by half the thickness of the sample, which was the average absorber facing a P^{33} β ray emerging from the sample. This fraction was then applied as the self-absorption correction for the P^{33} radiation, since the energies of the Pm^{147} and P^{33} betas are almost identical.

The self-absorption correction for Nb^{95} was established by approximation. The fraction of Pm^{147} β rays absorbed by the sample was determined as described above and the aluminum absorber thickness equivalent to the Nb^{95} sample determined. The fraction of the range of the 0.16-Mev β rays of Nb^{95} represented by this thickness was calculated.

Applying a Feather analyzer (36) the fraction of Nb^{95} β rays absorbed by this thickness of aluminum was computed. Half of this fraction was then applied as the self-absorption correction for the Nb^{95} sample.

The error inherent in the corrected absolute counting rate of the Nb^{95} samples is estimated to be ~2%, while the error introduced by the self-absorption correction in the case of P^{33} is less.

b. Background and Dead Time Corrections.

The customary corrections for dead time and background were applied for all counts. The first affected very high counting rates, the latter mainly the low counting rates.

It was attempted to prepare samples of sufficiently high counting rates during most of their decay, so that the daily variation of the background would have little or no influence on the precision, even if it had been neglected. With backgrounds of the order of 90 c/m and a variation of 10 c/m, it was attempted to count samples with activities greater than 1000 c/m. This was found to be of particular importance, since it was observed that dust would collect in the inside of the counting chambers while remodeling of the Chemistry Building was in progress and effected rises in the background rate by approximately 10% during the period of several days. The advantage of higher counting rates as far as statistics and counting time are concerned is apparent.

Practically all counts taken during these investigations with the β-ray counters had a standard error of less than 1% uncertainty. When the decay had progressed to count rates much below 1000 c/m careful background determinations were made before and after a sample was counted in order to preserve the precision.

As a rule of thumb it was found that a background count of the same length as the sample count would result in an absolute uncertainty smaller than that in the sample count, so that the statistical error in the background could be disregarded.

It might be of interest to note in this connection that for all counters employed in this research the background increased by a factor of about 40% on August 31, 1956, a few days after the explosion of a Russian hydrogen bomb over Siberia.

2. Absolute X-ray Counting.

In the course of the investigation of the $Zr^{90}(d, \alpha)Y^{88}$ reaction it became necessary to measure the disintegration rate of the Y^{88} product, an isotope decaying primarily by electron capture. This required the calibration of the x-ray counter or, in other words, a determination of the efficiency of the x-ray counter for Sr x-rays.

a. Calculation of the X-ray Counter Efficiency. To get an approximate idea of the geometrical efficiency, the

counter design was sketched on paper and the angle subtended by the counter window with its origin in the plane of the source drawn in. An average angle of 85° appeared a good first approximation. The surface of a sphere of radius 1 is 4π. The surface of the segment of that sphere subtended by a rotated angle of 85° is

$$S = 2\pi \cdot 1 \cdot (1 - \cos \frac{85}{2}) = 0.526\pi.$$

The fraction of the total surface subtended by the angle is thus 0.526/4 or 0.131 i.e. the superficial geometrical efficiency is 13.1%. It was estimated from the drawing that the average length of the trajectory of the x-rays in the gas is approximately 2.6 inch corresponding to an ~80% gas efficiency. From the beryllium absorption curve shown in Fig. 43 it was seen that Sr K-x-rays from Y^{88} are 97% transmitted by the 10-mil window making the efficiency for Y^{88} K-x-rays approximately

$$0.131 \cdot 0.80 \cdot 0.97 = 0.101 \text{ or } 10.1\%.$$

In some experiments only the K-x-ray photopeak of the Y^{88} was counted. The percentage of all counts that are found in the photopeak was determined to be approximately 94%. This resulted in the calculated efficiency of the counter for the photopeak of Sr K-x-rays of approximately 9.4%.

b. Measurement of Absolute Disintegration Rates by Means of the Coincidence Method. Attempts were made to determine the efficiency of the x-ray counter

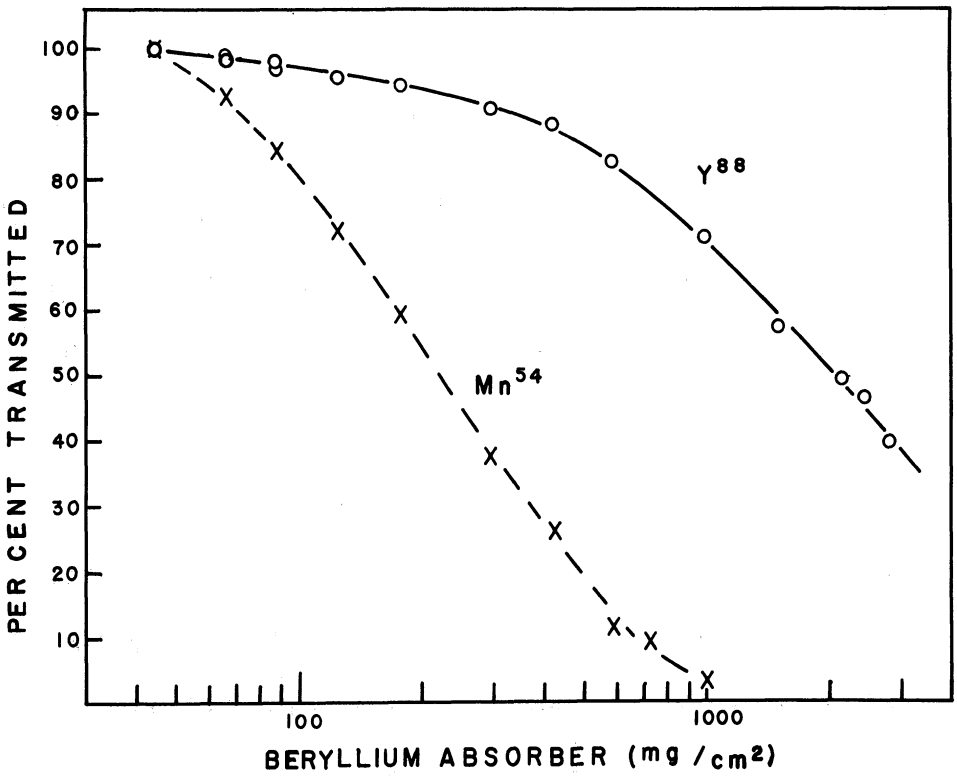

Fig. 43. Beryllium absorption curves for x-rays emitted by Y^{88} and Mn^{54}.

experimentally. For this purpose the absolute disintegration rate of a Y^{88} sample was determined by coincidence measurements.

Coincidence Method. The absolute disintegration rate of an isotope emitting two or more radiations in coincidence can be established, by counting the radiations simultaneously in two counters and measuring the coincidence rate of the pulses from these counters (112, 115). It is not necessary in this case to know the geometry and efficiencies of the two counters as the following considerations show:

If the efficiency of the first counter, counting only one type of radiation, is m for a sample in a given

position, then the absolute disintegration rate of the source is:

$$D = m\,A$$

where A is the count rate recorded in the counter. If n is the efficiency of the other counter, counting the other type radiation, then the absolute disintegration rate of the source is

$$D = n\,B$$

B being the count rate recorded in the second counter. The probability that a disintegration recorded by counter (a) is simultaneously detected in counter (b) is also n. The coincidence rate is thus $C = A/n$ or from this

$$D = \frac{D \cdot D}{D} = \frac{mA \cdot nB}{mnC} = \frac{A \cdot B}{C}$$

It is thus only necessary to establish the count rates in each of the two counters and the coincidence rate between them, to arrive at the desired absolute disintegration rate of the sample.

Absolute Disintegration Rate Determination for an Y^{88} Sample. In the case of Y^{88} there are three different γ-rays emitted in coincidence with the x-ray during an electron capture process (Fig. 44). The branching ratio between the two possible de-excitation paths was measured and found in agreement with the literature (97) to be of the order of 1%. For the purpose of the following

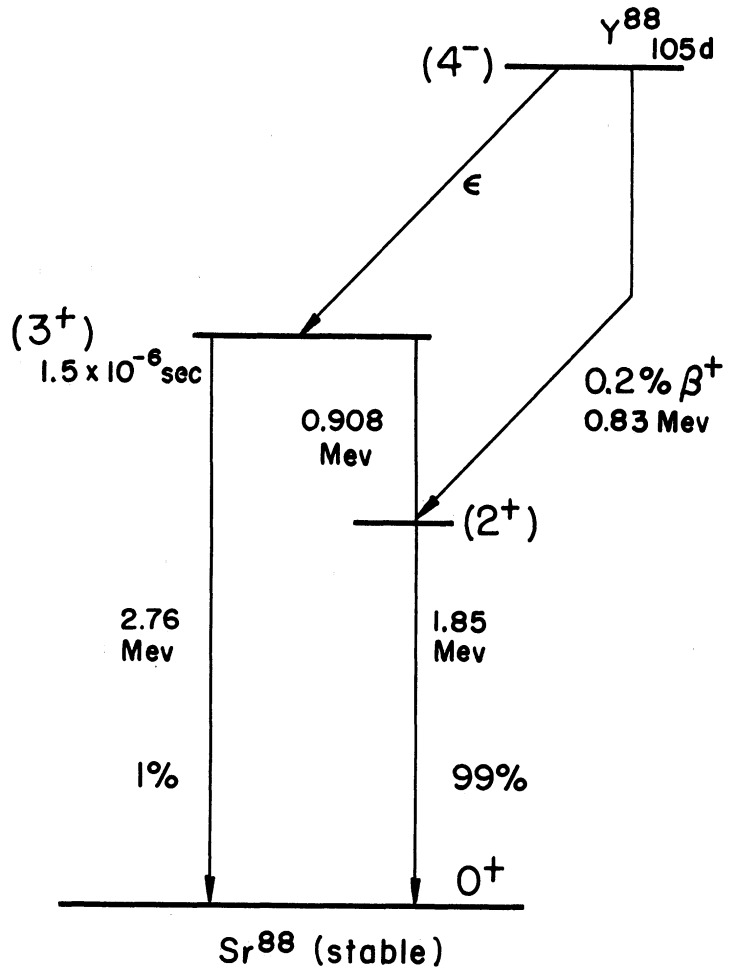

Fig. 44. Decay Scheme of Y^{88}

considerations it was assumed that this ratio was negligible and practically all transitions followed the path of the γ-ray cascade.

To determine the absolute disintegration rate of the Y^{88} sample, coincidence measurements were carried out between the x-rays and the 0.9-Mev γ rays, the x-rays and the 1.83-Mev γ rays, and between the 0.9-Mev and 1.83-Mev

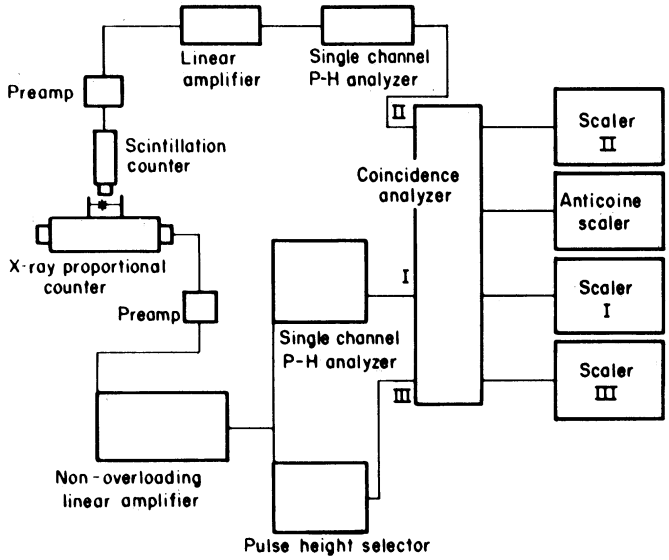

Fig. 45. Block diagram of x-ray–γ coincidence counter

γ rays. The block diagram of Fig. 45 indicates the circuit used for the x-ray–γ coincidence measurements.

Channel 1 recorded the γ-ray pulses produced by the γ rays of the desired energy in the scintillation counter. The channel width and base line of the pulse height analyzer was set for this purpose to include the entire photopeak, but exclude γ rays of different energy.

Channel 2 recorded all pulses produced in the x-ray counter whose heights were greater than the lower edge of the x-ray photopeak.

Channel 3 counted all pulses from the x-ray counter whose heights exceeded the photopeak x-ray pulses.

The true count of the x-rays in the photopeak was

obtained as the difference in the count rates recorded by channel 2 and 3.

Coincidences between channel 1 and 2 might be due to a coincidence between an x-ray and a γ ray of desired energy. In this case the coincidence should be considered. It might also be due to the coincidence of an x-ray with a high energy γ ray which interacted with the scintillation crystal by a Compton type interaction producing a pulse of the same energy as the photopeak of the desired γ rays. Since the γ rays in the case under discussion are in cascade, this effect does not disturb the result of the measurement. The coincidence count might, however, be due to the coincidence between a γ ray of desired energy and a γ ray of the other energy detected by the x-ray counter. Such pulses interfere with the measurement and should not be considered. To avoid counting these coincidences channel 3 was coupled in anti-coincidence with channels 1 and 2 so that γ-ray pulses produced in the x-ray counter and triggering channels 2 and 3 simultaneously would not be considered in the coincidence rate.

Corrections were applied to all observed rates for background and random coincidences. The latter correction was determined experimentally by using the same circuitry, but counting two different sources simultaneously in the two counters. The counters were separated by about 3 ft and several lead bricks were placed between them for these determinations.

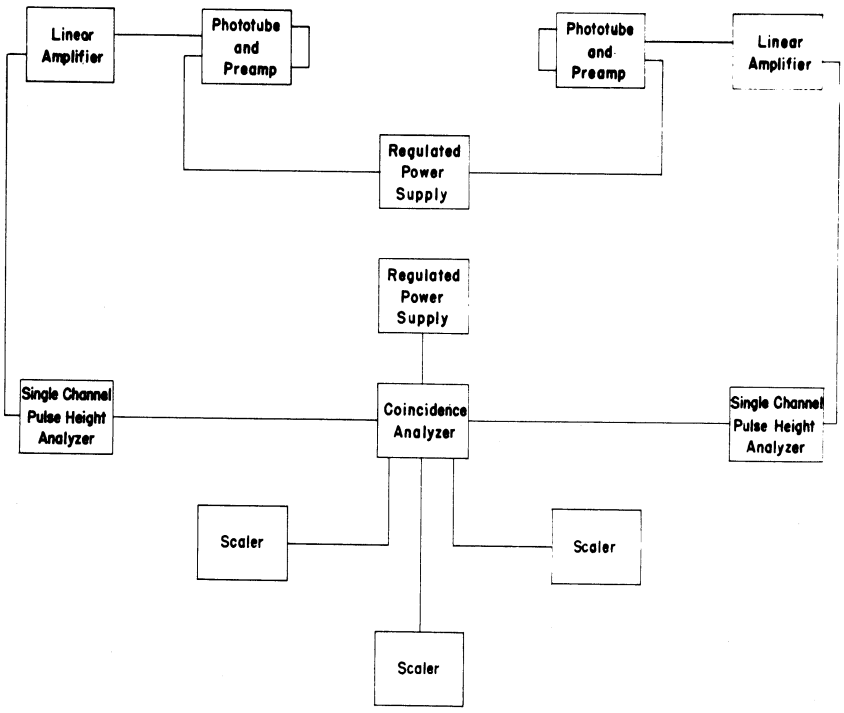

Fig. 46. Block diagram of γ-γ coincidence counter

For the γ-γ coincidence measurements the circuit given in Fig. 46 was used. One of the scintillation counters counted only the photopeak of the 1.83-Mev γ rays, the other the photopeak from the 0.9-Mev γ rays. The counter sensitive to the 0.9 Mev γ rays, however, recorded some of the Compton pulses from the 1.83-Mev γ rays as well as the 0.9-Mev photopeak. Corrections for the Compton fraction had to be applied. The value of this correction was determined experimentally from the γ-ray spectrum of the source taken with the same counter in the same geometry just before the coincidence measurements

Table VI. Data for the Determination of the Absolute Decay Rate of an Y^{88} Sample

Coincidence Method	x-ray count rate	γ rate	calculated absolute disintegration rate	efficiency of x-ray counter	efficiency of γ counter
x-rays – 0.9 Mev γ-rays	13,157 c/m	4,494 c/m	312,679 c/m		
x-rays – 0.9 Mev γ-rays	13,099	4,487	330,834		
x-rays – 1.8 Mev γ-rays	13,374		321,937		
X-rays – 1.8 Mev γ-rays	13,435		316,668		
average of above	13,266±1.04%	4,490	320,529±1.8%	4.13%	2.7%
0.9 and 1.8 Mev γ-rays			189,601 c/m		
			189,159 c/m		
			197,238		
average abs c/m from γ-rays			191,800±3%	6.97%	

were performed. The Compton plateau having a higher energy than the 0.9 Mev photopeak was extrapolated to the energy of the photopeak and its values for the range of the photopeak integrated. It was thus possible to determine the number of Compton pulses stemming from the 1.83-Mev γ-rays and having the same height as the photopeak of the 0.9-Mev γ-rays.

The results of the three attempts to determine the absolute disintegration rate of the Y^{88} sample are given in Table VI.

It is seen from Table VI that the absolute counting rate of the Y^{88} sample as determined by the x-ray—γ coincidence methods is about 1.5 times the decay rate found with the γ-γ coincidence method. The values of the efficiency of the x-ray counter vary accordingly.

Attempts to Calibrate the X-ray Counter with Sn^{113} and Mn^{54} Samples. To verify the efficiency values obtained for the x-ray counter from the above data, x-ray—γ coincidence measurements were carried out for samples of Sn^{113} and Mn^{54}. The x-ray spectra of both isotopes indicate only one γ-ray emitted during each electron capture process. (Fig. 47) It was thus expected that these γ-rays would be emitted simultaneously with the x-rays and coincidences between them obtainable. The results of the coincidence measurements carried out with the two samples are given in Table VII.

Table VII. Data for the Determination of the Absolute Decay Rates of a Sn^{113} and a Mn^{54} Sample

Isotope	Coincidence Method	x-ray count rate	γ rate	calculated absolute disintegration rate	efficiency of x-ray counter	efficiency of γ counter
Sn^{113}	x-ray—γ-rays	36,723	9,299	55,227,657	0.066%	0.017%
Sn^{113}	x-ray—γ-rays	36,733	9,274	36,933,361	0.099%	0.025%
Mn^{54}	x-ray—γ-rays	13,647	9,118	7,419,996	1.75%	0.122%
Mn^{54}	x-ray—γ-rays	13,675	9,168	7,004,040	1.95%	0.131%

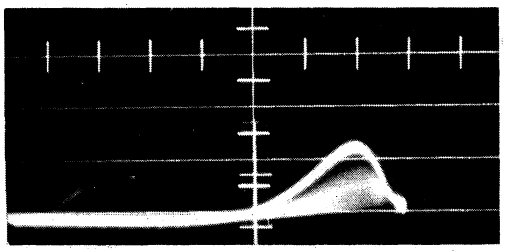

Sn^{113}

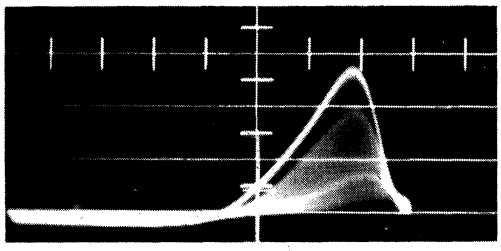

Mn^{54}

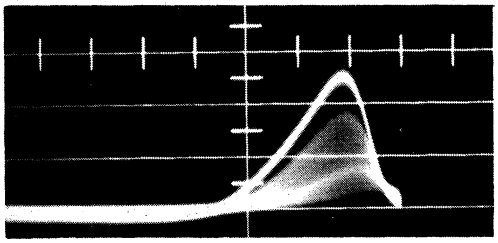

Nb^{95}

Fig. 47. Gamma-ray spectra of Sn^{113}, Mn^{54} and Nb^{95} taken with identical settings of amplifier and oscilloscope

A comparison of the values obtained for the x-ray counter efficiency for the x-rays emitted by the Sn^{113} and Mn^{54} and Y^{88} samples shows their great discrepancies. (The great fluctuation for the two values of the Sn^{113} experiments is due to the small number of true coincidences that could be collected).

To facilitate an explanation for these discrepancies the efficiency values of the γ counter might be compared for the 0.9-Mev γ rays of Y^{88}, the 0.26-Mev γ rays from

Sn^{113} and the 0.84-Mev γ rays from Mn^{54}. For the sodium iodide crystal employed, a greater efficiency would be expected for the 0.26-Mev γ rays from Sn^{113} than for the other two, of which again the 0.9-Mev γ ray from Y^{88} should yield the smaller efficiency. Comparing the experimental values it seems strange to encounter a variance of 10 and 100 in the opposite direction.

The following explanation is proposed to clarify the situation: after the electron capture process the nucleus is in a highly excited state. Two processes have to take place before a stable state is reached: the level of the electronic shell has to be refilled with emission of a characteristic x-ray; nuclear excitation energy has to be released by the emission of γ rays. To explain the experimental data it is assumed, that these two processes can be delayed with respect to each other. The x-ray is emitted after a very short time interval compared to the resolution time of the coincidence analyzer (1.94 microseconds). The nuclear de-excitation may, however, be delayed. In this case there exists an intermediary state, decaying randomly with a certain half-life.

As point in proof it may be mentioned that several cases of metastable states as intermediaries in electron-capture decay processes have been reported in the literature (46, 67). Metastable states seem to be encountered in all three of above cases. In this event the

number of coincidences observed is only due to those γ rays which are emitted while the coincidence analyzer is still sensitive after being triggered by the electron capture x-ray. The shorter the half-life of the metastable state, the more γ rays will still be considered and the truer the obtained absolute rate. The latter, however, will always be higher than the actual disintegration rate.

For Y^{88} - a fortunate case - two γ rays are emitted in cascade (Fig. 44), giving the true disintegration rate within 1%, if no intermediate of appreciable half-life is assumed for the cascade emission of the γ rays. This assumption is based on the agreement of the values obtained by the x-ray–γ coincidence measurements seen in Table VI. The difficulty in determining the absolute rate even from the γ-γ coincidences is the precision with which the Compton background can be determined. This background has to be subtracted from the γ-ray counting rate. As the part of the counting rate which is due to Compton pulses is rather large, an error of about 8% is inherent in the absolute rate determined for above Y^{88} sample.

From the experiments described above it appears that approximately 52% of the γ rays are emitted during the resolving time of the coincidence analyzer for the Y^{88}. This would indicate a half-life of 1.5×10^{-6} seconds for the metastable state. The half-lives for the intermediary states in the decay of Sn^{113} and Mn^{54} would be of

the order of 85 and 41 microseconds respectively. These estimates were made with assumption of a 6.9% x-ray counter efficiency as found from Y^{88}.

For the absolute counting of Y^{88} in the present research it was decided to use the value obtained from the γ-γ coincidence measurements as the true disintegration rate of the Y^{88} sample and assume the x-ray counter efficiency to be 6.9% for the photopeak.

The value thus obtained experimentally agrees reasonably well with the calculated efficiency of the x-ray counter.

Part 3

PROCEDURES AND RESULTS

The instruments used for determining the (d, α) reaction cross sections have been described in the previous sections and a general discussion of the procedures for the measurements given. A detailed report of their application to the experiments will be presented in this part. The experimental methods and results are treated for each reaction investigated.

The choice of the target nuclides was governed by the following factors:

1. The value of the experimental results for theoretical considerations.
2. The ability of the 7.8-Mev deuterons to induce the reaction.
3. The availability of the parent isotopes.
4. The detectability of the product nuclide.
5. The knowledge of the decay scheme for the product nuclide.
6. The possibility of resolving the expected decay curves.

The final choice made an optimum compromise of all the factors involved.

The reactions investigated in this research were the following:

$Zr^{94}(d, \alpha)Y^{92}$ *
$Zr^{92}(d, \alpha)Y^{90}$ *
$Zr^{90}(d, \alpha)Y^{88}$ *
$Mo^{98}(d, \alpha)Nb^{96}$ *
$Mo^{97}(d, \alpha)Nb^{95m}$
$Mo^{97}(d, \alpha)Nb^{95}$
$Mo^{92}(d, \alpha)Nb^{90}$
$Ti^{48}(d, \alpha)Sc^{46}$
$Ti^{46}(d, \alpha)Sc^{44}$
$S^{34}(d, \alpha)P^{32}$ *

The absolute cross sections for 7.7-Mev deuterons have been determined for all these reactions. Excitation functions were measured for the reactions with asterisks. Two of the above reactions had been investigated previously by another worker (47), but warranted a reinvestigation as the errors reported for them were rather large.

I. Bombardment Procedure

Targets were prepared by the methods reported in section II-A of part 2, and placed in the slots of the target probe assembly (Fig. 3). Several collimators consisting of empty aluminum target frames were placed before the target to reduce the

activity induced in the target frame, and behind the target to reduce the effect of secondary electrons emitted from the target.

The current integrator was warmed up for approximately one hour and tested if it was functioning normally. Current integrator readings were taken manually at various times during the course of the bombardment to have an estimate of the variation of the beam strength during the bombardment. After the bombardment the drift rate of the instrument was determined to apply a correction to the final current-integrator reading. This correction was usually less than 0.02%.

Occasionally a 1/2-mil Mylar scattering target was kept in the path of the beam (Fig. 1 N) during the bombardment to facilitate the focusing of the beam on the target. The reduction of the deuteron energy by this scattering target was calculated with the aid of Table I and considered for the final cross section values.

After bombardment the target and the substrate were dissolved and the (d, α) reaction products separated.

The final counting sample was prepared on VYNS-films (section III-C-1 of part 2) and its decay followed with the 4π counters and the x-ray and γ-ray counters.

II. The Zr(d, α)Y Reactions

The products of the (d, α) reactions on zirconium include four yttrium activities: the 17-minute Y^{94}, the 3.5-hour Y^{92}, the 64-hour Y^{90} and the 105-day Y^{88}. This can be seen from the chart of the nuclides for the zirconium region as given in Fig. 48. The Y^{94} decays rather rapidly with emission of a very strong 5.4-Mev β ray and was not observed during these bombardments. It had usually decayed out before the first counts were taken on the 4π counters. The 3.5-hour Y^{92} decaying with emission of β rays having maximum energies of 3.6, 2.7 and 1.3 Mev and several γ rays in coincidence with them could be well observed and the cross section of its formation determined.

Yttrium-90 decays with emission of one β ray only, having a maximum energy of 2.27 Mev. The 105-day Y^{88} decaying by an electron capture process and the emission of a weak 0.83-Mev positron merited some special attention in this research as it posed various interesting problems. A summary of the characteristics of these isotopes with the literature references is given in Table VIII.

Cassatt (18) showed that it was possible to obtain reasonable yields for the Zr(d, α)Y reactions with the 7.8-Mev deuteron beam of the Michigan cyclotron. He was able to identify all half-lives expected and resolved them from the gross yttrium decay curves. An attempt to

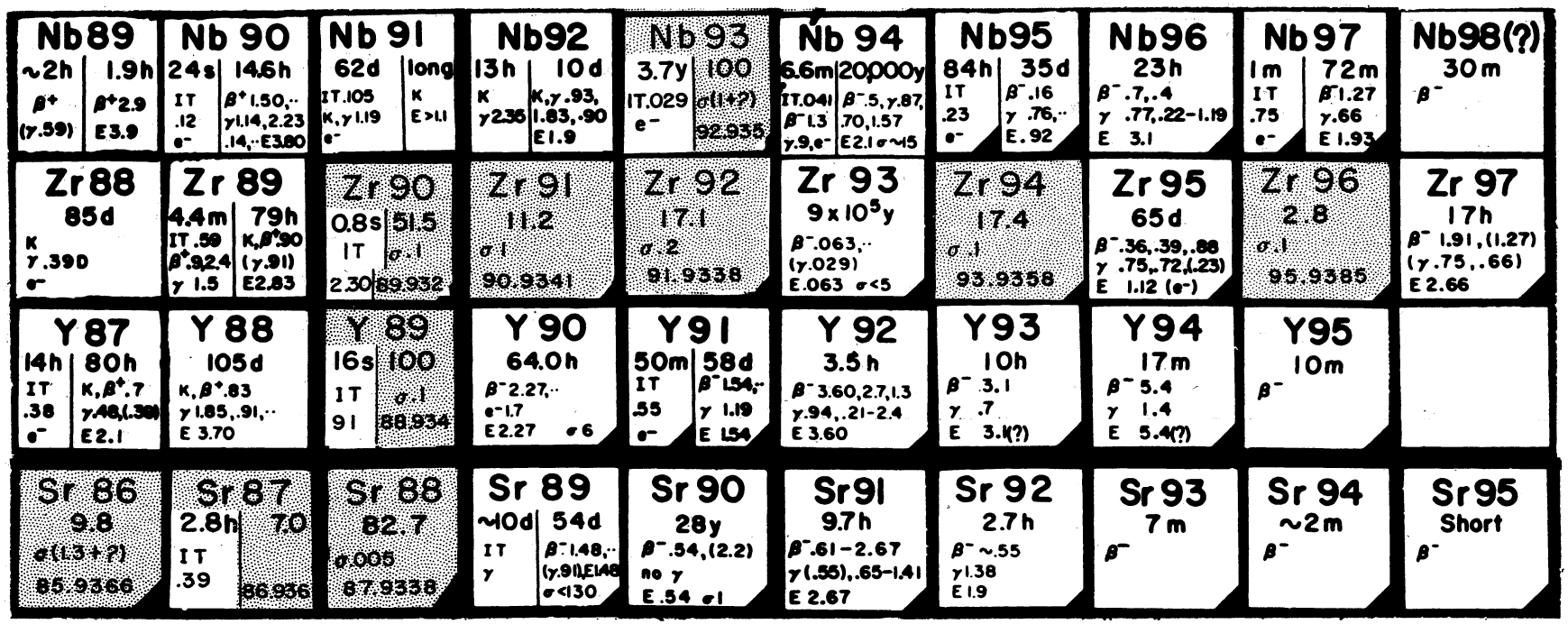

Fig. 48. Chart of Nuclides for Zirconium Region. The stable isotopes are presented in the dotted squares, the radioactive nuclides in the white fields. The first number under the symbol for the stable isotopes is their relative abundance in percent, the second number represents the activation cross section for thermal neutrons (in barns) and the third the isotopic mass on the physical scale. For the radioactive nuclides the half-life is given directly below the symbol. This is followed by the type of decay and the energy of the emitted radiation. K means electron capture process; e^- a conversion electron; IT the isomeric transition from an excited state to the ground state with emission of a γ-ray, while E represents the total energy of the decay.

(Section of Chart of the Nuclides published by General Electric Company, Knolls Atomic Power Laboratory, 5th edition, revised to April, 1956).

Table VIII. Properties of Yttrium Isotopes Encountered in this Research

Isotope	Half-life	Reference	Radiation	Relative amount	Energy	Reference
Y^{88}	105 days	104	EC	99+%	16 Kev	97
	104 days	124	β^+	0.2%	0.83 Mev	124
	105±1% *	this thesis	γ_1	100+	0.908 Mev	124
			γ_2	90+	1.85 Mev	124
			γ_3	0.5+	2.76 Mev	
				1+		97
				~1+		this thesis
Y^{90}	64.24 hrs	124	β^-	100%	2.26 Mev	124
	64.029 hrs	124			2.27 Mev	124
	64.18 hrs *	this thesis				
Y^{92}	3.60 hrs	124	β_1^-	11%	1.3 Mev	124
	3.5 hrs *	124	β_2^-	12%	2.68 Mev	124
	3.46±1%	this thesis	β_3^-	77%	3.6 Mev	124
	3.4	19				

* value used for calculations in this thesis

evaluate the cross sections, however, had not been made until this research.

A. Target Preparation

Some attempts were made to obtain thin, uniform zirconium targets by evaporating zirconium metal according to a method described by Lillie and Conner (77). The results were rather disappointing. Zirconium foils, 0.00013-inch thick, were rolled by the Arnold Engineering Company from a 0.002-inch stock obtained from the Foote Mineral Company of Philadelphia, Pennsylvania.

A spectrographic analysis of these foils was performed by LEDOUX and Company Inc. of Teaneck, New Jersey on April 4, 1957, with the following result:

Zirconium.....99.85%

Hafnium.....none detected, less than 0.1%.

Circular target disks of defined area were cut from the foils with a stamp-die. Their average thickness was determined within 0.3% by weighing on a semi-micro balance. To check the uniformity of the foil-thickness the absorption of the Pm^{147} β rays of the thin-film gauge was determined at five points. The variation of the amount absorbed remained within 2% for the majority of the foils used.

B. Chemical Separation

The (d, α) reaction products were separated from the bombarded targets by the carrier-free procedure given in Table IX. The procedure adheres to the following outline.

The tracer, previously deposited on Zapon film and counted, is dissolved together with the bombarded target and isotopic interchange obtained in a homogeneous solution under severe conditions. Primary separation from the bulk of the target and radioactive side products is achieved by two types of simultaneous precipitations. The carrier-free yttrium fraction is finally separated from its zirconium carrier and any interfering activities by an anion exchange step. The carrier-free yttrium activity contained in the eluate is regained by evaporation of the solvent.

C. Tracers

To determine the chemical yield for each particular separation following a zirconium bombardment tracers had to be used.

1. Yttrium-88

The 105-day Y^{88} decays predominantly by the electron capture process and was well suited for this purpose. Preliminary bombardments indicated that the Y^{88} count rate obtainable in the 4π counters from the yttrium product of

a two-hour bombardment represents only 1/10,000 of the counting rate of the product 4 hrs. after the bombardment. This fact made the use of Y^{88} as tracer very convenient.

To obtain enough pure Y^{88} activity for tracing the chemical yields a bombardment of several grams strontium oxide was performed with the 21-Mev deuteron beam of the cyclotron at the Argonne National Laboratory. Yttrium-88 was produced in relatively large amount by the efficient $Sr^{88}(d, 2n)Y^{88}$ and $Sr^{87}(d, n)Y^{88}$ reactions. The short-lived activities resulting from this bombardment were permitted to decay out for 11 months. The yttrium-88 was then separated from the target material in carrier-free form. The procedure for this separation involved several simultaneous precipitations of the Y^{88} with zirconium carrier followed by an ion exchange separation of yttrium from zirconium similar to the procedure given in Table IX.

a. Identification of Y^{88}. The resulting Y^{88} was identified by its x-ray spectrum seen in Fig. 37 and Fig. 38. A half-life determination over a period of several months (Fig. 49) with several samples resulted in values of 105 $\pm$ 1 days agreeing with the literature (97).

Investigation of the γ-ray spectrum of Y^{88} resulted in the picture seen in Fig. 42 showing the 0.91-Mev, and the 1.87-Mev lines.

The Co^{60} spectrum taken with the same amplifier and

Table IX

Chemical Separation of Yttrium from Zirconium Targets

(carrier-free)

Element	Separated from	Decontamination Factor
Y (carrier-free)	d. bombarded Zr	$\sim 10^5$

Time of Separation	Chemical Yield
~3.1 hours	~85%

Chemicals and Equipment

4 Pyrex beakers (50 ml.); centrifuge; centrifuge tubes 40 ml., 15 ml., (Pyrex); Lustroid tube (10 ml.); micro pipette 50; platinum wire; small anion exchange column (Fig. 20); medicine droppers; calcium carrier (10 mg/ml); zirconium carrier (10 mg/ml).

Dowex 2 (200-400 mesh); conductivity water; conc. H_2SO_4; conc. NH_4OH; conc. HCl; 30% H_2O_2; HCl-gas tank.

Procedures

(1) Cut the tracer yttrium, deposited on Zapon film, from aluminum sample plate and place in small beaker, add bombarded zirconium foil plus Mylar substrate. Add 1.5 ml. conc. H_2SO_4 and a few drops 30% H_2O_2. Heat to fumes until dissolved (cool and add more H_2O_2 at intervals). (Note 1)

(2) Transfer clear solution to a 40 ml. centrifuge tube, add 30 ml. H_2O and precipitate zirconium hydroxide with conc. NH_4OH. Stir with platinum wire; centrifuge and wash twice.

(3) Dissolve precipitate with a minimum amount of conc. HCl, add 3 mg calcium carrier and one drop $NbCl_5$ carrier (10 mg/cm^3). Transfer to 10 ml. Lustroid tube.

(4) Precipitate CaF_2 (and YF_3) with 3 ml. conc. HF. Centrifuge (water in centrifuge cups!) and wash twice.

(5) Transfer precipitate to a 15 ml. centrifuge cone, centrifuge, decant, add 0.5 ml. conc. H_2SO_4.

(6) Heat to fumes to drive off HF. Cool. Add 3 mg. Zr-carrier and dissolve residue in 10 ml. warm water.

(7) Precipitate zirconium hydroxide with conc. NH_4OH. Wash three times with conductivity water. (Note 2)

(8) Dissolve precipitate with a few drops conc. HCl and saturate with HCl gas.

Table IX (continued)

(9) Transfer solution to a small anion exchange column charged with 1 ml. Dowex 2 resin saturated with conc. HCl.

(10) Adsorb zirconium onto the resin slowly. After liquid level reaches resin bed add 5 drops of conc. HCl and permit to soak in. (Note 3)

(11) Elute carrier-free yttrium reaction product with 5 ml. conc. HCl at a rate of 1 drop in 7 seconds. (Note 4)

(12) Collect eluate when activity starts coming through. Evaporate to near dryness and plate for counting.

Notes

(1) A homogeneous solution is obtained under rather severe conditions. Complete isotopic interchange between the Y^{88} tracer and the reaction product is thus accomplished.

(2) This washing removes the calcium carrier and must be done thoroughly, if carrier-free yttrium is to be obtained.

(3) Try to wash the walls of the column free of activity with these 5 drops.

(4) The yttrium is not absorbed by the resin in hydrochloric acid but is easily eluted, while zirconium and niobium are strongly absorbed from a conc. HCl medium.

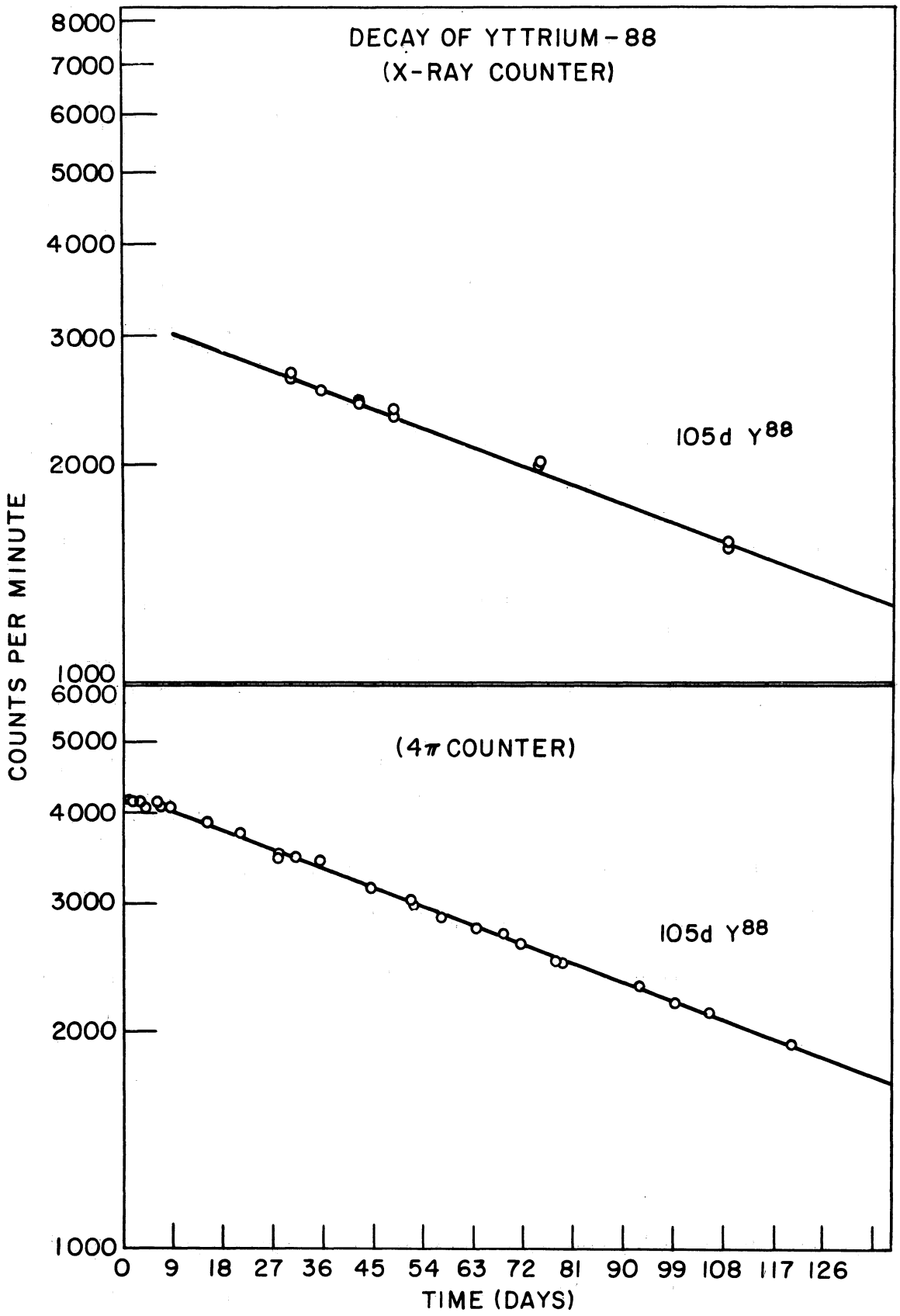

Fig. 49. Decay curves of Y^{88} taken with x-ray counter and 4π counter (two different samples)

oscilloscope settings served for the energy calibration.

Yttrium-88 Decay Scheme. In 1955 Alburger and Sunyar (2) reported that they could not observe any of the 2.76-Mev γ rays reported by W. C. Peacock and J. W. Jones (97) (cf. Fig. 44) The picture of the spectrum obtained with our Y^{88} (Fig. 50), however, clearly indicates the presence of this γ ray.

This picture as well as that of the Nb^{92} spectrum seen in Fig. 42, was taken by exposing the film for two minutes to the image of the two lower γ rays, then adjusting the trigger level of the oscilloscope to block out the traces of these energies and exposing the film for an additional hour to pulses resulting from γ rays with energies above about 2 Mev. The Co^{60} standards taken immediately after with the same amplifier and oscilloscope settings served for the calibration of the energies.

Manual counting of the peaks indicated a ratio of 0.0027 between the 2.76 and 0.9-Mev peaks. The latter was corrected for the Compton pulses stemming from more energetic γ rays. The experiment indicated a branching ratio of approximately 1 - 2%, if the efficiency of the 1 x 1.5-inch NaI crystal is taken into consideration for the two energy ranges. These findings together with the experimental results reported in section III-D-4 of part 2 verify the decay scheme for Y^{88} as given in Fig. 44.

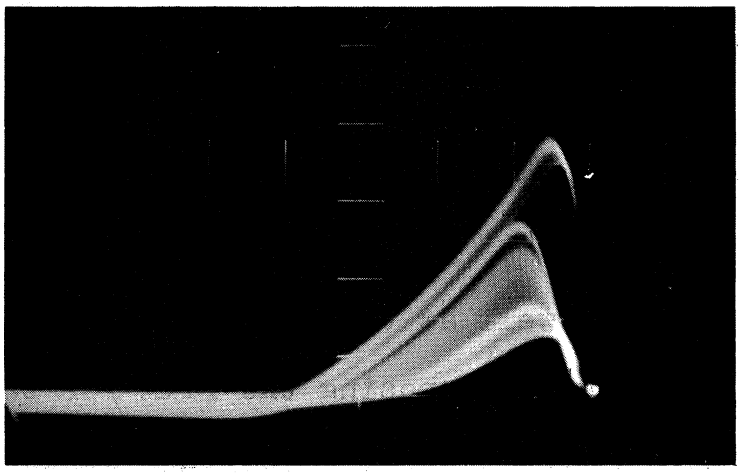

Y^{88}

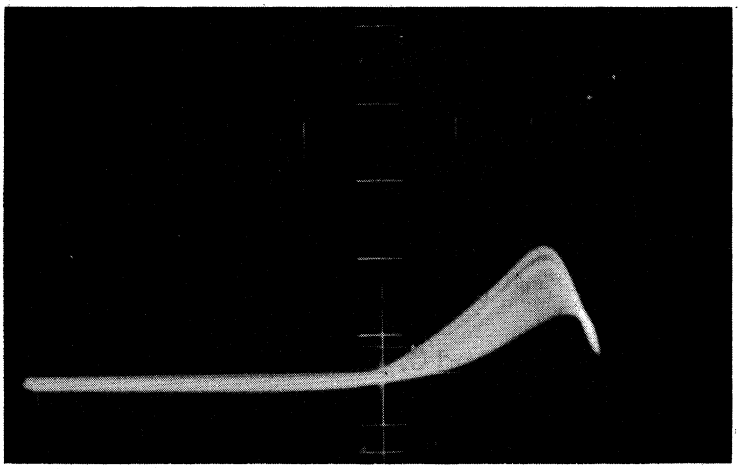

Co^{60}

Fig. 50. Gamma Spectra of Y^{88} and Co^{60}

b. Counting of Y^{88} Tracers. The identified Y^{88} was used for tracing the reaction yields of the $Zr^{94}(d, \alpha)Y^{92}$ and $Zr^{92}(d, \alpha)Y^{90}$ reactions. The desired amount of Y^{88} was deposited on a thin Zapon film and covered so as to form a weightless source. The decay rate of this source was determined by counting on the first shelf of the x-ray counter.

For the first few bombardments manual counts were taken in five-minute intervals covering the entire spectrum with a one-volt window. The area under the main peaks was integrated and this value used as the count rate of the tracer sample at that day. Errors of at least 3% were unavoidable by this method. For later bombardments the tracer Y^{88} was counted by the more exact and convenient method of counting the photopeak by difference as was described in section III-C-2 of part 2.

2. Tracer Y^{90}.

It was of special interest to determine the cross section of the (d, α) reaction for the magic number nuclide Zr^{90}. The reaction product for the $Zr^{90}(d, \alpha)Y^{88}$ reaction is here the same 105-day Y^{88} described above. To trace the chemical yields for this reaction, Y^{90} was used as tracer. The latter was isolated from several millicuries of SrY^{90} by 10 coprecipitation steps with zirconium hydroxide and the final separation from zirconium by the ion exchange steps mentioned above (Table IX).

The carrier-free Y^{90} thus obtained was plated on Zapon film and identified by its half-life of 64.18 $\pm$ 0.1 hrs. over a period of 25 days. To establish chemical yields the Y^{90} tracer as well as the separated samples from the bombardment were counted with the thin-window proportional beta counter in the same geometry.

D. Record of the Bombardments

Six bombardments were obtained to determine the cross sections and excitation functions of the Zr(d, α)Y reactions.

1. The $Zr^{92}(d, \alpha)Y^{90}$ and $Zr(d, \alpha)Y^{92}$ Reactions.

The products from these two reactions are β-ray emitters and could be counted absolutely with the 4π counters (Table VIII).

The dependability of the chemical separation procedure given in Table IX was proven by bombardments 4 and 7 and the relative yields for the formation of Y^{92}, Y^{94} and Y^{88} established for a two-hour bombardment with 7.8-Mev deuterons. The 4π counter decay curve for bombardment 7 is presented in Fig. 51. The three components into which the curve is analyzed can be readily identified from the gross decay curve.

The result of this bombardment helped to estimate the amount of Y^{88} tracer that should be used for the absolute cross section experiments to permit resolution of the decay curves and a minimum error in the yield determination. It was found that an Y^{88} sample counting between 10,000 and 15,000 counts per minute on the x-ray counter would well serve this purpose.

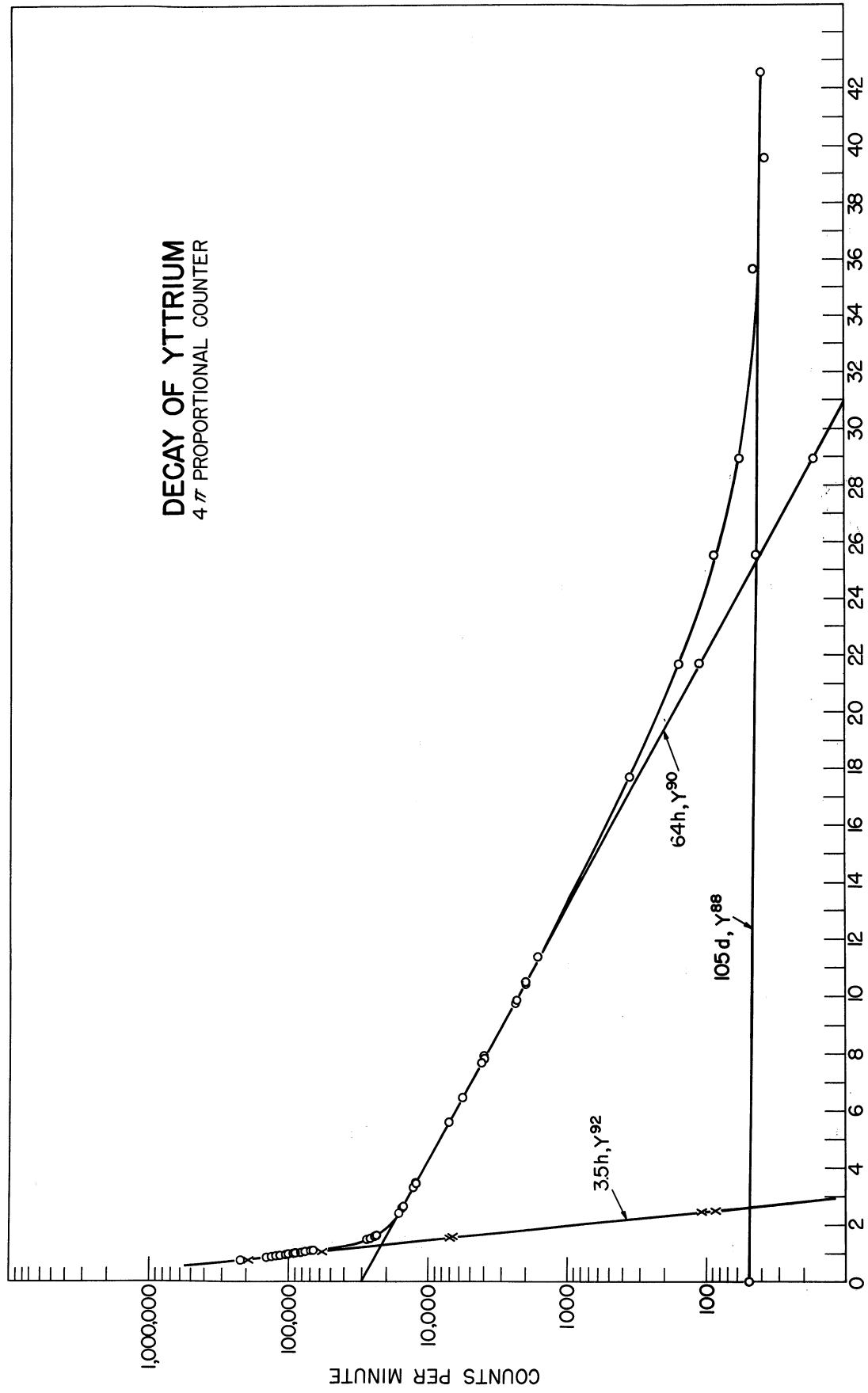

Fig. 51. Complex β-ray Decay Curve of Yttrium from Bombardment 7

The absolute cross section for the $Zr^{92}(d, \alpha)Y^{90}$ reaction for 7.56 ± 0.05 Mev deuterons was measured by two experiments. In bombardment 10 a zirconium foil was exposed to the full energy beam behind a 1/2-mil Mylar scattering target. The primary experimental data for the experiment are reported in Table X. The major source of error for this experiment was the uncertainty in the chemical yield. This was primarily caused by the difficulties of counting the x-rays from Y^{88} which were counted by integration under the photopeak of the K x-rays. This error could be reduced in bombardment 12b where the counting of the tracer was performed by the method described in section III-C-2 of part 2.

The agreement of the values obtained for the cross sections from the two bombardments: 3.76 ± 7% and 3.82 ± 6% millibarns respectively, is considerably better than indicated by the estimated experimental errors. The two experiments constitute the only case where a double determination of a cross section was performed, but they may serve for an estimate of the precision of these investigations.

The absolute cross sections for lower deuteron energies (6.97 and 4.78 Mev) were established by bombardments 11 and 12a. Difficulties were experienced with the resolution of the decay curves for bombardment 12a due to the low counting rate of the Y^{90} component. A better yield determination for this bombardment partially off-set the effect of this error on the cross section value.

Table X. Results of the Zr(d, α)Y Cross Section Determinations

The $Zr^{92}(d, \alpha)Y^{90}$ Reaction

Bombardment No.	Type	Average Deuteron Energy Mev	C_i	Chem. Yield %	Count Rate* c/m	Target thickness mg/cm^2	σ millibarns
10	abs.	7.56±0.05	4000±1%	43.4±4%	26,190±1.5%	3.515±0.3%	3.66±7%
12b	abs.	7.56±0.05	4002.1±1%	77.4±3%	48,938±1.5%	3.619±0.3%	3.72±6%
13	rel.	7.56±0.05	-	±5%	1,100±3%	3.56±1%	3.79±10%
11	abs.	6.97±0.08	4000±1%	30.1±4%	12,901±1.5%	3.515±0.3%	2.60±7%
13	rel.	6.37±0.08	-	±5%	400±3%	3.49±2%	1.39±10%
13	rel.	5.02±0.1	-	±5%	95±5%	3.48±2%	0.33±10%
12a	abs.	4.78±0.15	4002.1±1%	29.7±3%	949±3%	3.466±0.3%	0.197±8%
13	rel.	3.89±0.2	-	±5%	13±10%	3.42±2%	0.045±20%
13	rel.	2.48±0.3	-	±5%	2.5±20%	3.52±2%	0.008±50%

* For absolute experiments count rate at the end of the bombardment, for relative experiments at some later time.

Table X (continued)

The $Zr^{94}(d, \alpha)Y^{92}$ Reaction

Bombardment No.	Type	Average Deuteron Energy Mev	C_i	Chem. Yield %	Count Rate* c/m	Target thickness mg/cm^2	σ millibarns
10	abs.	7.56±0.05	4000±1%	43.4±4%	457,811±1.5%	3.515±0.3%	3.90±7%
13	rel.	7.56±0.05	-	-	8,300±3%	3.56±2%	4.3±10%
11	abs.	6.97±0.08	4000±1%	30.1±1.2%	241,809±1.5%	3.515±0.3%	2.89±7%
13	rel.	6.37±0.08	-	-	3,240±3%	3.49±2%	1.73±10%
13	rel.	5.02±0.1	-	-	745±5%	3.48±2%	0.39±10%
12a	abs.	4.78±0.15	4002.1±1%	29.7±0.9	26,473±2%	3.466±0.3%	0.329±7%
13	rel.	3.89±0.2	-	-	66±10%	3.42±2%	0.035±20%
13	rel.	2.48±0.3	-	-	0	3.52±2%	0.000±100%

The $Zr^{90}(d, \alpha)Y^{88}$ Reaction

6	abs.	7.56±0.1	30,248±1%	88.92±1%	21,552±8%	3.488±0.3%	2.28±12%
6	abs.	7.09±0.15	30,248±1%	70.83±1%	15,517±9%	3.480±0.3%	1.63±13%
6	abs.	5.2±0.6	30,248±1%	65.32±1%	4,784±14%	3.515±0.3%	0.50±20%
6	abs.	3.7±1.5	30,248±1%	81.16±1%	±100%	3.597±0.3%	0.00±100%

* For absolute experiments count rate at the end of the bombardment, for relative experiments at some later time.

The same three bombardments also established the cross section values for the $Zr^{94}(d, \alpha)Y^{92}$ reaction at the three energies. In bombardment 12 two foils (12a and 12b) had been exposed simultaneously to the deuteron beam, foil 12b, however, could only be worked up after its Y^{92} component had decayed out already. A recheck on the value obtained by bombardment 10 for the $Zr^{94}(d, \alpha)Y^{92}$ reaction with 7.56 Mev deuterons was thus not possible.

The experimental errors as reported in Table X are comparable to those reported for the $Zr^{92}(d, \alpha)Y^{90}$ reaction measured by the same bombardments. The only significant difference is the smaller error reported for the count rate from bombardment 12a. The improvement over the Y^{90} component was mainly due to the statistics.

The decay of the reaction products from the bombardments was followed with the 4π counters and in the order of 200 counts taken for each sample. This facilitated the resolution of the decay curves into the three components. (no additional half-lives were observed in the purified samples.) Scattering of the points remained largely within the statistical variation of the individual counts, which could be kept well below 1%.

Bombardment 13 was carried out in addition to the absolute runs described above. It represented a typical stacked foil experiment for determining the excitation functions of the two reactions. Table X gives the results normalized to the values from the absolute experiments.

Seven zirconium foils were interleaved with aluminum foils serving as absorbers (attenuators) of the cyclotron beam and as catchers of the recoils. Table XI gives the arrangement of the target foils and absorbers as employed in bombardment 13.

The chemical separation of the yttrium from the bombarded targets could be simplified for this relative experiment. It was only important that the chemical yields should be the same for the foils exposed to different bombarding energies. This was achieved by the procedure given in Table XII. The carrier-type separation could be performed rapidly to permit counting of the Y^{92} components of all samples and provided maximum uniformity of the chemical yields. It is estimated that the variation of the chemical yield from foil to foil did not exceed $\pm 5\%$ standard error.

The samples obtained from this bombardment were counted in sequence with the β-ray proportional counter for 22 hours continuously. An absorber of 640 mg/cm^2 aluminum was employed which favored strongly the 3.6-Mev β rays from Y^{92}, rejecting most of the 2.27-Mev Y^{90} activity as well as weaker β rays from other impurities. Relatively good decay curves with 3 - 4 hour half-lives were obtained and easily resolvable into their Y^{92} component.

After 22 hours the 3.6-hour Y^{92} components had largely decayed out and the samples were then counted through a 172 mg/cm^2 aluminum absorber. This aluminum absorber permitted the strong 2.7-Mev β rays of Y^{90} to be

Table XI. Arrangement of Zirconium Targets for Bombardment 13

Target or Absorber	Thickness (mg/cm^2)	Average Deuteron Energy Mev
Mylar	1.76	
Zr I	3.56	7.56
Aluminum	14.75	
Zr II	3.49	6.37
Aluminum	11.32	
Zr III	3.43	5.02
Aluminum	8.93	
Zr IV	3.42	3.89
Aluminum	8.93	
Zr V	3.52	2.48
Aluminum	8.93	
Zr VI	3.57	0 *
Aluminum	21.77	
Zr VII	3.53	0 *

* These two targets served to check the presence of reaction product from neutron induced reactions.

Table XII. Chemical Separation for Yttrium in Bombardment 13

Element	Separated from	Decontamination Factor
Y	d. bombarded Zr	10^3

Time of Separation	Chemical Yield
15 min.	90%

Chemicals and Equipment

Lusteroid tubes,40 ml; centrifuge; hot water bath; razor blade.

HF; yttrium carrier (10 mg/ml); calcium carrier (10 mg/ml).

Procedures

(1) Dissolve the Zr foil plus the aluminum substrate in dilute HF solution in a Lusteroid tube. Add 5 drops yttrium carrier plus 1 drop calcium carrier. Centrifuge for 4 minutes, decant.

(2) Flatten the bottom of the Lusteroid tube by dipping it in boiling water and pressing it against a lead brick.

(3) Cut off the bottom of Lusteroid tube, containing the precipitate, with a razor blade.

(4) Dry precipitate under a heat lamp and mount on sample card covered with 1/4-mil Mylar.

counted, but reduced the background of impurities due to incomplete chemical separation to a negligible minimum. Each sample was counted three times daily in intervals of approximately 8 hours over a period of 15 days. Very straight decay curves of the 64 hour Y^{90} were obtained.

2. Determination of the $Zr^{90}(d, \alpha)Y^{88}$ Cross Sections and Excitation Function.

The determination of the $Zr^{90}(d, \alpha)Y^{88}$ cross sections and excitation function proved considerably more difficult than the cross section determination discussed above. The product has a relatively long half-life and very little of it, in terms of activity, could be produced during the regular two-hour bombardments (Fig. 51). It was thus necessary to obtain a very much longer and more intense bombardment for this determination.

With the special cooperation of the cyclotron crew it was possible to arrange for a 10-hour bombardment which was used to bombard simultaneously five zirconium targets in the stacked-foil fashion. Their arrangement is seen from Table XIII. Unfortunately the Mylar substrates of all but the first target were damaged so severely by the beam that they broke, wrinkled and bent backward, resulting in higher actual bombarding energies for the last three foils, as well as loss of recoils. Fortunately the substrate of the first target remained intact and that of the second sufficiently so to be dependable for the cross section determinations at those energies. In

Table XIII. Arrangement of Zirconium Targets for Bombardment 6

Target or Absorber	Thickness (mg/cm^2)	Average Deuteron Energy Mev
Mylar	1.76	
Zr-6	3.488	7.56
Mylar	3.52	
Zr-5	3.480	7.09
Mylar	3.52	
Aluminum	10.78	
Zr-4	3.515	4.7
Mylar	3.52	
Aluminum	10.78	
Zr-3	3.597	2.7
Mylar	3.52	
Zr-1	3.479	1.7
Mylar	3.52	

addition the 1/2-mil Mylar scattering target used burned through during the latter part of the bombardment making the initial energy somewhat uncertain.

The targets were permitted to "cool" for several months to permit the Y^{90} and Y^{92} to decay completely. After this they were worked up and the chemical yields of the yttrium product traced with Y^{90}. The decay of the Y^{90} tracer was followed for one month to establish the chemical yields. Finally the samples were counted with the x-ray counter over a period of several additional months. It was possible by this method to determine the relative counting rates of four samples so as to establish a relative excitation function of the reaction. Large errors, however, had to be taken into consideration due to the partial destruction of the Mylar substrates resulting in a "curve" of which actually only the first two points are known to within 10%.

For the determination of the absolute cross section of the reaction from the two relatively undestroyed targets it was necessary to measure the absolute disintegration rate of Y^{88}. In effect this amounted to a determination of the efficiency of the x-ray counter for Y^{88} x-rays as was described in section III-D-4 of part 2.

With the calibrated x-ray counter efficiency for the Y^{88} photopeak the absolute counting rate of the samples from bombardment 6 could be determined with an estimated error of approximately 10%. The cross-section values

calculated from the experimental data are presented in Table X. Two points of the excitation curve are entered into Fig. 52. For the other values the uncertainties were too great to warrant entries.

E. Resolution of the Decay Curves

The resolution of the decay curves obtained for the yttrium products was carried out by the following method: A large graph of the gross decay curve, corrected for background and coincidences, was plotted on semi-log paper. The longest half-life (Y^{88}) was extrapolated to the end of the bombardment. The value of the extrapolated line was read from the graph for each time a count had been taken during the decay and subtracted from the gross decay curve. A plot of the difference resulted in a two-component curve. Small corrections could be applied to the extrapolated Y^{88} line to straighten out a slight curvature in the curve of the next shorter half-life (Y^{90}). The same process was repeated for the two-component curve until a straight line was obtained for the third component (Y^{92}).

The counting rate of a particular component at the end of the bombardment was then calculated from the resolved decay curve in the following way: arbitrary points, lying on the decay curve drawn with the "known" half-life of the component through the resolved points, were chosen.

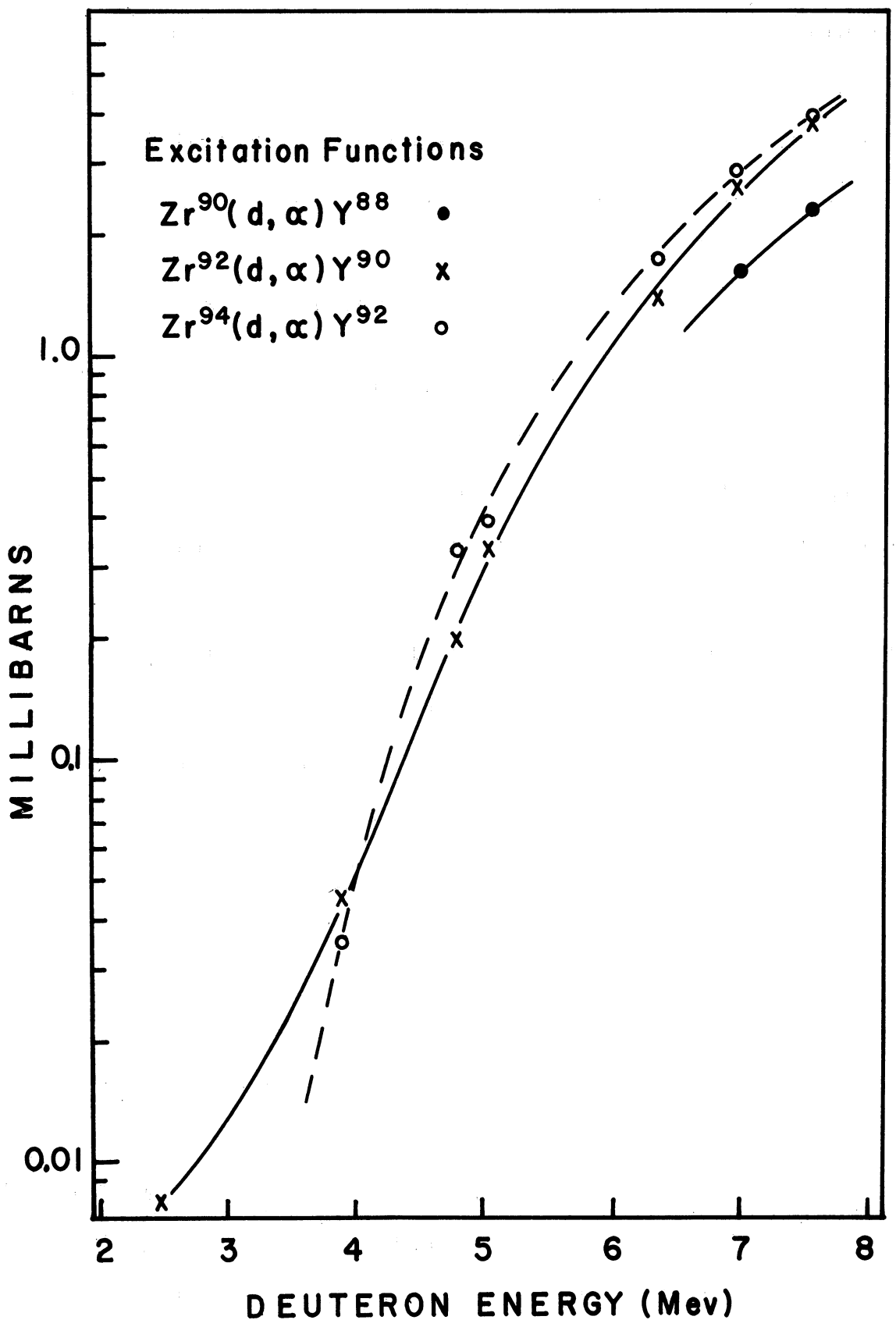

Fig. 52. Excitation Functions for the Zr(d, α)Y Reactions.

With the aid of the decay constant the count rate at the end of the bombardment could be computed from these points and the obtained values used to estimate the error.

It is believed that the much more laborious analysis of the decay data by means of a least-squares method would not result in error limits exceeding those quoted, since very good data was available for the analysis. The resolved points scattered little around a line fitted to them representing a half-life in good agreement with values reported in the literature.

III. The Mo(d, α)Nb Reactions

The molybdenum reactions were considered of interest as a comparison to the reactions involving zirconium. The atomic number of the target element is two units larger than that of zirconium.

The chart for the nuclides of the molybdenum region is shown in Fig. 53. The (d, α) reaction products from molybdenum include seven daughter isotopes with 11 different activities. Of these only four isotopes were found in this research and only four cross sections determined. Niobium-98 with a half-life of 30 minutes, as well as the isomers Nb^{94m} and Nb^{90m} with 6.6-minute and 24-sec. half-lives respectively had decayed out before the samples could be counted. The 20,000-year Nb^{94} was not obtained in sufficient quantity to be detected.

Niobium-92, although not resolved from the 4π β-decay curves, could be identified by its characteristic x-ray with the x-ray spectrometer. Its spectrum can be seen in Fig. 54. To verify this spectrum, a sample of the 10-day Nb^{92} was prepared by deuteron bombardment of zirconium and subsequent ion exchange separation. (Niobium is eluted from a small Dowex 2 column with 4 M HCl, while zirconium and yttrium, the other two products of a zirconium bombardment, are eluted by 7 M and 12 M HCl respectively (cf. Table II).

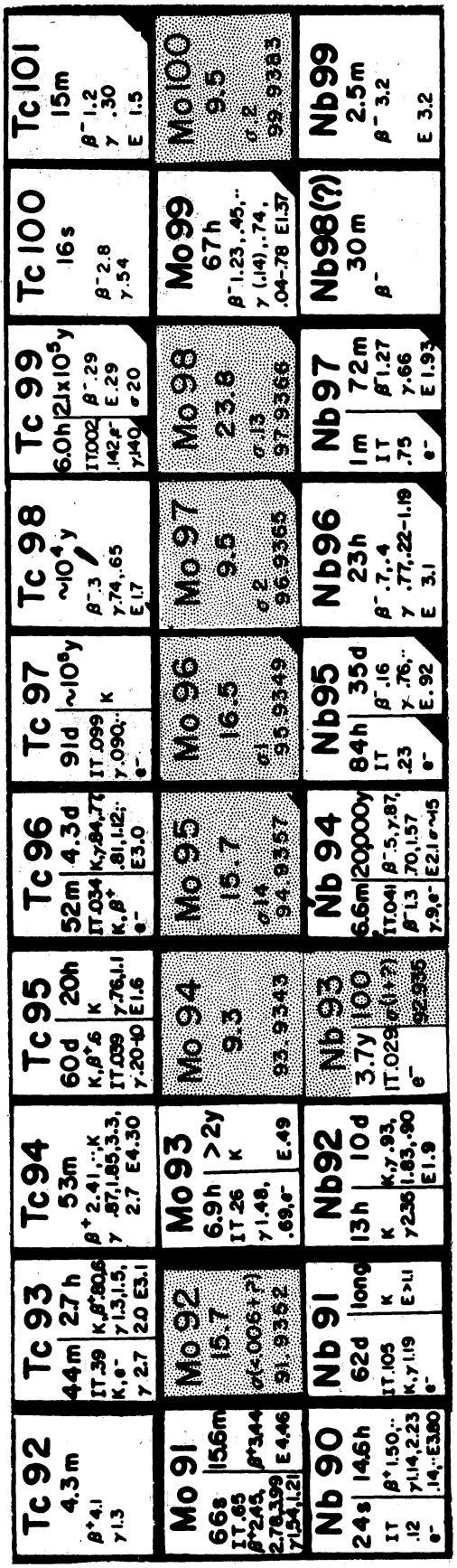

Fig. 53. Chart of Nuclides in the Molybdenum Region (for explanation see Fig. 48).

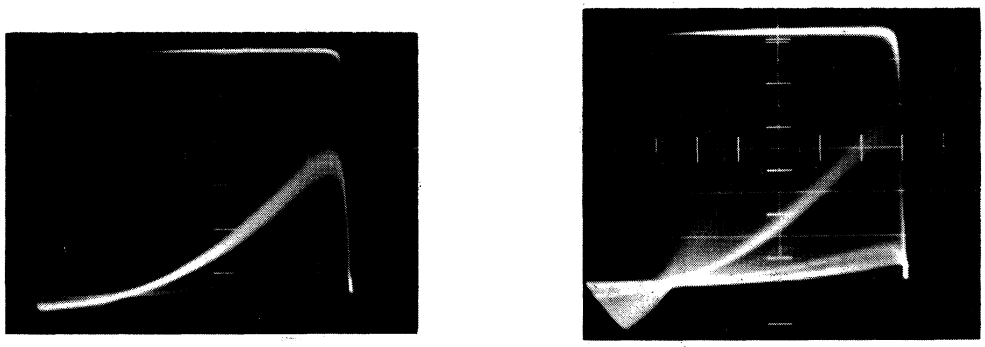

Y^{88} MoNb-14

Fig. 54. X-ray spectra of Y^{88} and niobium fraction from bombardment 14 taken 12 days after the end of the bombardment.

Y^{88} Nb^{92}

Fig. 55. Nb^{92} X-ray Spectrum

Fig. 55 shows the x-ray spectrum of this sample. It is essentially the same as the niobium spectrum in Fig. 54.

The 13-hour activity also reported for Nb^{92} could not be identified. By resolving the niobium β-decay curves obtained with the 4π counters into only four components (Fig. 57 and 58), any contribution by the 13-hour Nb^{92} was added to the Nb^{90} component, decaying with a 14.6-hour

half-life. The contribution of the Nb^{92} was thus included in the calculation of the $Mo^{92}(d, \alpha)Nb^{90}$ cross section making this value an upper limit for the (d, α) cross section of the magic Mo^{92} parent.

The following niobium isotopes could be identified in the β-decay curves of the molybdenum bombardment products: The 23-hour Nb^{96}, the 35-day Nb^{95}, the 84-hour Nb^{95m}, and the 14.6-hour Nb^{90} emitting a 1.5-Mev positron together with three γ rays. A list of the properties of these isotopes is seen in Table XIV.

A. Targets

Like zirconium, molybdenum is a rather refractory metal and could not be satisfactorily evaporated with the equipment available for this research. Metal foils were thus used for the targets. Through the courtesy of the Arnold Engineering Company foils of pure molybdenum metal were obtained with a thickness of approximately 5 mg/cm^2 (0.13 mil). The targets were prepared by cutting the foil into disks by means of a stamp die and mounting them onto a Mylar substrate which was stretched over the aperture of an aluminum target-frame. The average thickness of the disks was determined by weighing with a micro-balance to within 0.1% and the uniform thickness determined by means of the Pm^{147} gauge as in the case of zirconium.

Table XIV. Properties of Niobium Isotopes Encountered in this Research

Isotope	Half-life	Reference	Radiation	Amount	Energy	Reference
Nb^{90}	14.6 hrs.	a	β^+	4.5+	0.55 Mev	124
	14.7	a		8.5+	0.865	124
				87+	1.5	
					$f_e/f^+=0.76$	124
					1.7	
			γ_1	very weak	0.133	124
			γ_2	135+	1.40	124
				135°		124
			γ_3	3.5°	0.372	124
			γ_4	130°	1.130	124
				380°	1.14	124
			γ_5	40°	1.27	124
			γ_6	120°	2.201	124
				230+	2.20	124
Nb^{92}	10.1 days	a	EC	100%	17.9 Kev	124
	9.8		no β^+			
	11		γ_1	1.3+	0.900 Mev	124
			γ_2	~100+	0.933	124
				97.8+	0.934	124
			γ_3	2.2+	1.83	124
				~1+	1.84	
Nb^{95}	35 days *	b	β^-	100%	0.160	64
	37		γ	100%	0.745	64
Nb^{95m}	90 hrs.	b, c	γ		0.236	27
	84 hrs. *	b				

Table XIV(continued)

Isotope	Half-life	Reference	Radiation	Amount	Energy	Reference
Nb^{96}	23.35 hrs.	b	β_1^-	92%	0.75	64
	22.9 hrs.	b				
	23 hrs. *	d	β_2^-	8%	0.37	64
			γ		0.216	99
					0.230	99
					0.451	99
					0.560	99
					0.725	99
					0.770	99
					0.804	99
					0.840	99
					1.078	99
					1.187	99

Table XV

Chemical Separation of Niobium from Molybdenum Targets

(carrier-free)

Element	Separated from	Decontamination Factor
Nb (carrier-free)	d. bombarded Mo	$\sim 10^5$

Time of Separation	Chemical Yield
~4 hours	~50%

Chemicals and Equipment

Pyrex beakers (50 ml.); centrifuge; centrifuge tubes 40 ml., 15 ml.; medicine droppers; micropipette 50λ; platinum wire 6 inch; small anion exchange column (Fig. 20); molybdenum carrier (10 mg/ml); aluminum carrier (10 mg/ml).

Dowex-2 (200 - 400 mesh); conductivity water; conc. H_2SO_4, NH_4OH, HCl, HNO_3; 30% H_2O_2; HCl-gas tank.

Procedures

(1) Place tracer niobium in small beaker, add bombarded molybdenum foil plus Mylar substrate. Add 30 drops of conc. H_2SO_4 and a few drops H_2O_2. Heat to fumes until dissolved. (Cool and add H_2O_2 together with a few drops of conc. HNO_3 at intervals.) (Note 1)

(2) Transfer clear yellow-brown solution to 40 ml. centrifuge cone, add 30 ml. H_2O and 2 mg aluminum carrier. Stir well. Make alkaline with conc. NH_4OH. Centrifuge and wash twice. (Note 2)

(3) Dissolve precipitate with a minimum of conc. HCl, dilute and reprecipitate with conc. NH_4OH. Centrifuge and wash twice.

(4) Dissolve precipitate in conc. HCl, add few drops of molybdenum carrier, dilute and reprecipitate with conc. NH_4OH. Centrifuge and wash twice.

(5) Dissolve precipitate in minimum amount of conc. HCl and saturate with HCl gas. (Note 3)

(6) Transfer this solution to a small anion-exchange column charged with 1 ml. Dowex-2 resin saturated with conc. HCl.

Table XV(continued)

(7) Permit to absorb slowly. When liquid level reaches the resin bed add five drops conc. HCl and try to wash glass walls with this. Permit to soak in and add about 1 ml. conc. HCl.

(8) Elute the aluminum plus some salt (NH_4Cl) with 12 ml. of 7 M HCl. (Note 4)

(9) Elute carrier-free niobium with 25 ml. of 4 M at a rate of 1 drop in 5 - 7 seconds.

(10) Evaporate the niobium fraction to near dryness and plate for counting.

Notes

(1) Complete mixing of tracer and reaction product is achieved in the homogeneous solution. All elements are oxidized to their highest valence state.

(2) Ammonium molybdate and ammonium pertechnate are soluble and thus not precipitated together with the aluminum.

(3) During most bombardments the precipitation of salt, be it $AlCl_3$ or NH_4Cl, was observed when the solution was saturated with HCl. This, however, did not interfere with the ion-exchange step.

(4) The specifications given in the procedure have to be rigidly observed as they are rather critical.

B. Chemical Separation

The (d, α) reaction products were separated from the bombarded targets by the carrier-free procedure given in Table XV. This chemical procedure followed in its outline very closely the ideas described for the zirconium-yttrium separation, and was found to be very dependable and effective.

The elution of niobium from the Dowex-2 column as carried out in the last step of the procedure is somewhat difficult and only approximately 60% of the niobium activity is removed by the 25 ml. of 4 M HCl. Formation of a radio-colloid at this HCl concentration inside the resin particles may be the reason for this behavior. At 50 ml. molybdenum starts eluting. A safety factor of 2 is thus observed, if only the 25 ml. fraction is retained.

Technetium was not found in the columns after elution with 50 ml. 2 M HCl, proving the precipitation steps a rather effective separation of niobium from that element.

C. Tracer for the Mo(d, α)Nb Reactions

The most readily available long-lived niobium isotope is the 35-day Nb^{95}.

1. Procurement.

To procure Nb^{95} in sufficient quantity it was separated from its parent Zr^{95} by the procedure given below. (Table XVI)

Table XVI

Chemical Separation of Niobium from Zirconium Targets

(carrier-free)

Element	Separated from	Decontamination Factor
Nb (carrier-free)	Zr^{95} from fission products	10^5

Time of Separation	Chemical Yield
4 hours	50%

Chemicals and Equipment

2 Pyrex beakers (50 ml.); centrifuge; 2 centrifuge cones 15 ml.; medicine droppers; platinum wire 6 inch; small anion exchange column (Fig. 20); zirconium carrier (10 mg/ml).

Dowex 2 resin (200 - 400 mesh); conductivity water; conc. H_2SO_4, HCl, NH_4OH; 30% H_2O_2; HCl-gas tank.

Procedures

(1) Destroy oxalate complex with 1 ml. conc. H_2SO_4 plus 3 drops 30% H_2O_2.

(2) Dilute with 10 ml. H_2O and precipitate zirconium-hydroxide with conc. NH_4OH. Centrifuge, wash once. Repeat step 2 once more.

(3) Dissolve precipitate with minimum amount conc. HCl, saturate with HCl gas and apply to small anion exchange column charged with 1 ml. Dowex 2 which had been saturated with conc. HCl.

(4) Absorb slowly. When liquid level reaches the resin bed add 10 drops conc. HCl and try to wash sides of column wall. Permit to soak in.

(5) Elute elements like alkalis, earths and zirconium with two 5 ml. portions of 7 M HCl.

(6) Elute Nb^{95} tracer with 7 ml. of 2 M HCl made up with conductivity water. Discard the first ml. and use rest as tracer.

A first attempt to identify Nb^{95} in the separated fraction indicated that the old Zr^{95} sample on hand contained several extraneous activities. A new sample was thus obtained from the Oak Ridge National Laboratory. The latter was purified by the procedure given in Table XVI.

2. Identification and Use as Tracer.

The tracer thus purified was identified by its γ-ray spectrum seen in Fig. 56. The Nb^{95} tracer was not used for any experiments until all of the 84-hour Nb^{95m} had decayed out so as not to complicate matters unduely.

The method used for tracing the niobium fraction of the bombardment product from molybdenum varied from that described for the zirconium bombardments. Three tracer samples were prepared and mounted on gold-plated Zapon film. Two had equal amounts of activity and one ten-times their strength. Relative counting rates for all three samples were obtained for the identical setting and geometry with a γ counter counting the photopeak of the 0.74-Mev γ ray of Nb^{95}. The two weaker samples were counted in addition in the 4π counter and their counting rate ratio established. One of these samples was used as tracer for the bombardment and the other two preserved.

After all but the Nb^{95} component had decayed out of the sample from the molybdenum bombardment, counts were again taken with a γ counter and 4π counter and the ratios of the count rates established. After subtraction of the Nb^{95}

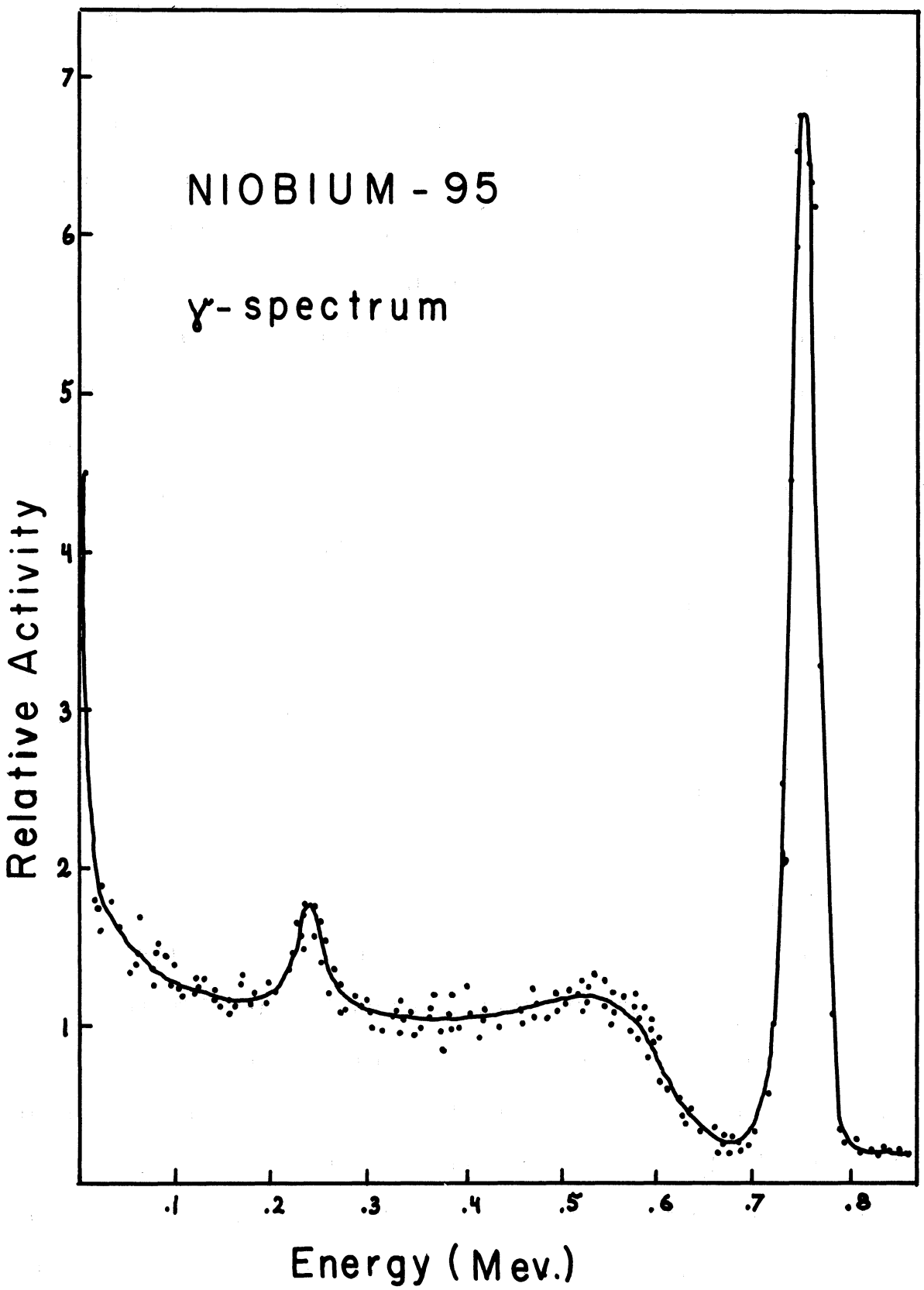

Fig. 56. Gamma Spectrum of Nb^{95} Tracer

fraction stemming from the $Mo^{97}(d, \alpha)Nb^{95}$ reaction the chemical yield could be established immediately without further extrapolation to the time before the bombardment.

This procedure has the advantage of being independent of the counters which may vary in their efficiency from day to day. It is also independent of the accurate knowledge of the decay constant of the tracer. These two facts make the method preferable, if enough pure tracer activity is available. The only requirement for the method is, that the tracer has been purified previously by the same method by which the sample from the bombardment is purified afterwards.

D. Records of the Bombardments

Four bombardments were obtained to determine the cross sections and excitation functions of the Mo(d, α)Nb reactions.

Bombardment 5 served to check the dependability of the chemical separation procedure and to identify the reaction products. The relative yields of the product activities was established by bombardment 14 for a two-hour bombardment with 7.8-Mev deuterons. The ratio determined between the count rates of the Nb^{95} component and the other activities was to be used in the yield calculations for the absolute cross-section experiment of bombardment 18.

The molybdenum target was exposed to the full energy

beam in bombardment 18. The niobium product was chemically separated from the bombarded target together with 31,000 c/m Nb^{95} added tracer. The separated niobium fraction was followed in its decay with a 4π counter over a period of several months. To establish the absolute count rate of the Nb^{95} component a self-absorption correction had to be applied. This correction was determined by the method described in section III-D-1 of part 2 and found to be $6 \pm 1\%$ for the sample counted.

The primary data and the cross section values for the $Mo^{97}(d, \alpha)Nb^{95}$, $Mo^{97}(d, \alpha)Nb^{95m}$, $Mo^{98}(d, \alpha)Nb^{96}$ and $Mo^{92}(d, \alpha)Nb^{90}$ reactions are reported in Table XVII. An internal-conversion coefficient of 90% was assumed for the 0.23-Mev γ ray of Nb^{95m}. No corrections were applied for any electron-capture processes accompanying the decay of Nb^{90}. The errors quoted in Table XVII were estimated in the same way as was discussed for the zirconium bombardments. The values are based entirely on the experimental data as obtained with the 4π counters.

The decay curve obtained from bombardment 18 is seen in Fig. 57. The size of the points of these figures is in no relation to the experimental errors which were much less than the circles indicate. Only with gross data of this type was it possible to analyze the four component decay curve of the niobium reaction product with the small errors quoted.

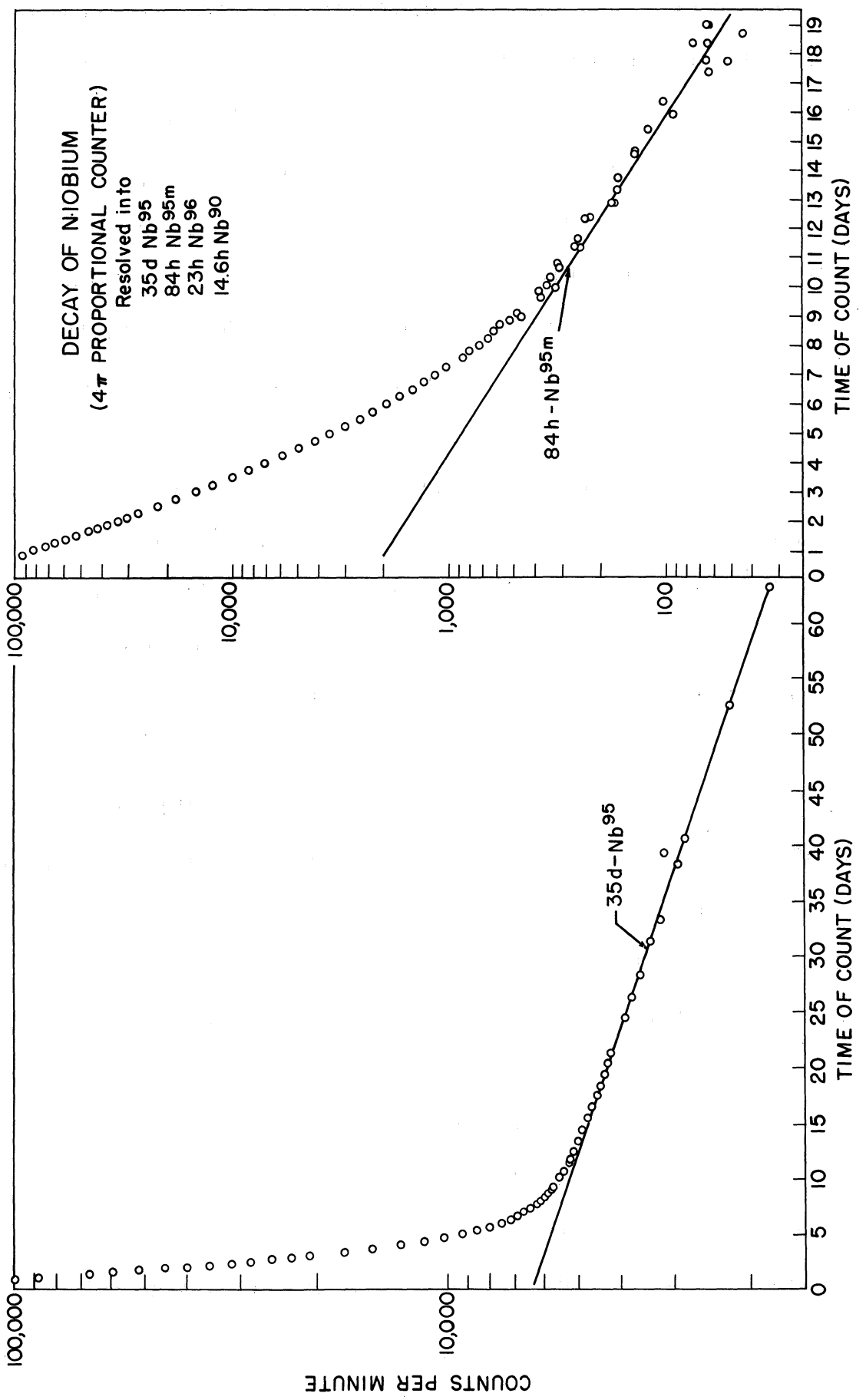

Fig. 57. Complex β-ray Decay Curve of Niobium from Bombardment 18

Table XVII. Results of the Mo(d, α)Nb Cross Section Determinations

Bombardment No.	Type	Average Deuteron Energy Mev	C_i	Chem. Yield %	Count Rate* c/m	Target thickness mg/cm^2	σ millibarns
				The $Mo^{97}(d, \alpha)Nb^{95}$ Reaction			
18	abs.	7.71±0.05	5496±1%	18.7±1.6%	537±2.5%	4.992±0.1%	2.35±6%
14	rel.	7.54±0.05	-	±5%	1,999±1.5%	4.959±0.1%	-
15	rel.	7.54±0.05	-	±5%	120±3%	4.8±2%	2.3±10%
15	rel.	5.61±0.1	-	±5%	85±5%	4.86±2%	1.63±10%
15	rel.	3.82±0.25	-	±5%	34±10%	4.9±2%	0.65±20%
15	rel.	2.25±0.3	-	±5%	3.3±20%	4.85±2%	0.6±50%
				The $Mo^{97}(d, \alpha)Nb^{95m}$ Reaction			
18	abs.	7.71±0.05	5496±1%	18.7±1.6%	2,058±5%	4.992±0.1%	0.98±10%
				The $Mo^{98}(d, \alpha)Nb^{96}$ Reaction			
18	abs.	7.71±0.05	5496±1%	18.7±1.6%	54,859±1.5%	4.992±0.1%	2.53±5%
				The $Mo^{92}(d, \alpha)Nb^{90}$ Reaction			
18	abs.	7.71±0.05	5496±1%	18.7±1.6%	66,187±1.5%	4.992±0.1%	2.95±5%

* For absolute experiments count rate at the end of the bombardment, for relative experiments at some later time.

Bombardment 15 was performed to establish the relative excitation functions for the Mo(d, α)Nb reactions. A stacked foil technique with aluminum absorber substrates was used as in bombardment 13 mentioned above for zirconium. The arrangement of the targets and absorbers for this experiment is given in Table XVIII.No tracers were employed for the yield evaluation, but strict conformity of the simultaneously performed separations permitted an error limit of not more than about ±5% for the chemical yields.

The six samples obtained from this bombardment were counted in sequence with the proportional counter. Counts were taken continuously for five days following the bombardment to permit resolution of the 14.6-hour Nb^{90} and the 23-hour Nb^{96}. The remaining activities stemming from Nb^{95} and Nb^{95m} were followed in their decay for an additional two months to permit good resolution of the curves.

The relative cross sections for Nb^{95} are normalized to the absolute value obtained in bombardment 18 and entered in Table XVII. A plot of the excitation curve for the Mo^{97}(d, α)Nb^{95} reaction is seen in Fig. 60.

Gamma spectra were taken twice during the decay of the niobium sample from bombardment 18. They can be seen in Fig. 59 indicating a strong enrichment of the 0.76-Mev Nb^{95} line with time.

Table XVIII. Arrangement of Molybdenum Targets for Bombardment 15

Target or Absorber	Thickness (mg/cm^2)	Average Deuteron Energy Mev
Mylar	1.76	
Mo I	4.79	7.54
Aluminum	11.32	
Mo II	4.85	5.61
Aluminum	14.75	
Mo II	4.91	3.82
Aluminum	8.93	
Mo IV	4.84	2.25
Aluminum	4.46	
Mo V	5.06	1.0
Aluminum	4.46	
Mo VI	4.80	0 *
Aluminum	4.46	
Mo VII	5.00	0 *
Aluminum	14.75	
Mo VIII	5.00	0 *

* These targets served to check the presence of products from neutron-induced reactions.

E. Resolution of the Decay Curves

The decay curve of the niobium product from bombardment 18, seen in Figs. 57 and 58, may serve as an illustration of the resolution problems encountered. The 35-day Nb^{95} and 84-hour Nb^{95m} activities could be subtracted from the gross β-decay curve by the same procedure employed for resolving the yttrium curves described earlier. The resulting two-component curve could not be analyzed, however, by continued subtraction. The following consideration aided in its resolution:

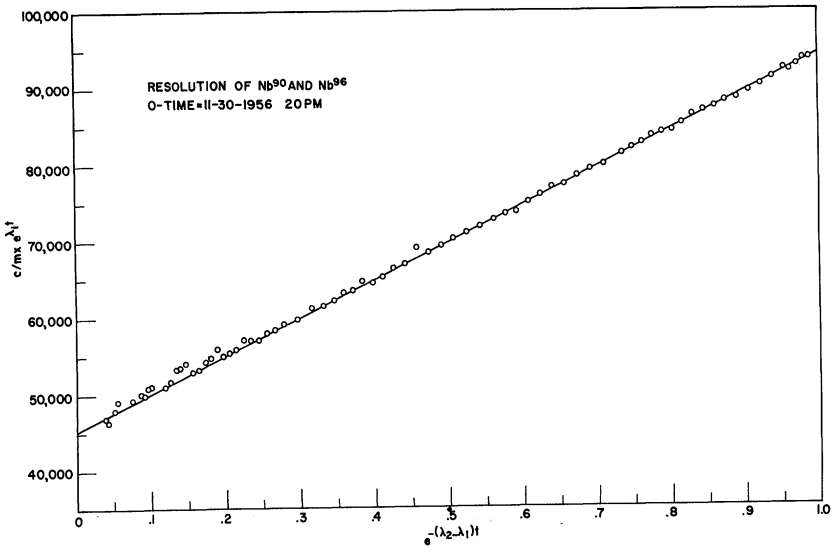

Fig. 58. Resolution of the Nb^{90} and Nb^{96} components of the niobium decay curve from bombardment 18 (cf Fig. 57)

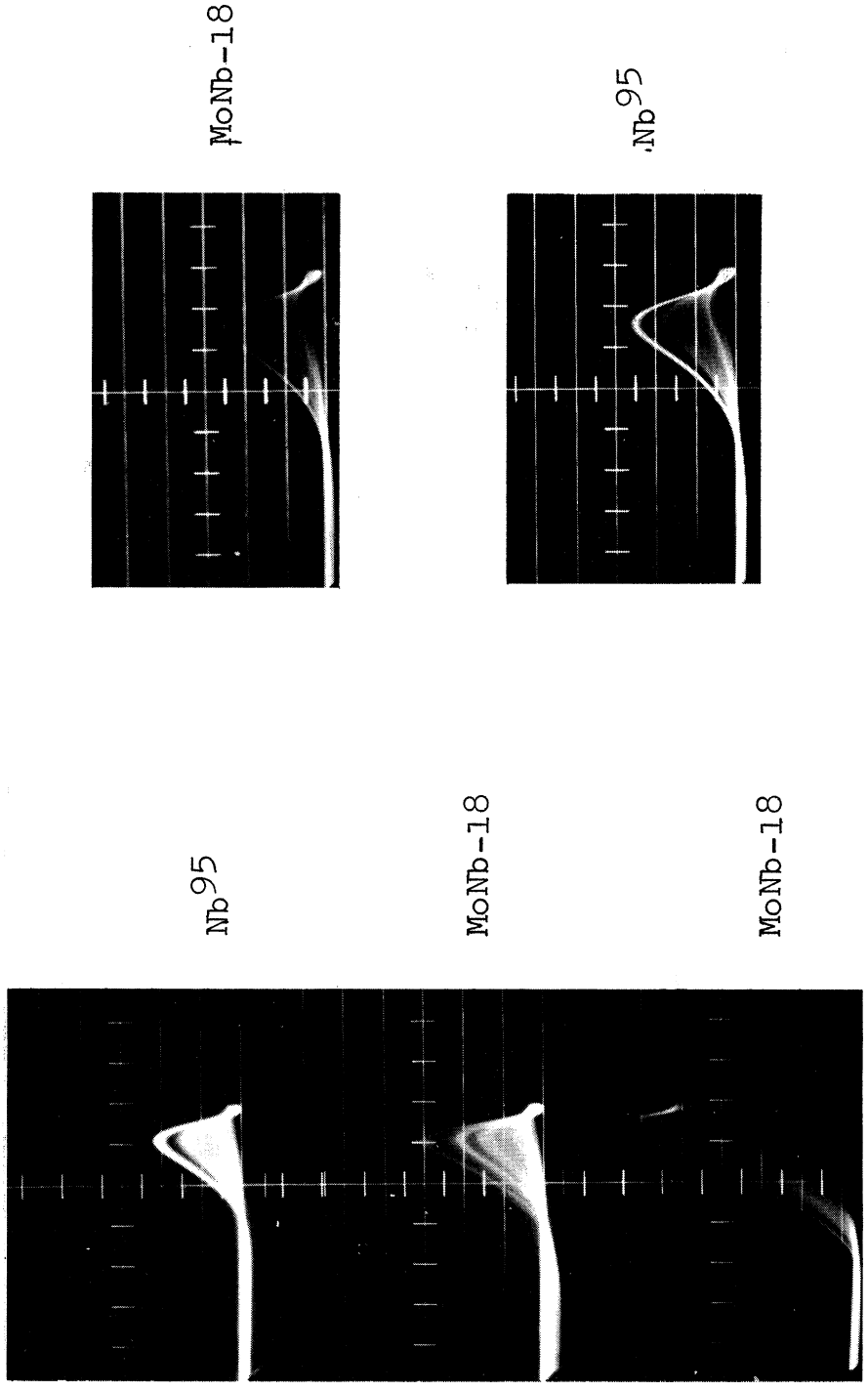

Fig. 59. Gamma Spectra of Niobium Sample from Bombardment 18, one day and ten days after bombardment. (Nb^{95} spectra for energy calibration)

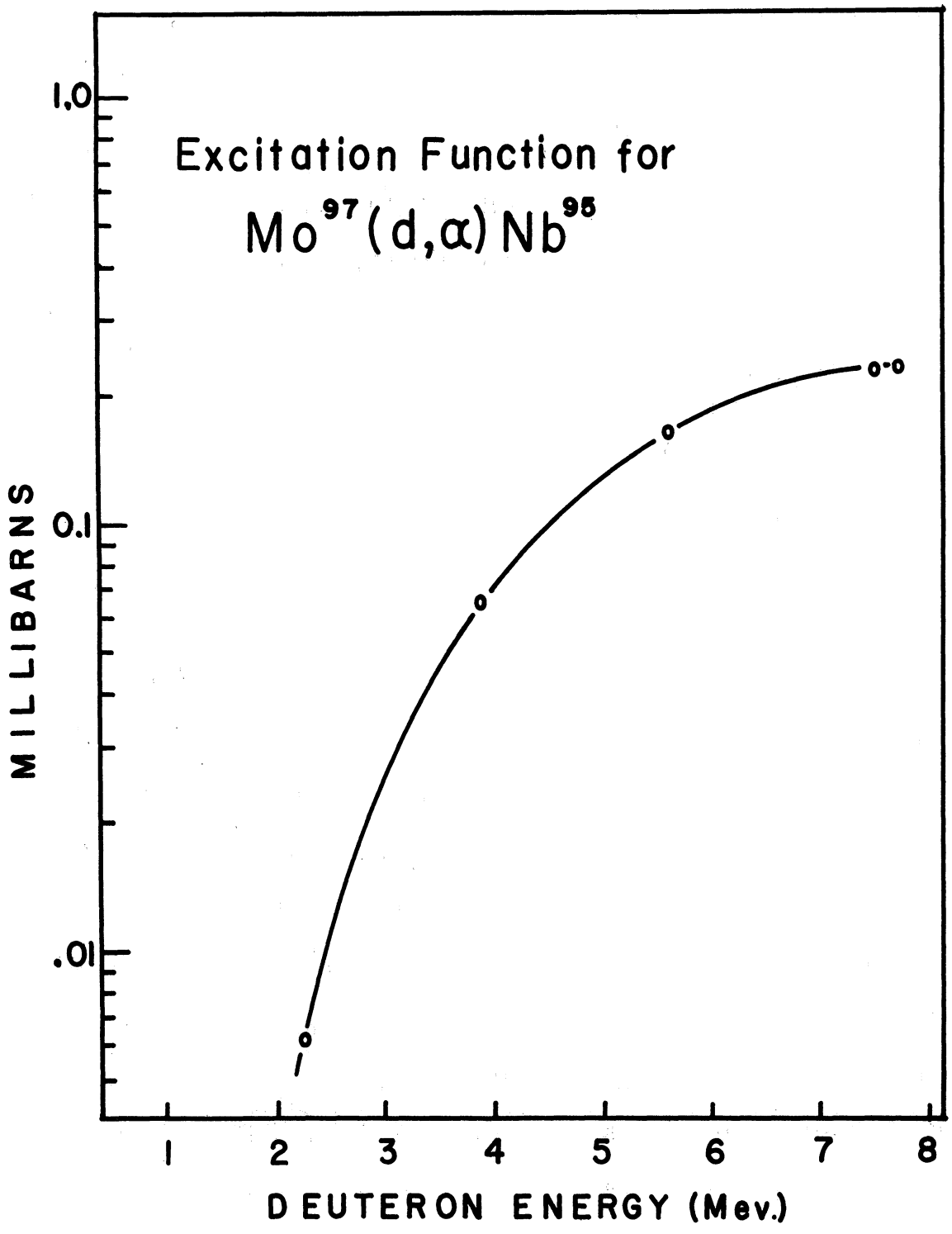

Fig. 60. Excitation Function for the $Mo^{97}(d, \alpha)Nb^{95}$ Reaction

The decay rate of a sample containing two radioactive species is given by:

$$A = A_1 e^{-\lambda_1 t} + A_2 e^{-\lambda_2 t}$$

where λ_1 is the decay constant of the longer lived, and λ_2 the decay constant of the shorter-lived activity. Transposition of above equation yields:

$$Ae^{\lambda_1 t} = A_1 + A_2 e^{-(\lambda_2 - \lambda_1)t}$$

or

$$Ae^{\lambda_1 t} = A_1 + A_2 e^{-\Delta\lambda t}$$

It is seen from the last equation that a plot of $Ae^{\lambda_1 t}$ vs. $e^{-\Delta\lambda t}$ will yield a straight line with an intercept at $e^{-\Delta\lambda t} = 0$ or $t = \infty$ representing A_1 and a value for $t = 0$ or $e^{-\Delta\lambda t} = 1$ representing $A_1 + A_2$, the sum of the decay rates of the two components at time 0.

A plot of this type is given in Fig. 58 for the Nb^{90} and Nb^{96} components of the niobium decay curve from bombardment 18. For this type analysis the exact knowledge of the decay constants is very essential. Resolution of the two components was possible within approximately 1.5% for the two components. The labor involved in this analysis, however, was extensive.

IV. The Ti(d, α)Sc Reactions

The titanium reactions were considered of interest partly for the challenging chemical problems and the fact that Ti^{50} containing 28 neutrons is a magic nucleus. Hall attempted the cross section determination of the $Ti^{48}(d, \alpha)Sc^{46}$ reaction but obtained only rather uncertain values. His main difficulties rested with the chemical separation employed and the fact that no 0.0001-inch titanium foils were available to him.

The chart of the nuclei in the titanium region is seen in Fig. 61. Six half-lives should be expected in the (d, α) reaction products on a titanium target. Five of these were observed in the present studies. Only the 20-sec isomer of Sc^{46} had decayed out by the time the separated reaction products could be counted. The isotopes observed in the reaction products were the following:

a) The 44-hour Sc^{48}, emitter of a 0.64-Mev β ray and several γ-rays.

b) The 81-hour Sc^{47}, emitting a 0.44-Mev or 0.60 Mev negatron as well as a 0.16 Mev x-ray.

c) The 85-day Sc^{46}, emitting a weak 0.36-Mev β particle with two γ rays.

d) The 4.1-hour Sc^{44}, emitting a 1.47-Mev positron together with several γ rays.

e) The isomeric Sc^{44m} decaying by internal transition with emission of a 0.14-Mev γ ray with a half-life of 57 hours.

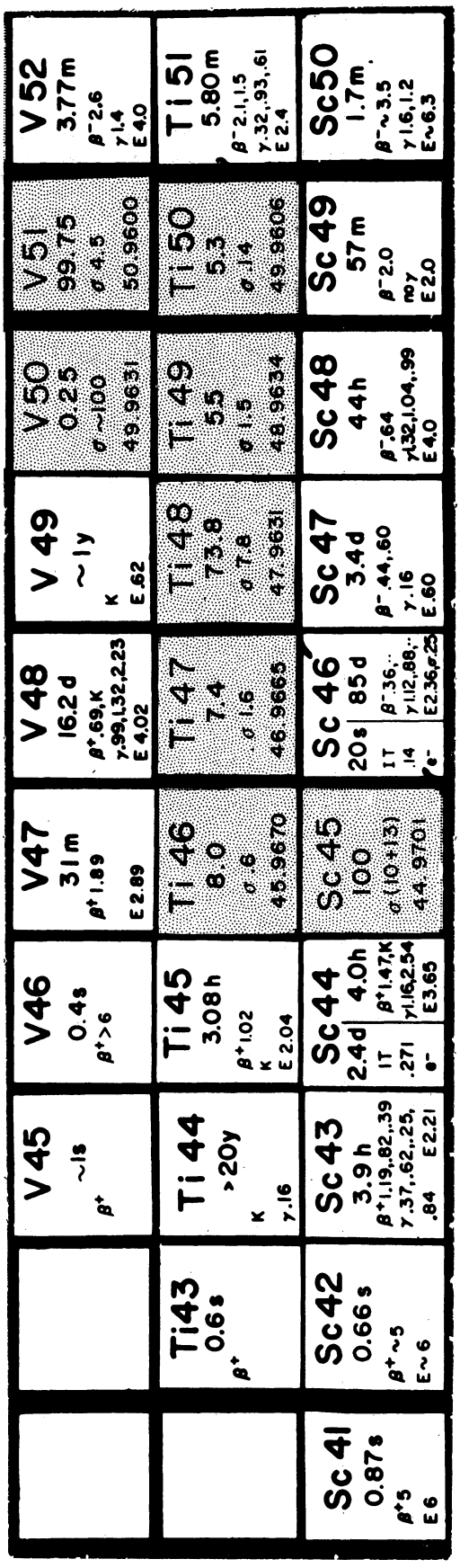

Fig. 61. Chart of Nuclides in the Titanium Region (for explanation see Fig. 48)

Table XIX. Properties of Scandium Isotopes Encountered in this Research

Isotope	Half-life	Reference	Radiation	Relative amount	Energy	Reference
Sc^{44}	3.92 hrs.	124	EC	6±1%	4.0 Kev	124
	3.90	124		~2%		
	3.96	124	β^+	94%	1.47 Mev	124
	4.10±2% *	5	γ_1	~100%	1.16	
			γ_2	0.12%	2.54	
Sc^{44m}	2.44 days	124	γ	100%	0.27	124
	2.46	124				
Sc^{46}	85 days *	124	β_1^-	100%	0.36	124
	84	124	β_2	1%	1.48	124
				1%	1.25	68
			γ_1		0.885	124
			γ_2		1.119	124
			γ_3	10^{-5}%	2.23	124

* value used for calculation

Table XIX (continued)

Isotope	Half-life	Reference	Radiation	Relative amount	Energy	Reference
Sc^{47}	3.43 days	124	β_1^-	74%	0.450	124
	3.40	124				
	3.3	5	β_1^-	26%	0.610	124
	3.45	79	γ	100+	0.160	124
					0.185	
Sc^{48}	1.83 days	124	β^-	100%	0.64	
			γ_1	100%	0.99	
			γ_2	100%	1.04	
			γ_3	100%	1.33	

A summary of the decay characteristics of these isotopes is given in Table XIX.

Although very good data were obtained for the decay curves of the Ti(d, α)Sc reaction products as can be seen in Fig. 62, resolution of the curve was only possible for the 85-day Sc^{46} activity and the 4.1-hour Sc^{44}. The combined components due to the 44-hour Sc^{48}, the 57-hour Sc^{44m} and the 81-hour Sc^{47} forming the 62-hour component seen in Fig. 62 could not be resolved into the three activities by the means available. This made the determination of the cross sections for the Ti^{50}(d, α)Sc^{48}, Ti^{49}(d, α)Sc^{47} and Ti(d, α)Sc^{44m} reactions impossible. The value reported for the (d, α) reaction on Ti^{46} is to be considered only a partial cross-section value, since the amount of Sc^{44m} could not be measured and simultaneous decay of the Sc^{44} by the electron-capture process was not entered into the calculations. Application of a correction for the latter effect would increase the value obtained for the (d, α) cross section by about 6 ± 1%; the relative yield of the Ti^{46}(d, α)Sc^{44m} reaction is estimated to be of the order of 5% compared to the Ti^{46}(d, α)Sc^{44} reaction.

A. Targets

Again, as in the cases of zirconium and molybdenum, thin titanium foils were used for the targets. The foils were rolled to a thickness of 4.4 mg/cm^2 (0.15 mil) by the Arnold Engineering Company from 2-mil titanium stock, kindly supplied by the

Titanium Corporation of America. These foils were cut with the die, mentioned previously, and mounted on Mylar. The average thickness of the foil disks was determined by weighing with a micro-balance within ± 0.1% and the uniformity of the thickness checked with the Pm^{147} gauge (± 3%).

B. Chemical Separations

The chemical procedure for separating the scandium reaction products from the bombarded targets combined a radio-colloid purification step with an anion exchange separation. The yields were relatively small for this separation, but the effected purification excellent (Table XX).

After preliminary separation from vanadium, the bulk of titanium was reduced to approximately 1/20 by a homogeneous precipitation of $Ti(OH)_4$ while the Sc^{+++} remained in solution. The anion-exchange step was carried out in a strongly oxidizing medium which permitted the titanium and vanadium to remain in their highest oxidation states. Ti^{+4} and V^{+5} were not eluted from the Dowex-2 column by more than 50 ml conc HCl - $KClO_3$ under these conditions (Table II).

The final "radio-colloid" step (43) freed the carrier-free scandium from any macro amounts of NaCl and $KClO_3$ which accompanied it in the eluate from the anion-exchange separation. The carrier-free scandium activity was then obtained by elution from the filter paper with 4 M HCl.

Table XX

Chemical Separation of Scandium from Titanium Targets

(carrier-free)

Element	Separated from	Decontamination Factor
Sc (carrier-free)	d. bombarded Ti	10^5

Time of Separation	Chemical Yield
4 hours	50%

Chemicals and Equipment

4 Pyrex beakers (50 ml); centrifuge; centrifuge tubes 40 ml., 15 ml.; platinum wire 6 inch; Erlenmeyer flask 250 ml.; medicine droppers; glass fritt filter funnel, coarse; Whatman 42 filter paper; micropipet 50λ; small ion-exchange column Fig. 20.

Dowex-2 resin (200 - 400 mesh); conductivity water; conc. H_2SO_4, HNO_3, HCl, NH_4OH; 30% H_2O_2; NaOH (solid pellets); $NaHCO_3$ (saturated solution); $KClO_3$ (crystals); HCl-gas tank.

Procedures

(1) Place tracer scandium in small beaker, add Mylar substrate. Add 2 ml conc H_2SO_4 plus a few drops of 30% H_2O_2. Add bombarded titanium foil, heat until dissolved. Oxidize purple solution with few drops of HNO_3 (some TiO_2 precipitates at this point, if solution is too hot, but this does not interfere). (Note 1)

(2) Transfer to 50 ml centrifuge cone and precipitate $TiO_2 \cdot aq$. with several pellets of NaOH. Wash twice.

(3) Dissolve with conc HCl. (If solution is not complete, try adding water and heat gently). Centrifuge and transfer supernate to another centrifuge cone.

(4) Add slowly a saturated solution of $NaHCO_3$ until initial precipitate still dissolves on stirring. (Note 2)

(5) Heat gently to effect homogeneous precipitation of $TiO_2 \cdot aq$. Do not permit the pH to rise above about 5.5.

(6) Repeat steps 3, 4 and 5 and combine the supernate with that of step 5.

(7) Saturate combined supernates with HCl gas (Cool!). Centrifuge off the NaCl.

(8) Evaporate to 5 ml and repeat step 7.

Table XX (continued)

(9) Add a crystal of $KClO_3$, shake and transfer to a small anion exchange column charged with 1 ml. Dowex-2 resin which has been saturated with conc. HCl containing a few mg $KClO_3$ per 100 ml.

(10) Permit to absorb. When liquid level reaches the resin bed add five drops of conc. HCl with $KClO_3$ and permit again to reach the bed-level. Elute the scandium activity with approximately 12 ml. conc. HCl-$KClO_3$. (Check with monitor when activity is eluted).

(11) Pour the eluate rapidly into a 250 ml. Erlenmeyer flask containing 30 ml. of a solution made of 11 parts 8 N NH_4OH and 1 part 30% H_2O_2. Shake vigorously. (Note 3)

(12) After fumes subside, cool the clear solution and pass it twice through a double-layer of Whatman 42 filter paper positioned over a glass-frit funnel. (The scandium activity remains on the filter in radio-colloidal form).

(13) Wash filter paper with 10 ml. of the mixture of step 11 to which about 3 ml. conc. HCl has been added.

(14) Wash with 5 ml. alkaline distilled water followed by a wash with 5 ml. conductivity water.

(15) Elute the scandium activity from the filter paper by passing 5 ml. of 4 M HCl twice through the filter paper (some of the activity will still remain on the paper, but most of it will be eluted).

(16) Evaporate to near dryness and plate for counting.

Notes

(1) The Mylar is dissolved first, since titanium forms a precipitate in hot conc. H_2SO_4 solution containing peroxide.

(2) $Ti(OH)_4$ is precipitated homogeneously from a solution of pH 2, while the $Sc(OH)_3$ precipitates only from a pH of 7.

(3) A sudden increase of the pH in a strongly oxidizing medium transforms any titanium present into the titanate ion whose ammonium salt is soluble, while the trace amount of scandium, being insoluble in the medium "precipitates" in the form of a radio-colloid.

At times it was possible to elute only about 3/4 of the scandium from the filter paper to which it is very strongly adsorbed. Relatively low yields were the results of this effect.

C. Tracer for the Ti(d, α)Sc Reactions

The most readily available long-lived scandium isotope is Sc^{46} with a half-life of 85 days. This isotope was obtained in carrier-free form from the Oak Ridge National Laboratory and stored for approximately one year. To ensure a pure tracer, the Sc^{46} activity was purified previously to bombardment 19 by the same chemical procedure as given in Table XX. Some inactive Ti foil was added to serve as carrier of the scandium during the first steps. The tracer Sc^{46} was identified by its γ spectrum and half-life. The spectrum is seen in Fig. 63.

The method used for tracing the scandium fraction of the titanium bombardments followed in essence the method described above for the Mo(d, α)Nb bombardments. Two Sc^{46} samples were prepared and the 1.12-Mev photopeak of the γ spectrum counted. The counting rate ratio for γ rays in the two samples was thus established. One of the samples (A) was used in tracing the chemical separation, the other (B) preserved for later comparison. After the short-lived activities of the bombardment product had decayed out, the ratio of the sample (C) from the bombard-

ment product and tracer sample (B) was determined. At the same time the ratio between the sample (B) and the bombardment product from a previous bombardment, for which no Sc^{46} tracer had been used, was determined. This ratio was normalized to the time of the end of the absolute bombardment and to the same activity of the shorter-lived reaction products. (Bombardments of equal lengths were used for this comparison). From these ratios the amount of Sc^{46} present in sample (C) due to the $Ti^{48}(d, \alpha)Sc^{46}$ reaction could be calculated and subtracted from the total Sc^{46} activity. The remainder, stemming from the added tracer, was then used to determine the chemical yield. It is estimated that an error of less than 2% was introduced in this experiment by the tracing.

D. Record of the Bombardments

The absolute cross sections of the Ti(d, α)Sc reactions for 7.7-Mev deuterons were determined with the aid of two bombardments. Bombardment 17 served to check the chemical procedure and establish the identities as well as the relative yields of the reaction products. The latter was important for the yield determination of the tracer experiment of bombardment 19. Counts were taken with the 4π counters as well as with the γ-ray spectrometer.

Two 4π-counter samples were made from the bombardment product, one weaker to follow the short lived Sc^{44} and one approximately 29 times as strong to follow the longer-lived components. The ratio of the counting rates of the two samples was carefully determined after the Sc^{44} activity had decayed out, and the curves, corrected for background and coincidences, combined into one. This procedure permitted to count samples not exceeding 100,000 c/m and yet left a strong enough sample to follow the 85-day Sc^{46} component over many half-lives.

The complex β-decay curve of the scandium fraction from bombardment 17 is seen in Fig. 62. Many more points were taken than are indicated in the figure. Those presented are, however, typical for the data obtained.

The titanium target was exposed to the full energy of the cyclotron beam in bombardment 19. After the chemical separation two samples were prepared. One was followed in its decay with the 4π counter, the other for a period of two days with the γ-ray spectrometer. Spectra of this sample taken at various times after the bombardment can be seen in Fig. 63 giving an indication of their complexity. From a sequence of spectra taken by automatically sweeping the γ-ray spectrum for a period of two days following the bombardment, the decay of the 0.5-Mev positron annihilation line could be followed. It decayed with a half-life of approximately 4 hours, eventually going into a much longer half-life.

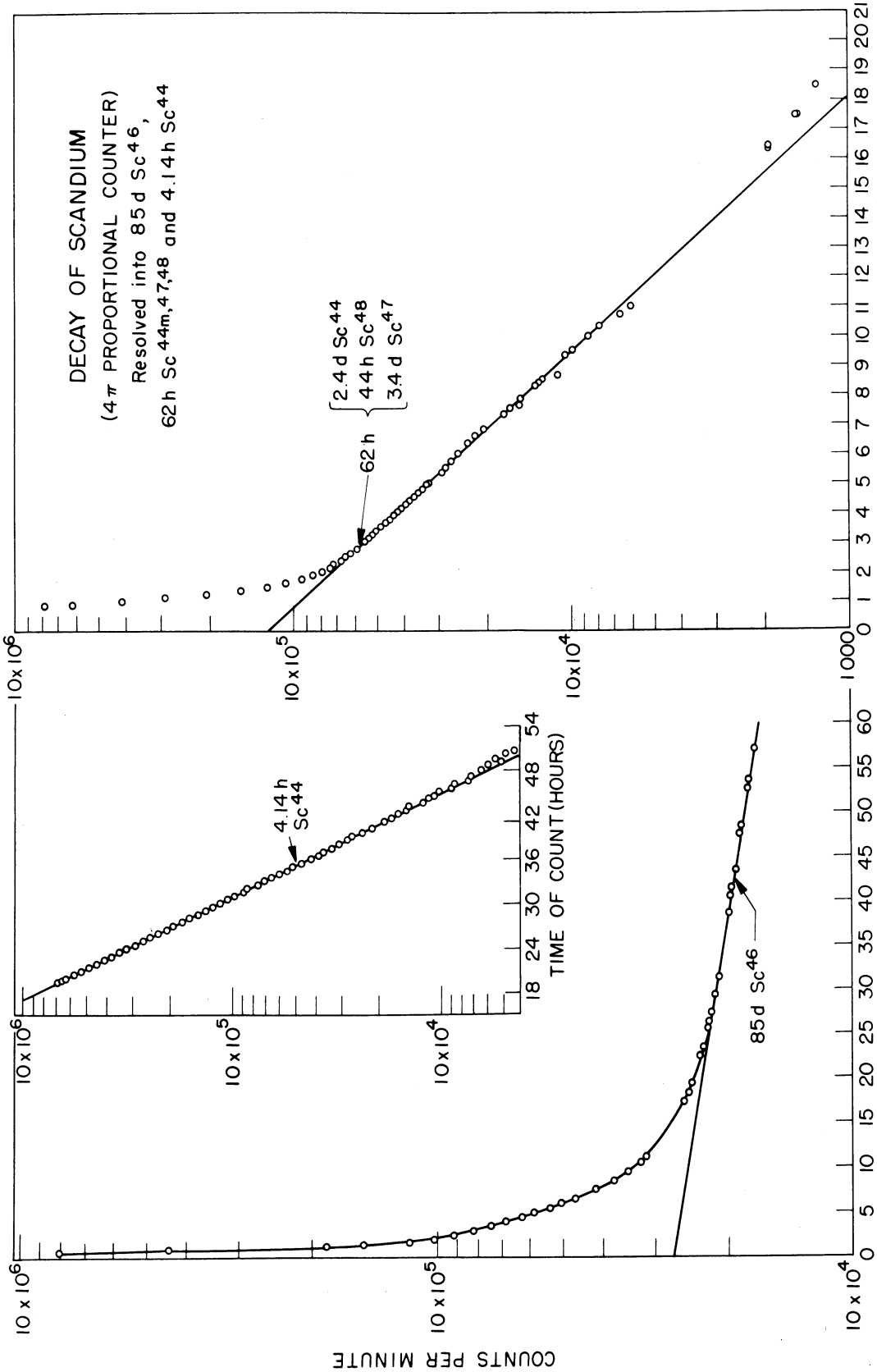

Fig. 62. Complex β-ray Decay Curve of Scandium from Bombardment 17

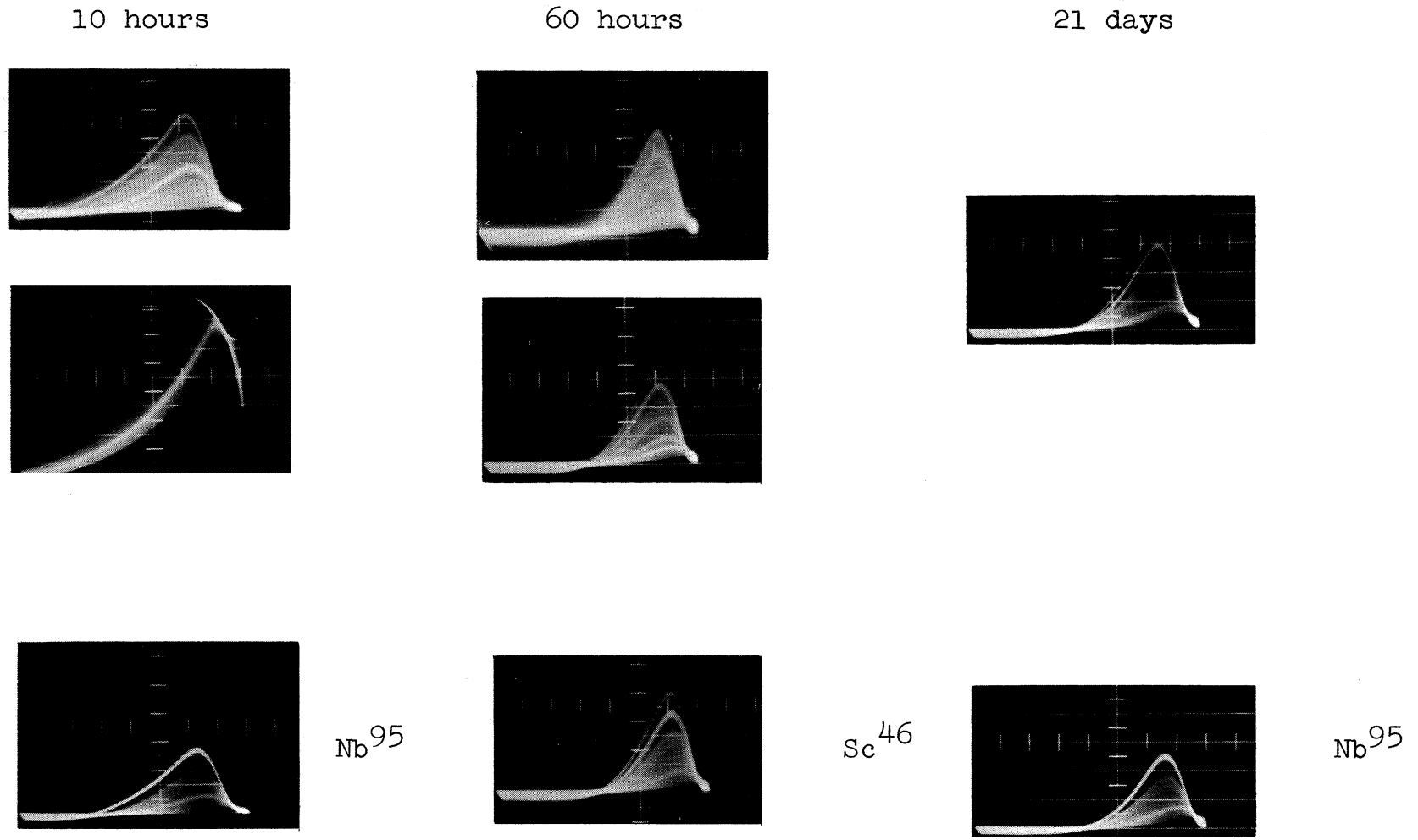

Fig. 63. Gamma Spectra of Scandium, ten and sixty hours and 21 days after the end of bombardment 19. (Reference standards of niobium-95 and scandium 46)

The results from bombardment 19 are given in Table XXI. Self-absorption of 1% was applied for the Sc^{46} count rates as determined by Hall (55). The error estimates are again based on the principles discussed for the case of the zirconium bombardments. The somewhat larger error in the count rate determination of the Sc^{46} is due to the uncertainty caused by using this isotope as the tracer for the chemical yield.

As was mentioned above, the cross-section value reported for the $Ti^{46}(d, \alpha)Sc^{44}$ does not include the $Ti^{46}(d, \alpha)Sc^{44m}$ reaction and has thus to be considered as a partial cross section. This is in contrast to the case of the $Mo^{97}(d, \alpha)Nb^{95}$ reaction mentioned earlier where the $Mo^{97}(d, \alpha)Nb^{95m}$ was included into the cross section value of the over-all reaction.

E. Resolution of the Decay Curves

Figure 62 represents the complex decay curve of the scandium product from bombardment 17 as obtained with the 4π counter. A partial analysis into its Sc^{46} and Sc^{44} components was obtained by the method of consecutive subtraction discussed for the zirconium bombardments. Resolution of the combined Sc^{44m}, Sc^{47} and Sc^{48} yielded an average half-life of approximately 62 hours which could not be resolved any further with the means available.

Table XXI. Results of the Ti(d, α)Sc Cross Section Determination

Bombardment No.	Type	Average Deuteron Energy Mev	C_i	Chem. Yield %	Count Rate* c/m	Target thickness mg/cm^2	σ millibarns
				The $Ti^{48}(d, \alpha)Sc^{46}$ Reaction			
19	abs.	7.71±0.05	3362.1±1%	3.83±1.5%	5,037±2.5%	4.525±0.1%	28.53±6%
17	rel.	7.71±0.05	3500±1%	-	26,742±1.5%	4.464±0.1%	
				The $Ti^{46}(d, \alpha)Sc^{44}$ Reaction			
19	abs.	7.71±0.05	3362.1±1%	3.83±1.5%	456,144±1.5%	4.525±0.1%	52.39±5%

* Count rate at the end of the bombardment

V. The $S^{34}(d, \alpha)P^{32}$ Reaction

The S^{34} reaction was considered of value for this research to establish the trend of the (d, α) reactions for non-magic number nuclei in the low-atomic weight range. Hall (54) attempted the determination of the cross section for this reaction, but experienced difficulties with the elemental sulfur targets employed, thus introducing rather large uncertainties in his values.

The chart of the nuclides in the sulfur region is given in Fig. 64. There are three phosphorus isotopes obtainable by the (d, α) reaction on sulfur. Only one of them, however, has a long enough half-life to be observable after the chemical separations necessary to obtain it in carrier-free form. Only P^{32} was thus observed in these investigations. This isotope decays by emission of a strong 1.71-Mev β particle without any γ radiation.

The half-life of P^{32} was of great importance for the analysis of the decay curves and had thus to be determined experimentally. The value of 14.221 ± 0.005 days determined in this work may be compared to some of the values found in the literature as given in Table XXII.

Most of the authors quoted in Table XXIIworked with P^{32} samples that were not pure and corrections had to be applied for the presence of S^{35} and P^{33}. The majority

NUCLIDE CHART OF THE SULFUR REGION

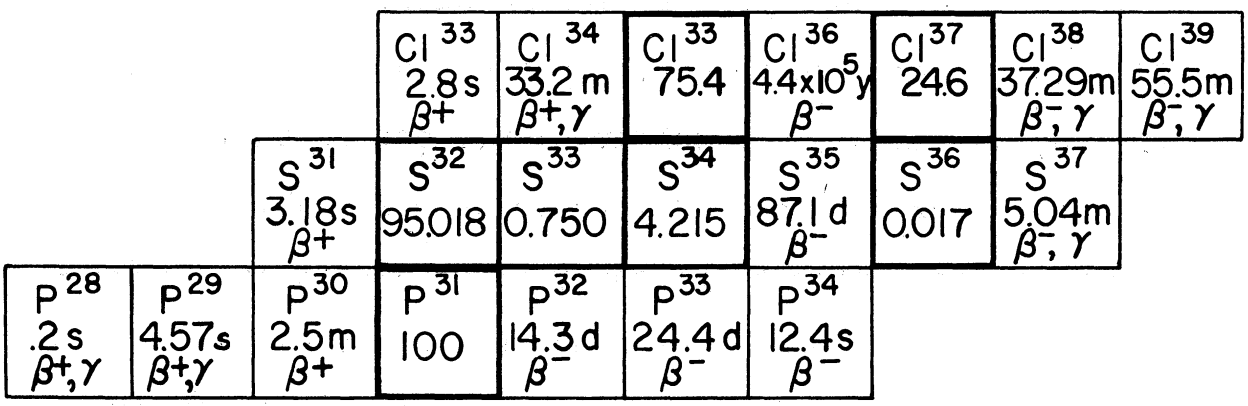

Fig. 64. Chart of Nuclides in the Sulfur Region

Table XXII. Summary of Half-lives Reported for Phosphorus-32

Half-life (days)	Authors	Period Observed	Method and Possible Difficulties
14.30 - 0.03	Cacciapuoti (6)		
14.08 - 0.07	Mulder, Hoeksema, Sizoo (92)	4 half-lives	GM counter and electroscope S^{35} impurity
14.35 - 0.05	Klema, Hanson (72)	2 half-lives	GM counter bremsstrahlen from S^{35} and, or P^{33}
14.60 - 0.05	Sinclair, Holloway (116)	3 half-lives	electroscope S^{35} and, or P^{32}
14.30 - 0.09	Bayly (8)	3 half-lives	calorimeter GM counter
14.50 - 0.02	Lockett, Thomas (78)	5 half-lives	electroscope S^{35}
14.221 - 0.005	this research	11 half-lives	4π proportional counter

of the determinations were made by following the decay of the P^{32} for less than six half-lives and carried out with instruments for which the reproducibility of the counting geometry, change of atmospheric conditions in the optical path and linearity of detection posed problems. The method used in this determination improved on the isotopic purity of the sample used, and avoided some of the errors by counting a carrier-free sample with a 4π counter. Following the decay for 11 half-lives increased the reliability of the experimental value (Fig. 65).

A. Target Preparation

Targets for the sulfur experiments were prepared by evaporating chemically pure ZnS onto roughened Mylar film in the high vacuum. (cf. section II-A-1 of part 2) The evenness of the deposit was tested with the Pm^{147} gauge and found to vary within less than 1% (the sensitivity limit of the gauge) over the entire target-area. The average thickness was determined to within 1% from the weight difference of the empty target frame plus Mylar substrate, and the weight after the ZnS had been deposited. The target area was defined by the area of the collimator-mask used in the deposition of the zinc sulfide.

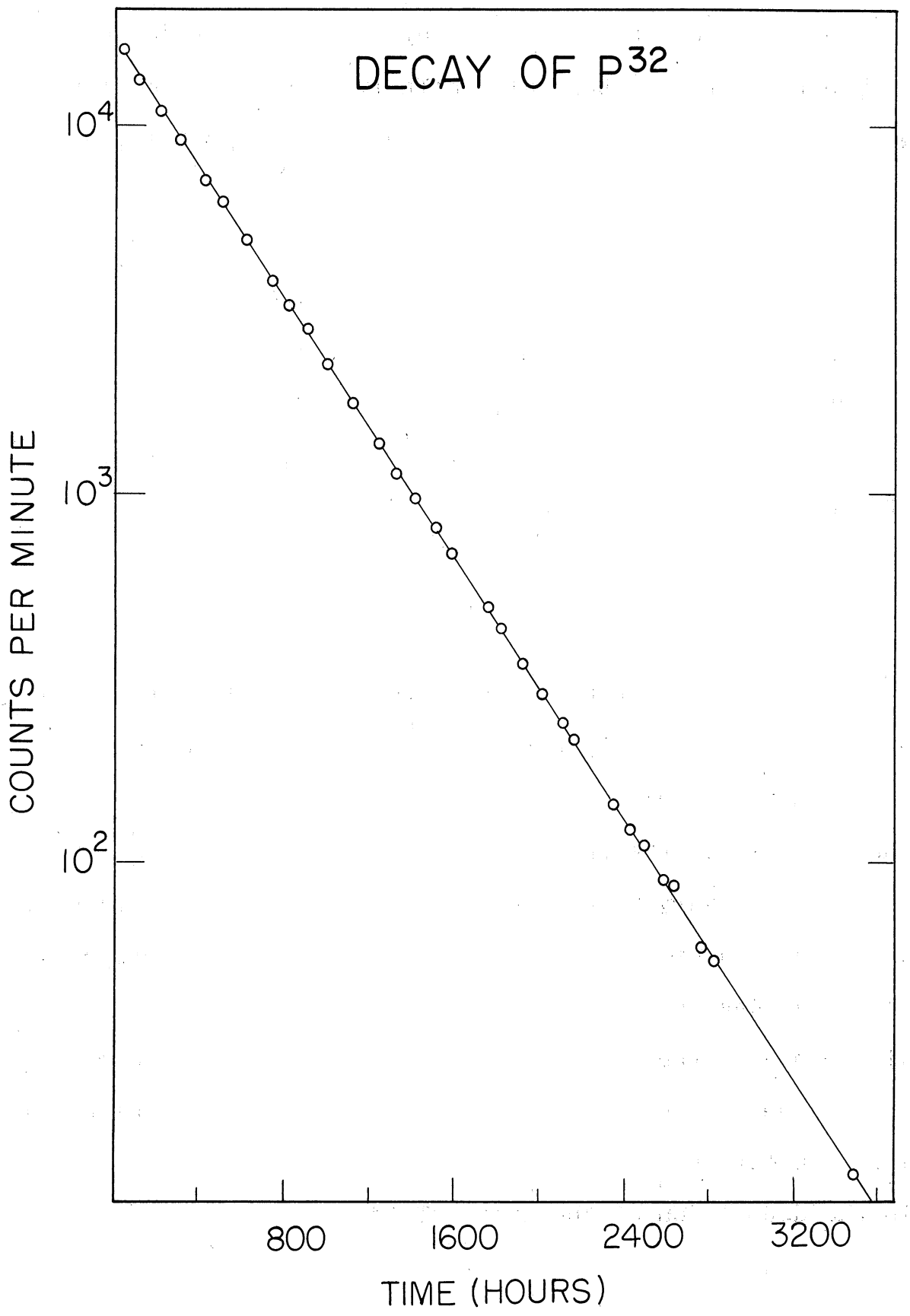

Fig. 65. β-ray Decay Curve of P^{32} from Bombardment 1 over 11 half-lives

Table XXIII

Chemical Separation of Phosphorus from Zinc Sulfide Targets

(carrier-free)

Element	Separated from	Decontamination Factor
P (carrier-free)	d. bombarded ZnS	10^4

Time of Separation	Chemical Yield
6 hours	70%

Chemicals and Equipment

Pyrex beakers (800 ml); 1 Phillips beaker (250 ml); centrifuge; pH meter; 2 centrifuge tubes, 50 ml; Erlenmeyer flask, 1000 ml; 3 ion exchange columns, 25 cm long, 1 cm diameter.

Dowex 50 resin (100 - 200 mesh); $FeCl_3$ solution (1/2 saturated); bromine; carbon tetrachloride; conc. HNO_3, H_2SO_4; NaOH(pellets); Na_2CO_3 powder; conductivity water; 30% H_2O_2.

Procedures

(1) Place target into 250 ml. Phillips beaker containing the P^{33} tracer plated on Zapon film. Add a mixture of 20 ml. CCl_4 and 5 ml. Br_2 and 5 ml. conc. HNO_3. Permit to react for 1/2 hour, shake at intervals. (Note 1)

(2) Heat gently and narrow down to near dryness, shake occasionally.

(3) Add 3 - 4 ml. conc. H_2SO_4 to dissolve the Mylar (Polyester film) and the Zapon film of the tracer sample. Don't heat. (Note 2)

(4) After clear solution is obtained, add water to hydrolize Mylar. Centrifuge off the precipitate. Decant and save supernate.

(5) Add a NaOH pellet with a drop of water. The precipitate dissolves with little residue. Dilute, centrifuge and add supernate to that of step 4. (A milky solution results. Treat residue with a few drops H_2SO_4 and add it to supernates. (Note 3)

(6) Centrifuge for 4 minutes to get rid of the colloidal terephthalic acid. Add supernate into a 1 liter Erlenmeyer flask and dilute to approximately 500 - 600 ml. (depending on how much H_2SO_4 had been used).

(7) Pass the solution through a cation exchange column charged with 10 ml. 100 - 200 mesh Dowex-50 in hydrogen form. The metallic ions are retained by the resin.

Table XXIII (continued)

(8) Evaporate eluate to less than 500 ml. Neutralize to pH 6.5 with less than 4 gr. solid Na_2CO_3 anhydr. Heat while adjusting pH.

(9) Pass solution slowly through a Dowex-50 $Fe(OH)_3$ column (Fig. 21 E) that has been prepared as described below. Wash with 50 ml. H_2O. Phosphorus is retained by the column. (Note 4)

(10) Elute phosphorus activity from column with 100 ml. of 0.125 N NaOH and pass it directly through a Dowex-50 column in its hydrogen state. Wash columns with 20 ml. H_2O.

(11) Evaporate eluate to near dryness. Destroy dissolved column resin (~1 mg) with a few drops 30% H_2O_2 and plate for counting after H_2O_2 has been destroyed by gentle heating.

Notes

(1) The solution of Br_2 in CCl_4 oxidizes the sulfide to sulfate and avoids formation of colloidal sulfur which would interfere with attaining an initial homogeneous solution. Escape of phosphine is also avoided in the oxidizing medium.

(2) Phosphoric acid is volatile when heated to the fuming temperature of sulfuric acid.

(3) A homogeneous solution of the terephthalic acid monomers results in the alkaline solution. It is expected that only a negligible amount of P^{32} is carried by the reprecipitating acid before isotopic exchange with the P^{33} tracer has occurred. Steps 8, 9, 10 form a unique method of separating phosphorus activity from sulfur.

(4) The Dowex-50 $Fe(OH)_3$ column was prepared by the method given by McIsaac and Voigt. (85) Dowex-50 (100 - 200 mesh) obtained from Bio · Rad Company, Berkeley, California, was filled into the column and washed with distilled water. Conc. HCl and again distilled water was passed through the column until eluate did not change red litmus. A solution 1 N in $FeCl_3$ and 0.1 N in HCl was then passed through the column until eluate turned yellow. It was then rinsed with water to free it from excess iron. 50 ml. of 2 N NH_4OH was passed through next, turning the resin purple in color. The column was finally rinsed with distilled water to remove excess ammonia.

B. Chemical Separation

The chemical procedure employed for separating the phosphorus reaction product from the bombarded target is given in Table XXIII.

The unique method reported by McIsaac and Voigt (85) for the separation of trace phosphorus from macro amounts of sulfur by the use of a kation-exchange resin in the ferric-hydroxide form was applied for the present purpose. It had been known previously that $Fe(OH)_3$ precipitated from a $FeCl_3$ solution by ammonia is a good carrier for any phosphorus activity present as phosphate. McIsaac and Voigt produced this precipitate inside the particles of a cation exchange resin and found that trace phosphorus will be retained by the resin from a solution containing macro amounts of sulfate. As the $Fe(OH)_3$ precipitated from a strongly alkaline solution is less able to absorb phosphate ions, the phosphate traces were found to be eluted from the resin bed by 0.125 N NaOH. Carrier-free phosphorus is obtained from this eluate by passing the solution through another column charged with a cation exchange resin in the hydrogen form.

The steps preceding this separation as given in Table XXIII aim to free the solution containing the dissolved ZnS target from its content of radioactive metallic ions and render a solution identical to the one employed by McIsaac and Voigt.

C. Tracer for the $S^{34}(d, \alpha)P^{32}$ Reaction

The only available long-lived phosphorus isotope other than P^{32} is P^{33}. It has practically all the disadvantages a tracer can have. It is difficult to obtain at all, practically impossible to obtain in isotopically pure form and in sufficient quantity. The half-life of P^{33}, only 1.7 times that of the P^{32}, has not been determined very accurately making the resolution of the decay curves difficult. The activity of P^{33} is only a relatively weak β with no γ ray accompanying its decay. The determination of the cross section for the above reaction thus offered its greatest challenge in this tracing step.

Phosphorus-33 is produced in a nuclear reactor by the (n, p) reaction on sulfur. It thus accompanies all P^{32} activity obtained by this method as an impurity of approximately 1% the initial activity. Due to the difference in half-life the P^{33} content of a decaying P^{32} sample is enriched with time, although its absolute amount decreases. To obtain sufficient P^{33} tracer for this research, a 10-mc P^{32} shipment was obtained on April 5, 1956, from the Oak Ridge National Laboratory and permitted to decay until November 1956. The relative abundance of P^{33} in this sample was thus increased to approximately 66%. The phosphorus tracer was purified from any S^{35} content it might contain and other impurities by the chemical procedure given in Table XXIII.

The method for tracing the chemical yield of the bombardment was the following: Two samples of the P^{33}- P^{32} tracer mixture were prepared and counted in the 4π counter. The self-absorption for the P^{33} activity was found as described in section III-D-1 of part 2 and the ratio of the counting rates determined. One of the tracer samples was used for tracing the bombardment, the other was preserved as reference and followed in its decay. The amount of P^{33} both in the tracer sample and the bombardment product was resolved from the decay curve, after corrections for self-absorption had been applied. The chemical yield of the separation was thus established. The amount of P^{32} added with the tracer P^{33} to the bombardment product was calculated from the relative amount in the preserved sample and subtracted from the P^{32} fraction in the bombardment product to obtain the absolute disintegration rate of the fraction produced by the $S^{34}(d, \alpha)P^{32}$ reaction only.

D. Record of the Bombardments

Three bombardments were performed to investigate the $S^{34}(d, \alpha)P^{32}$ reaction. Bombardment 1 served to check the chemical procedure and determine the half-life of the bombardment product. The latter was followed for 11 half-lives with the 4π counter. The decay curve of this sample is seen in Fig. 65. The half-life was determined by the least squares method* applied to the logarithms of the count rates and found to be 14.221 ± 0.005 days. From this result it could be assumed that no P^{33} was produced during the bombardment, which served as proof that the threshold of the (d, αn) reaction was not exceeded by the 7.8-Mev deuterons even for elements as low in the periodic table as sulfur.

The absolute cross section for 7.8-Mev deuterons was determined by bombardment 16. The target was exposed to the full-energy beam and the phosphorus product separated several days after the bombardment. The tracer mixture of P^{33} - P^{32} added to determine the chemical yield counted approximately 69,000 c/m in the 4π counter. The self-absorption correction necessary for evaluation of the P^{33} content of the purified sample from bombardment 16 was determined to be $4 \pm 0.5\%$. (Section II-D-5 of part 2.) Table XXIV gives the data and results from this bombardment. The errors reported were estimated from the principles discussed earlier (section II-E). They are in general

*Non-weighted least squares method was used.

Table XXIV. Results of the S(d, α)P Cross Section Determination

The $S^{34}(d, \alpha)P^{32}$ Reaction

Bombardment No.	Type	Average Deuteron Energy Mev	C_i	Chem. Yield %	Count Rate* c/m	Target thickness mg/cm^2	millibarns
16	abs.	7.73±0.05	2501.4±1%	36.1±2%	76,317±3%	1.652±0.8%	330.3±7%
3	rel.	7.73±0.05	-	±5%	18,486±1%	1.390±0.8%	330±10%
3	rel.	6.55±0.1	-	±5%	8,139±1%	1.594±0.8%	126±10%
3	rel.	5.05±0.1	-	±5%	4,532±1%	1.786±0.8%	63±15%
3	rel.	3.15±0.3	-	±5%	3,050±1%	1.902±0.8%	39±20%
3	rel.	0.7±0.5	-	±5%	2,205±1%	1.967±0.8%	28±30%

* For absolute experiments count rate at the end of the bombardment, for relative experiments at some later time.

somewhat large due to the difficulties experienced with analyzing the decay curves. The error of the target thickness has to be ascribed to the uncertainties introduced by weighing the ZnS deposits by difference.

Bombardment 3 served to establish the relative excitation function for the $S^{34}(d, \alpha)P^{32}$ reaction. The target arrangement for the bombardment is given in Table XXV. The targets were worked up simultaneously by the carrier-free procedure given in Table XXIII, and the purified P^{32} products counted over a period of several months with the proportional counter. A series of straight decay curves was obtained for the samples with little scatter of the individual points. A graph of the excitation functions is seen in Fig. 66.

E. Resolution of the Decay Curves

The difficulties in resolving the decay curves of the tracer and the sample from bombardment 16 may be illustrated by Fig. 67. The decay curve of the tracer is given to illustrate the amount of P^{33} contained in the six-month-old shipment from the Oak Ridge National Laboratory. Analysis of the curve was performed by the method discussed in section III-D for the case of the molybdenum bombardments.

Although the half-life of P^{32} was experimentally checked in this research, uncertainties in the "known" half-life of P^{33} made the analysis difficult. To obtain the resolved curve seen in the insert of Fig. 67, a half-life of 24.2 days

Table XXV. Arrangement for Zinc Sulfide Targets for Bombardment 3

Target or Absorber	Thickness (mg/cm^2)	Average Deuteron Energy Mev
ZnS XI	1.39	7.74
Mylar	3.52	
Aluminum	10.78	
ZnS VII	1.594	6.55
Mylar	3.52	
Aluminum	10.78	
ZnS V	1.786	5.05
Mylar	3.52	
Aluminum	10.78	
ZnS XII	1.902	3.15
Mylar	3.52	
ZnS IV	1.967	0.7
Mylar	3.52	

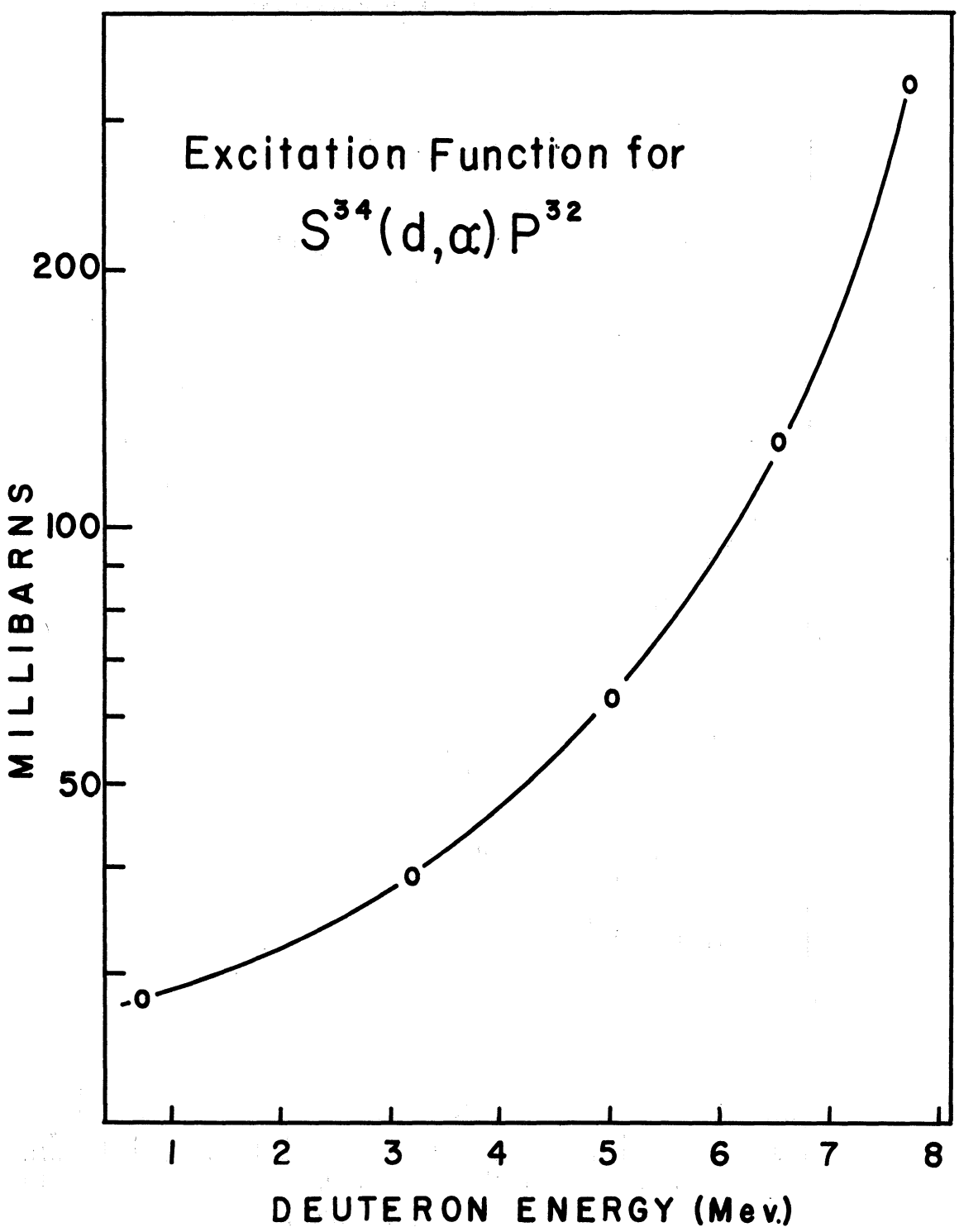

Fig. 66. Excitation Function for the $S^{34}(d, \alpha)P^{32}$ Reaction

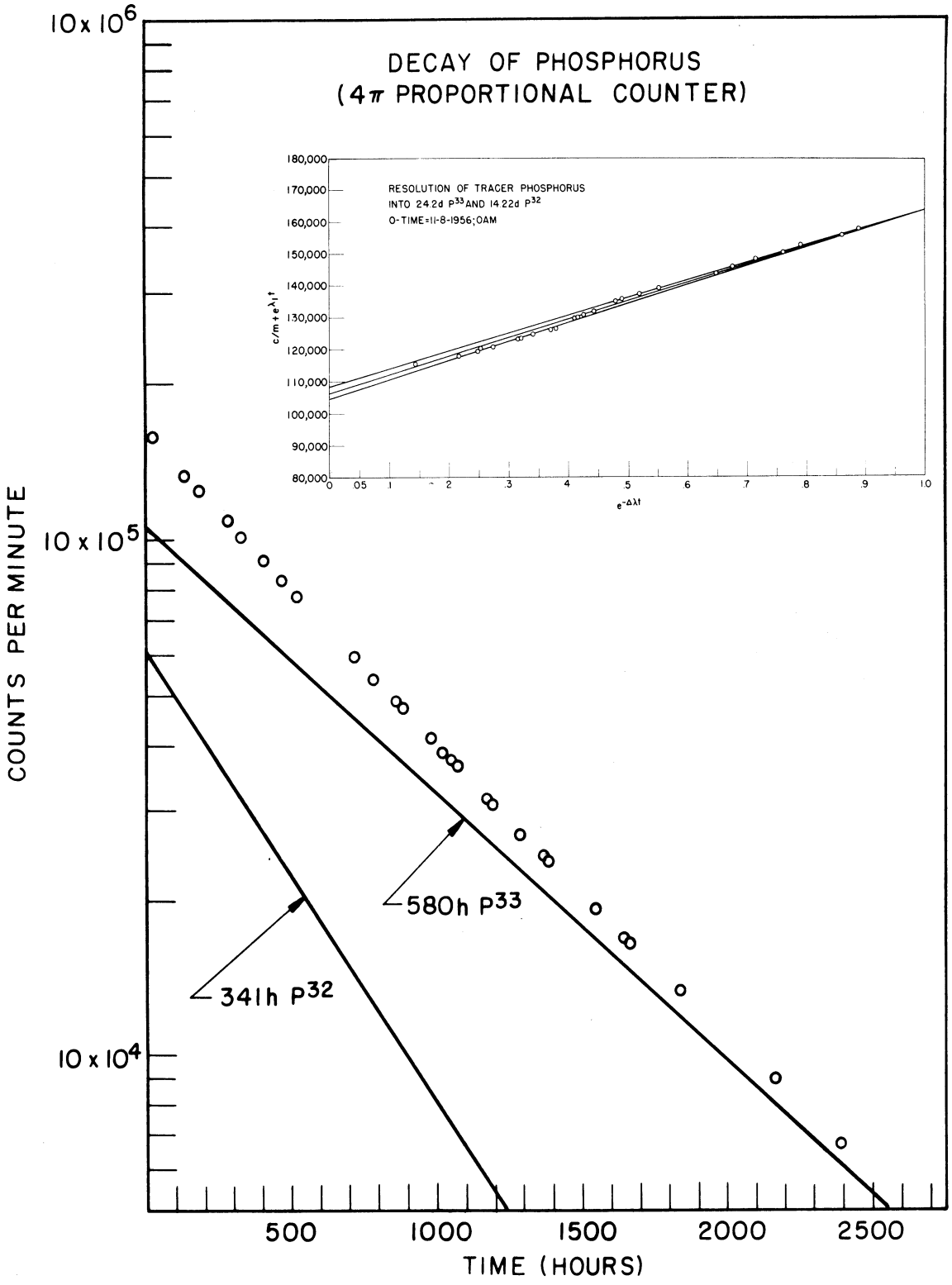

Fig. 67. Complex Beta Decay Curve of P^{32} - P^{33} Tracer

seemed to fit the data best. Taking this into consideration it may be that the error quoted for the absolute cross section in Table XXIV is somewhat optimistic.

VI. The $Fe^{56}(d, \alpha)Mn^{54}$ Reaction

For calibration of the x-ray counter it was desirable to have a standard sample emitting characteristic x-rays of approximately 6 kev. Manganese-54, an isotope decaying by electron capture with the emission of a 0.84-Mev γ ray and a half-life of 290 days seemed well suited for this purpose. To produce a sufficient quantity of this isotope a bombardment of an iron foil was obtained at the Argonne National Laboratory with the 21-Mev deuteron beam. The (d, α) reaction on the natural mixture of iron isotopes yields a certain amount of short-lived products as can be seen from the chart of the nuclides in the iron region given in Fig. 68. Interference from these products, however, was avoided by permitting them to die out before the remaining Mn^{54} was used.

A. Target

The aim of the bombardment was to produce a relatively high yield of Mn^{54}. To achieve this in a two-hour bombardment a relatively thick 10-mil pure iron foil was silver-soldered onto a thick copper backing plate to withstand the 100 micro-ampere current of the cyclotron beam. Special solder containing the eutectic mixture of silver and copper was flowed onto the copper backing plate with a flux consisting of 50% H_3BO_3 and 50% $Na_2Br_4O_7 \cdot 10\ H_2O$

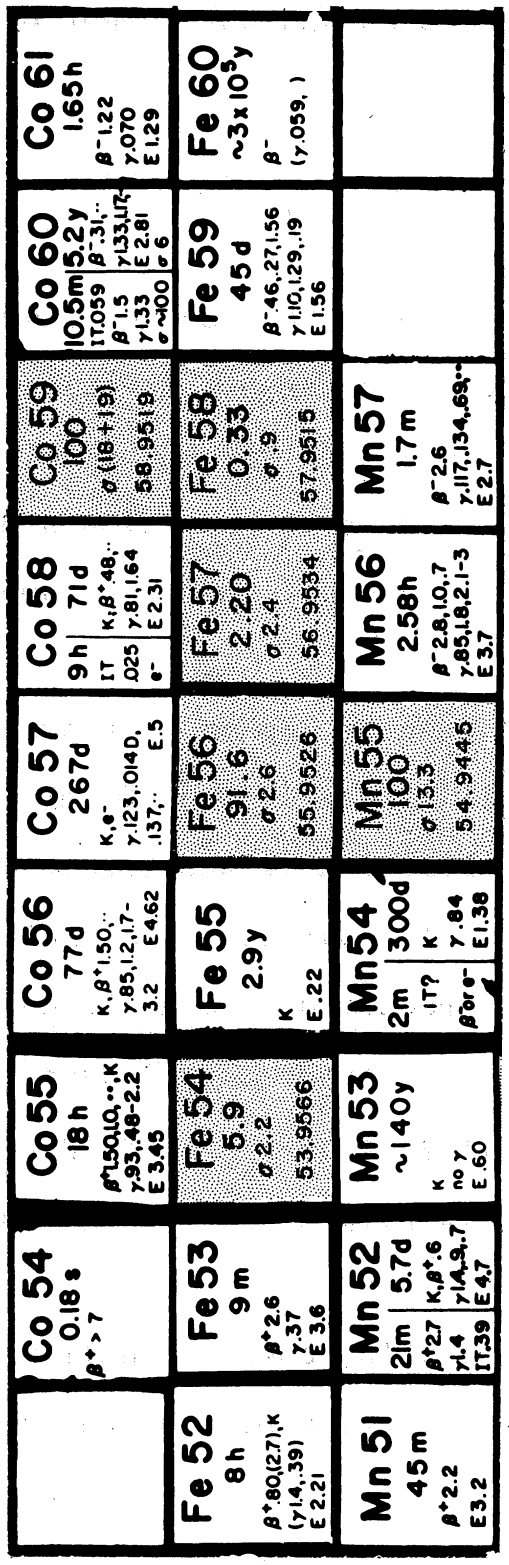

Fig. 68. Chart of Nuclides in the Iron Region (for explanation see Fig. 48)

plus water and the iron foil laid on the liquid solder. Excess flux and solder was removed and the target exposed to the deuteron beam.

B. Chemical Separation

The chemical separation procedure used to separate the manganese reaction product from iron and cobalt as well as from copper, zinc, nickel, silver and cadmium combined an initial solvent extraction step with simultaneous precipitation and ion-exchange steps. The procedure is given in Table XXVII.

The solvent extraction step employs a continuous extractor described in detail by Willard and Diehl (128) to remove all iron from the solution of the target with a minimum amount of handling. (The target had a radiation intensity of approximately 1 roentgen at a distance of 2 cm). This step was based on the data reported by Dodson, Forey and Swift on the extractability of certain metals from a hydrochloric acid medium by isopropyl ether as given in Table XXVI.

The simultaneous precipitation steps as well as the anion exchange steps follow the principles discussed in section III-B-2 of part 2.

Table XXVI

The Extraction of Various Elements from 7.75 N HCl Solutions by an Equal Volume of Isopropyl Ether*

Element	% In Isopropyl Ether Layer
Fe^{III}	99.00
Cu^{II}	0.00
Co^{II}	0.00
Mn^{II}	0.00
Ni^{II}	0.00
Al^{III}	0.00
Cr^{III}	< 0.01
Ti^{IV}	0.00
V^{V}	0.00
SO_4 in presence of Fe	0.30
PO_4 in presence of Fe	trace
Mo in presence of Fe	trace
$V^{V + IV}$	trace

C. Identification of Reaction Product and Side Products

The Mn^{54} reaction product was used as a standard for the x-ray counter. Its x-ray photopeak as seen in Fig. 37 and the γ spectrum seen in Fig. 47 identified the isotope.

* Dodson, R. D., Farney, G. J., Swift, E. H., J. Am. Chem. Soc. 58, 2573 (1936). The extraction of ferric chloride from hydrochloric acid solutions by isopropyl ether.

Table XXVII

Chemical Separation of Manganese from an Iron Target

(carrier-free)

Element	Separated from	Decontamination Factor
Mn (carrier-free)	d. bombarded Fe, Cu and Ag	10^4

Time of Separation	Chemical Yield
10 hours	50%

Chemicals and Equipment

Continuous extractor(128); blowtorch; Pyrex beaker, 200 ml., 50 ml.; filter crucible; Erlenmeyer flask, 250 ml.; porpous plate; aluminum foil; 2 centrifuge tubes, 15 ml. centrifuge; platinum wire, 6 inch; 2 small ion exchange columns (Fig. 20); medicine droppers.

Dowex-2 resin (200 - 400 mesh); conc. HNO_3, HCl, NH_4OH; conductivity water; iso-propyl ether; HCl-gas tank; iron carrier (10 mg/ml).

Procedures

(1) Heat target in hood and free iron foil from backing plate.

(2) Place iron foil with adhering solder in beaker and add conc. HNO_3. Warm gently and permit copper and silver to dissolve. Decant green solution and store after ebullition ceases.

(3) Dissolve remaining iron foil in dilute HCl.

(4) After the iron is dissolved filter off any AgCl present, add 5 ml. conc. HNO_3 and evaporate to dark yellow syrup of about 10 ml.

(5) Transfer to bulb of continuous extraction apparatus and add 25 ml. conc. HCl and 5 ml. H_2O to make about 9 M in HCl.

(6) Place approximately 175 ml. iso-propyl ether into 250 ml. Erlenmeyer flask; add a small piece of porous plate, and connect to extractor and place condensor on top of extractor. Wrap extractor bulb with aluminum foil and place in beaker with water. Heat the Erlenmeyer flask to boil moderately and permit to extract in dark over night.

Table XXVII (continued)

(7) Evaporate extracted aqueous solution to near dryness, take up with few ml. conc. HNO_3. Add 3 drops Fe-carrier.

(8) Transfer to 15 ml. centrifuge cone and precipitate with NH_4OH. Wash twice and dissolve with dil. HCl.

(9) Precipitate with NH_4OH and wash twice.

(10) Dissolve precipitate with conc. HCl and saturate with HCl gas.

(11) Apply solution to an anion exchange column charged with approximately 1 ml. Dowex-2 resin saturated with conc. HCl.

(12) Permit to adsorb. Add 5 drops conc. HCl and soak in slowly.

(13) Elute Mn^{54} with 12 ml. of conc. HCl.

(14) Evaporate eluate to near dryness. Take up with 9 M HCl.

(15) Apply to second column charged with approximately 1 ml. Dowex-2 saturated with 9 M HCl.

(16) Permit to adsorb. Add 5 drops 9 M HCl and soak in slowly.

(17) Elute Mn^{54} with 12 ml. 9 M HCl.

Side products such as Cd^{109} and Co^{57} from the above bombardment were separated by carrier-methods from the solutions encountered in above procedure and were also used for standards. The x-ray spectrum for Cd^{109} is seen in Fig. 38.

Part 4

DISCUSSION

I. Nuclear Shell Model

In recent years vast progress has been made in establishing theories regarding the atomic nucleus. One of the most successful attempts in describing the behavior of nuclear particles inside the nucleus is presented by the "Nuclear Shell Model". The foundations for this model were laid by Hartree (57), Elsasser (28 - 32) and Bethe (10) in the 1930's in their attempts to find an "Independent Particle Model" for the structure of the nucleus. In 1948 Maria G. Mayer (81 - 2) pointed out several significant discontinuities in the trend of the properties of nuclei as a function of the atomic number, which seemed to indicate the existence of distinct energy shells inside the nucleus. The new idea bringing forth the shell model was conceived simultaneously by Maria Mayer (83) and Haxel, Jenson and Suess (60) in 1949. Assuming strong spin-orbit coupling of the nuclear particles resulting in splitting of the nuclear energy levels, the shell model can account for the discontinuities of nuclear properties and permits the calculation of these properties by an adaptation to the independent particle model as known before.

The level scheme proposed by the Shell Model is given in Fig. 69 indicating the presence of relatively large energy-level spacings at the points for which discontinuities of nuclear properties had been proven. The discontinuities occur at the "magic numbers" 2, 8, 20, 28, (40), 50, 82, 126.

A. The (n, γ) Reaction Cross Sections

One of the postulates of the Nuclear Shell Model is the relatively great stability of nuclei containing "magic" numbers of either neutrons or protons. The nuclear reaction cross section is a quantity related to the stability of the nucleus. Hughes (66) was thus able to prove the greater stability of closed shell nuclei with a plot of the capture cross sections for thermal neutrons as given in Fig. 70. In this plot certain isotopes such as Kr^{86}, Rb^{87}, Sr^{88}; Xe^{136}, Ba^{138}, Pb^{208}, Bi^{209} etc., containing a magic number of neutrons, reveal significantly lower cross-section values. This reveals a certain inertness toward nuclear reactions for these nuclei and is an indication of their relatively greater stability.

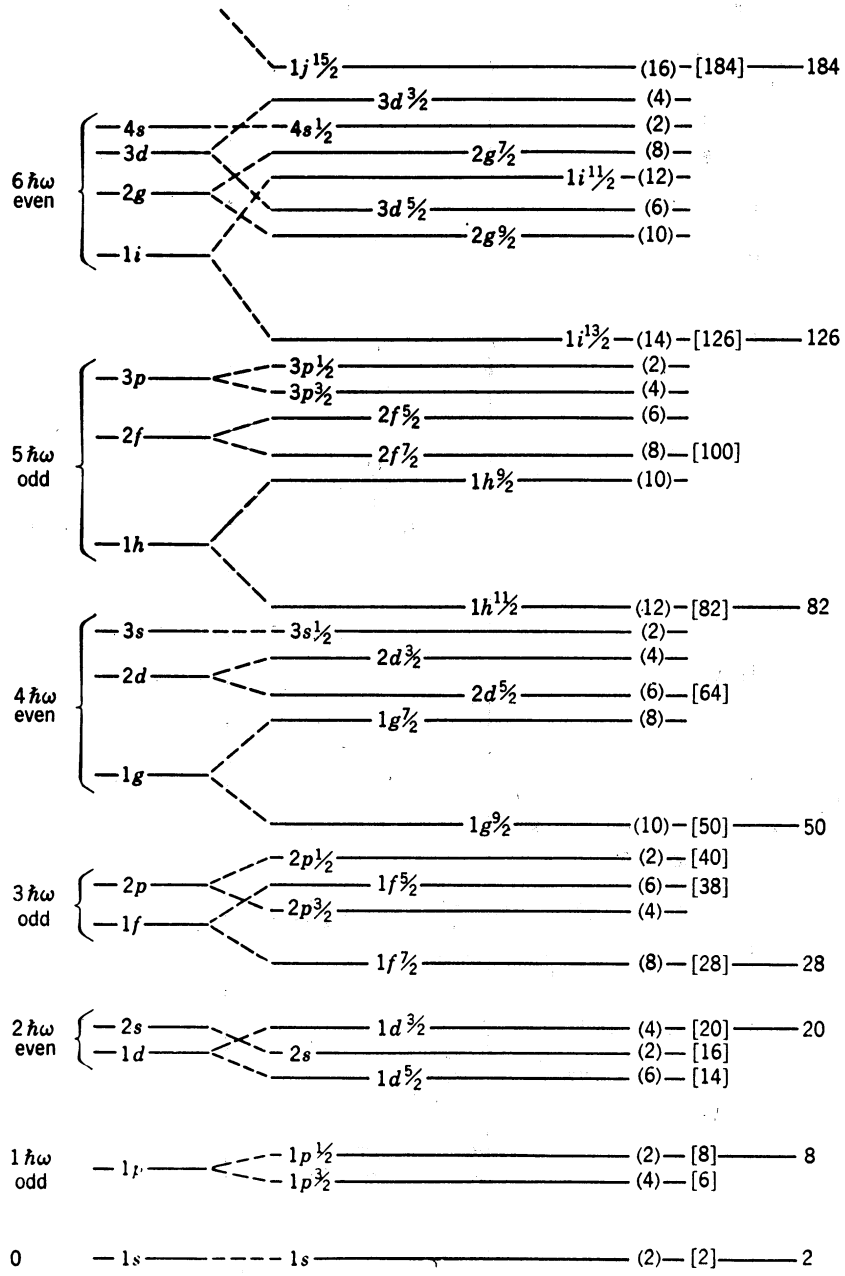

Fig. 69. Schematic Diagram of Nuclear Level Systems with Spin-Orbit Coupling

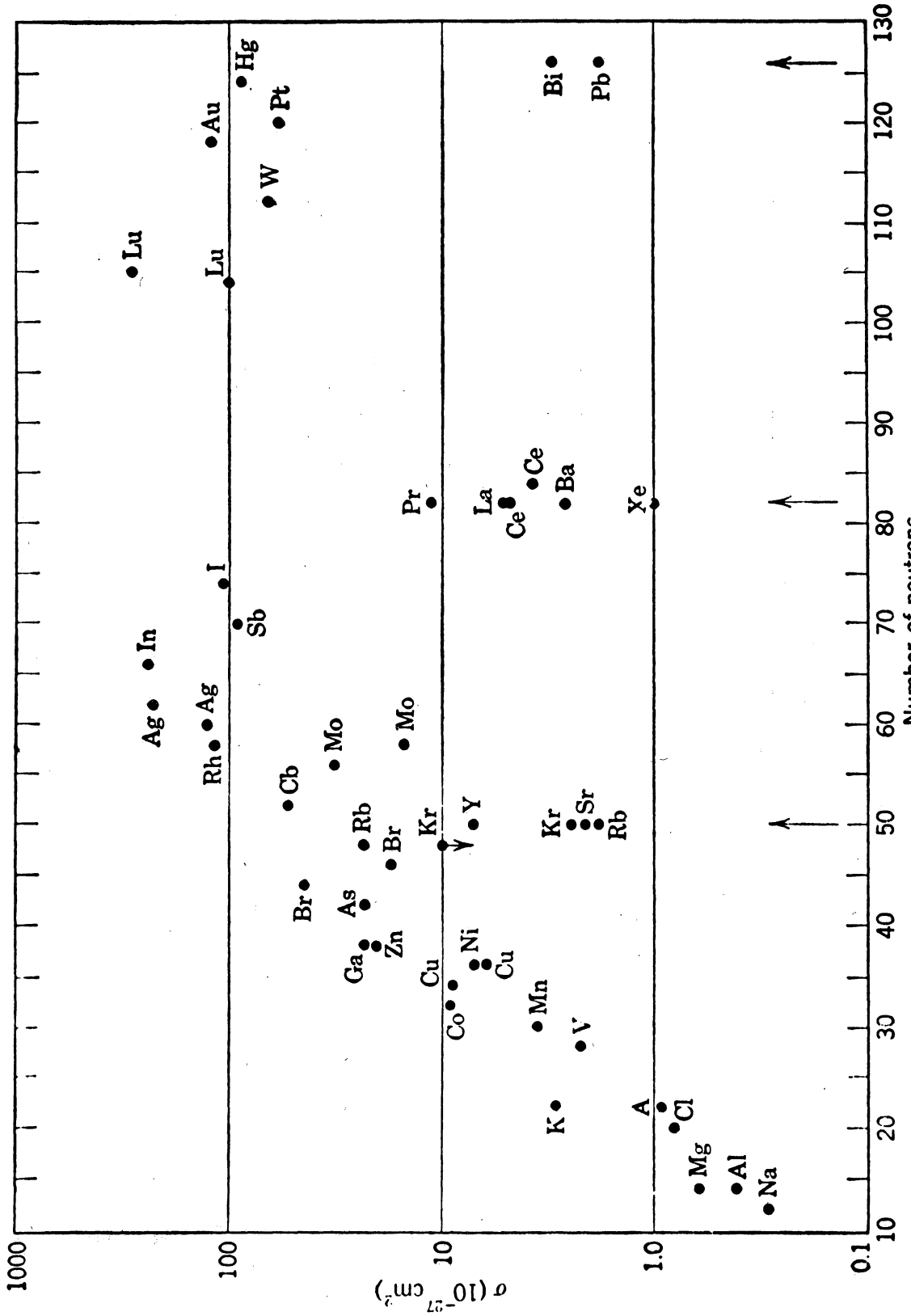

Fig. 70. Capture Cross Section for 1-Mev Neutrons. (Reference 66)

B. The (p, n) Reaction Cross Sections

To illustrate the same principle by means of the (p, n) reaction Blaser, Boehm, Marmier and Scherrer (13) investigated the cross sections and excitation functions for the (p, n) reactions of many target isotopes. A plot of the (p, n) cross sections which they determined for 6.7-Mev protons vs. the neutron content of the target nuclei resulted in values for magic-number nuclei lying below the general trend. The values for 6.7-Mev protons, however, did not show significant deviation for all magic nuclei. Those deviating most significantly in their (p, n) cross section values belonged to so called "double magic" nuclei, featuring a magic number content of both neutrons and protons.

C. The (d, α) Reaction Cross Sections

Essentially the same type of investigation as mentioned above for the (p, n) reaction was attempted by the present research for the (d, α) reaction. It was expected that the deviation of the cross sections for magic-number nuclei would be much less significant than for the two reactions mentioned above and, that measurements giving values with an accuracy better than 10% would be required, to prove any significant difference in the cross-section values for closed-shell nuclei as compared to

their non-magic neighbors. This expectation was based on the fact that approximately 2.5 times as much energy is released when the 7.8-Mev deuteron interacts with the target nucleus than in the capture of a thermal neutron. (The relatively high-energy deuterons had to be used to give sufficient yields for the nuclear reactions). This energy effect is likely to overshadow any small rest energy differences in the magic-number target nucleus which are relatively important for the (n,γ) case (32, 110).

The most significant results were expected from the comparison of the cross-section values of a nucleus having closed shells for both protons and neutrons, Zr^{90}, with those of its non-magic isotopes.

The results of this research appear to verify the expectations. Figure 71 is a plot of the (d, α) reaction cross sections for 7.7-Mev deuterons as determined in this research. The values for cadmium and magnesium were determined by Hall (43) and are included to round out the picture. The errors for the points in Fig. 71 are listed in the tables for the various reactions (Tables X, XVII, XXI, XXIV).

Two closed-shell nuclides with a content of 50 neutrons have been investigated. While the value for Mo^{92} does not seem to deviate from the trend established by the cadmium, molybdenum and zirconium isotopes, the value for the double-closed-shell Zr^{90} is seen to lie significantly below it.

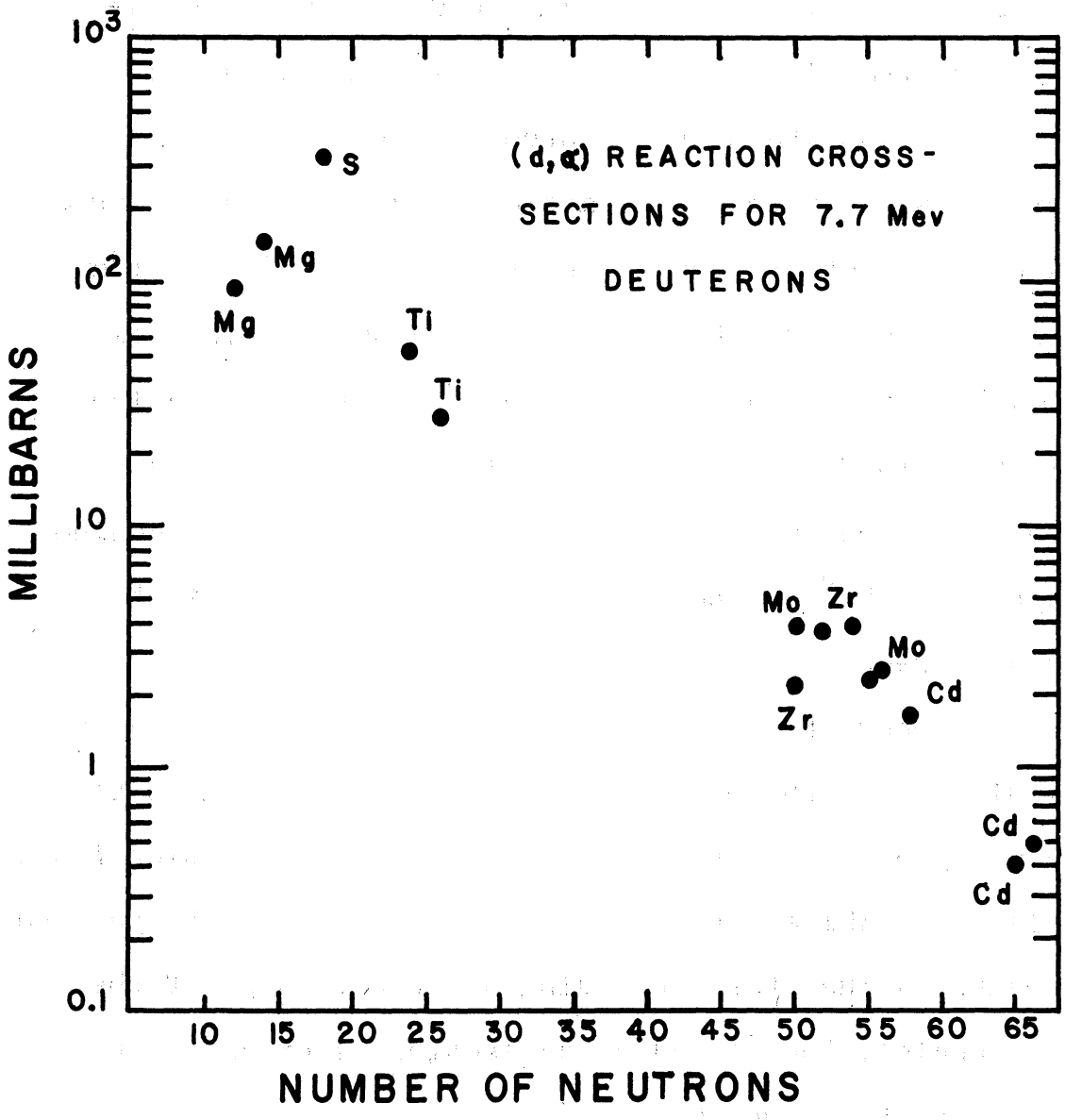

Fig. 71. (d, α) Reaction Cross Sections for 7.7 Mev Deuterons

The relatively high cross-section value for sulfur is not easily explained. Although the decay curve of the phosphorus reaction product as seen in Fig. 65 seems to exclude any admixture of P^{33} stemming from the $S^{36}(d,\alpha n)P^{33}$ reaction, some of the P^{32} reaction product may still originate by the neutron-induced reaction $S^{32}(n, p)P^{32}$. The latter is also suspected from the curvature of the low-energy excitation function of the $S^{34}(d, \alpha)P^{32}$ reaction, as is seen in Fig. 67. A comparison of this curve and those presented in Fig. 52 and Fig. 60, for the zirconium isotopes and Nb^{95} respectively, will readily elucidate this difference in character.

The trend of the (d, α) reaction cross section values is indicated by the points in Fig. 71 and is seen to be distinctly different from that of the (n, γ) reaction found in Fig. 70. While the non-magic number cross sections tend to greater values for increasing neutron content of the target nuclei, the (d, α) cross sections decrease with increasing atomic weight.

Thermal neutrons do not have to overcome a potential barrier to strike the nucleus. The probability of interaction, i.e., the capture cross section, thus increases with the size of the target nucleus. In the case of deuterons as bombarding particles a certain minimum energy is required before the projectile can penetrate to the nucleus of the target atom. This threshold energy is the

greater, the greater the positive charge of the target nucleus. For a given laboratory energy of the deuterons the threshold energy is exceeded more for low-atomic number nuclei than for those higher in the periodic table. The cross section, however, is energy dependent as could be seen in Fig. 52, and a steep rise of the excitation function is experienced in the vicinity of the threshold. This makes a slight excess of deuteron energy above the threshold account for a large increase of the cross sections (14).

To obtain a plot more closely analogous to Fig. 70, the (d, α) reaction cross sections should be plotted for those laboratory energies for which the deuterons have the same kinetic energy when reaching the nuclear surface. Such a plot would partially compensate for the effect of the Coulomb barrier, which is not encountered in the case of neutron capture.

To establish such a plot, very exact values for the cross sections must be known for the respective ranges of the excitation functions. The energy range that could be covered by the means available for this research, however, did not suffice for such a plot. It was thus only attempted to determine the absolute cross sections for one energy, and to find some relative values of the excitation functions to determine the character of these functions.

A rather complete search for charged-particle-reaction excitation functions reported in the literature was undertaken during the initial stage of this research.* Very few excitation functions for (d, α) reactions were found in this search, thus pointing out the need for additional data of this kind.

II. Considerations for Future Experiments

Further experiments on the (d, α) reaction cross sections by the techniques presented in this report may be planned as an extension of the present research. The considerations entering into the choice of the reactions should be essentially the same as the ones governing the choices for this investigation.

The energy of the available deuterons may exclude as target materials all elements for which the threshold of the (d, α) reaction is not exceeded. For the 7.8-Mev deuterons of the cyclotron of the University of Michigan this would exclude all elements with atomic number greater than 66 (dysprosium) as was found experimentally.

The following elements had to be excluded, since the

---

* Anders, O. U., Meinke, W. W., Excitation Functions and Cross Sections, document No. 4999, American Documentation Institute, Washington 25, D. C., U. S. A. (1956).

(d, α) reaction products form stable nuclei: Be, C and the odd atomic-number elements: N, F, Na, Al, P, Sc, V, Mn, Co, As, Y, Nb, Tc, Rh, In, I, Cs, La, Pm, Tb. Investigation of the (d, α) reactions of these elements would have to follow a completely different approach. This would probably include either detection of the primary α particles emitted during the reaction, or the use of a mass-spectrometer.

Of the remaining 44 elements some were excluded because the counting rates of the (d, α) reaction products would be too low to measure due to the low relative abundance of the parent isotopes and too long or too short half-lives of the products. These elements are shown in Table XXVIII.

Inability to bombard gaseous materials and count gaseous products with the equipment on hand excluded the following elements from consideration: He, Li, Ne, A, K, Kr, Rb, and Xe.

Difficulties in analyzing decay curves of the (d, α) reaction products were anticipated for a number of other elements. The critical isotopes of these elements are shown in Table XXIX.

Several elements posed difficulties in tracing their (d, α) reaction products through the chemical separations:

No suitable tracer could be found for the Cl^{37}(d, α)S^{35} reaction since all radioactive sulfur isotopes, but S^{35}, have half-lives below 10 minutes.

Table XXVIII. Elements Excluded from Investigation because of Half-Lives of (d, α) Reaction Products or Low Abundance of Parent Isotopes

Element	Parent Isotope	Abundance	Half-Life of (d, α) Reaction Product
B	B^{10}	18.8	4×10^{-15} sec
O	O^{18}	0.204	7.4 sec
Si	Si^{28}	92.17	10^6 years
	Si^{30}	3.12	2.3 min
Ca	Ca^{40}	96.9	7.7 min
	Ca^{42}	0.64	3.9×10^9 years
	Ca^{44}	2.1	12.5 hours
	Ca^{46}	0.0032	22 min
	Ca^{48}	0.18	unknown
Br	Br^{81}	49.4	7×10^4 years
Pd	Pd^{106}	27.3	4.4 min, 42 sec
Ru	Ru^{99}	12.7	10^5 years
	Ru^{100}	12.7	10^4 years
	Ru^{101}	17.0	2×10^5 years
Ag	Ag^{109}	48.6	7×10^6 years
Eu	Eu^{153}	52.2	80 years

Table XXIX. Elements Excluded from Investigation because of Decay Curve Analysis Problems

Element	Parent Isotope	Half-Life of (d, α) Reaction Product
Sn	Sn^{112}	5 hours, 66 min
	Sn^{114}	21 min, 2.5 sec, 14 min
	Sn^{115}	1.73 hours
	Sn^{117}	4.5 hours
	Sn^{118}	54 min, 13 sec
	Sn^{119}	1.9 hours, 1.1 hours
Te	Te^{120}	3.5 min, 5.1 hours
	Te^{122}	5.8 days, 17 min
	Te^{124}	3.5 min, 2.8 days
	Te^{126}	21 min, 1.3 min, 60 days
	Te^{128}	9 hours, 28 days
	Te^{130}	1 hour
Nd	Nd^{146}	17 min
	Nd^{148}	24 min
Sm	Sm^{147}	25 years
	Sm^{148}	2 years
	Sm^{149}	2.6 years
Gd	Gd^{152}	14 hours
	Gd^{154}	9 hours, 13 years
	Gd^{156}	16 years
	Gd^{157}	1.7 years
Ba	Ba^{134}	6.2 days
	Ba^{138}	13 days

Difficulties were anticipated in procuring tracers for the (d, α) reactions on Zn, Ge, Ce, and Pr. As tracer for the Zn(d, α)Cu reactions the 61-hour Cu^{67} should be used. This isotope can be obtained either by the $Zn^{67}(n,p)Cu^{67}$ reaction or the Zn^{70}(d, αn)Cu^{67} reaction, but both would necessitate the use of isotopically enriched targets. The Ge(d, α)Ga reactions may be traced by the 14.1-hour Ga^{72} which would have to be produced by a preliminary bombardment of germanium. For the Ce(d, α)La reaction no good tracer is available. La^{141} with a 3.8-hour half-life may serve to trace the Ce^{142}(d, α)La^{140} reaction but its procurement by the low-yield Ba^{138}(α, p)La^{141} reaction is difficult and close timing of the bombardments has to be observed to make use of it.

Without use of enriched Ce^{140} no pure tracer Ce^{141} can be obtained which would be necessary to trace the Pr^{141}(d, α)Ce^{139} reaction. The use of separated isotopes was, however, avoided in the present research due to their high cost and lack of availability.

(d, α) reactions involving Mg, Cd (47) and Cr * had been investigated by previous workers, so that the final choice had to be made from the ten remaining elements.

---

* Kafalas, P., Ph. D. Thesis, Massachusetts Institute of Technology (August 1954).

The cross sections of the (d, α) reactions on iron were not measured since the thin, high-purity iron foil necessary could not be obtained during the course of the investigation. Nickel bombardments producing 77-day Co^{56}, 71-day Co^{58} and 5.2-years Co^{60} were not performed, although thin targets could be produced by electrodeposition. The bombardment times necessary for sufficient amounts of reaction products would have been relatively long and the resolution of the decay curves of the products difficult.

Gallium and selenium containing no magic number isotopes were of relatively small interest for an investigation of the effects of nuclear shell structure on the (d, α) reactions.

This left only S, Ti, Zr, Mo, Sr, and Sb. The (d, α) reaction cross sections of the first four were investigated in the present research.

Improvements of the data obtained in this research could be made by employing the various techniques developed for tracing the reaction products more methodically. In this connection it should be kept in mind that the method using a reference sample is independent of the knowledge of the decay constants of the tracers as well as of the reproducibility of a given counter over a long period of time.

The determination of the self-absorption of β rays in the 4π sources may be studied in order to improve some

of the errors quoted. Finally, the analysis of the decay curves may be facilitated by the use of a computer, making the resolution of many-component decay curves quicker and less laborious. This would also permit the resolution of decay curves involving isotopes whose half-lives differ by less than 50 percent.

Nevertheless, it is believed that the method of determining the (d, α) reaction cross sections has by now been sufficiently developed to obtain data precise enough for theoretical treatment. The work should now be expanded to include various other nuclides to permit a good quantitative correlation of the trends in the (d, α) reactions. More excitation functions should be measured which could be normalized to the absolute points.

The techniques developed in the present research are applicable without alteration to the study of the (d, n) reaction and, with little improvement on the chemical separations, for all reactions for which the product is different than the target element. For such reactions more attention has to be given, however, to effects of side-reactions having the same product.

III. Summary

The purpose of this research was the determination of the cross sections and excitation functions of various (d, α) reactions induced by the 7.8-Mev deuterons from the University of Michigan cyclotron. Measurements were performed for reactions of isotopes of zirconium, molybdenum, titanium and sulfur. Special attention was given to reactions involving closed-shell nuclei in order to detect any significant deviation of the cross-section values for these reactions when compared with values for non-magic number nuclei. These deviations were expected to be relatively small and precision measurements had to be performed to detect them. New techniques and instruments were developed for this purpose and others improved, which had been evolved by previous workers. It was thus possible to obtain absolute cross-section values with standard errors between 5 and 10 percent and reproducibility within 2 percent.

The accuracy obtained for the cross sections measured in this research compared favorably with values reported by other authors in the literature. Blaser, Boehm, Marmier and Scherrer (13) quote errors of the order of 24 millibarns. Aamodt, Peterson and Phillips (1) report values for the $C^{12}(p, pn)C^{11}$ reaction cross sections with errors of 7 millibarns. For this research the sensitivities were of the order of 0.1 - 2 millibarns.

The values were determined for the relatively low-yield (d, α) reactions. Determination of the cross sections was not possible by measuring the particles emitted during the reaction itself. The reaction products had to be purified by carrier-free procedures and counted absolutely with 4π proportional counters and coincidence methods. This added several steps introducing errors, which could be avoided by workers measuring cross sections by physical means only.

For the present research no compromise could be made lessening the achievable accuracy of the measurements, because of the small magnitude of the effects sought. A compromise thus had to be made in the number of reactions investigated. The final selection presents a compromise between the available man-hours and the expected efforts required for precision measurements on a particular isotope.

The instruments constructed for measuring the intensity of the cyclotron beam included a current integrator permitting readings with standard deviation of less than 1 percent and a negative high voltage power supply to provide a potential of -1000 volts to the suppressor ring.

Chemical separation methods were developed to purify the (d, α) reaction products by carrier-free techniques and prepare carrier-free tracers used for determining the yields of the chemical separations. A beta gauge was designed and built for measuring the evenness of cyclotron targets of a few mg/cm^2 thickness with errors of approximately 1 percent.

Various counters, including two 4π-proportional counters and a 4-inch diameter x-ray counter, were constructed together with several electronic circuits. The performance of these counters was studied in detail and optimum conditions for proper operation found for them. Absolute counting techniques were developed for counting x-rays and β rays and experience gained in x-ray and γ-ray spectroscopy using proportional and scintillation counters.

Excitation functions were measured for several of the investigated reactions by the "stacked foils" technique and a rough correlation of the cross section values for 7.7-Mev deuterons attempted.

APPENDIX

Integration of equation 4

$$\frac{dN}{dt} = I\,\sigma\,\frac{n}{A} - \lambda N$$

Transpose $$\frac{dN}{dt} + \lambda N = I\,\sigma\,\frac{n}{A}$$

Let $S\frac{dN}{dt} + S\,\lambda N$ be the derivative of some combination.

We obtain $$S\frac{dN}{dt} + S\,\lambda N = \frac{d}{dt}(SN) = S\frac{dN}{dt} + N\frac{dS}{dt}$$

This holds if $$\frac{dS}{dt} = S\,\lambda$$

then $$\frac{dS}{S} = \lambda\,dt$$

$$\ln S = \int \lambda\,dt$$

and $$S = e^{\int_0^t \lambda\,dt} = e^{\lambda t}$$

now $$S\frac{dN}{dt} + S\,\lambda N = S\left(I\,\frac{\sigma\,n}{A}\right)$$

substituting for S

$$e^{\lambda t}\left(\frac{dN}{dt}\right) + e^{\lambda t}\,\lambda N = e^{\lambda t}\left(I\,\frac{\sigma\, n}{A}\right)$$

By integration we obtain

$$e^{\lambda t}\,N = \int_0^N e^{\lambda t}\left(I\,\frac{\sigma\, n}{A}\right) dN + C$$

$$e^{\lambda t}\,N = \frac{1}{\lambda}\int_0^N e^{\lambda t}\left(I\,\frac{\sigma\, n}{A}\right) \lambda dN + C$$

$$e^{\lambda t}\,N = \frac{1}{\lambda}\left(I\,\frac{\sigma\, n}{A}\right) e^{\lambda t}\,\Big]_0^t$$

$$e^{\lambda t}\,N = \frac{1}{\lambda}\left(I\,\frac{\sigma\, n}{A}\right) e^{\lambda t} - \frac{1}{\lambda}\left(I\,\frac{\sigma\, n}{A}\right) = \frac{1}{\lambda}\left(I\,\frac{\sigma\, n}{A}\right)\left(e^{\lambda t} - 1\right)$$

$$N = \frac{1}{\lambda}\left(I\,\frac{\sigma\, n}{A}\right)\left(1 - e^{-\lambda t}\right)$$

Table XXX. Data for the Beryllium Absorption Curve of X-rays Emitted by Y^{88} and Mn^{54}

Beryllium Absorber mg/cm^2 *	Y^{88} count rate** c/m	% Transmitted	Mn^{54} count rate** c/m	% Transmitted
44.8	17,091 ± 8	100	3101	100
67.6	16,907	98.9		
67.6	16,764	98.1	2873	92.6
89.6	16,776	98.1		
89.6	16,583	97.0	2613	84.2
126.1	16,377	95.8	2239	72.2
178.8	16,129	94.4	1844	59.4
297.5	15,560	91.0	1177	37.9
423.6	15,069	88.2	825	26.6
591.8	14,136	82.7	361	11.6
724.8			305	9.8
1000	12,176	71.2		
1000	12,140	71.0	116	3.7
1503	9,839	57.5		
2188	8,415	49.2		
2475	8,026	47.0		
2475	8046	47.1		
2846	6726	39.4		

* Beryllium absorber plus 44.8 mg/cm^2 beryllium counter window.

** Count rate corrected for background statistical variation 1-2% per point.

Table XXXI. Data for Aluminum Absorption Curve of Pm^{147} Beta-rays

Absorber mg/cm^2	Count rate counts per minute
0.00	13,834
1.46	9,544
2.72	7,235
3.25	6,594
3.59	6,191
4.66	5,343
6.18	4,143
13.9	1,557
21.8	836
25.1	729
39.7	566
46.6	532
54.3	505
1710	189.5

BIBLIOGRAPHY

(1) Aamodt, R. L., Peterson, V., Phillips, R., Phys. Rev. 88, 739-44 (1952). $C^{12}(p, pn)C^{11}$ cross section from threshold to 340 Mev.

(2) Alburger, D. E., Sunyar, A. W., Phys. Rev. 99, 695-702 (1955). Decay of Bi^{207}.

(3) Anders, O. U., Nucleonics 13, No. 7, 46 (1955). Millicurie beta-ray point source.

(4) Anders, O. U., Meinke, W. W., Rev. Sci. Instr. 27, 416-7 (1956). Beta gauge for localized measurements on thin films.

(5) Anderson, G., Phil. Mag. 45, 621 (1954). Electromagnetic separation of spallation products.

(6) Aron, W. A., Hoffman, B. G., Williams, F. C., U. S. Atomic Energy Commission, Rept. AECU-663 (May 1951). Range-energy curves.

(7) Bach, D. R., Ph. D. Thesis, University of Michigan (1955). An investigation of the low-lying levels in O^{18}.

(8) Bayly, J. G., Can. J. Research 28A, 520-9 (1950). Calorimetric measurement of the disintegration rate of a phosphorus-32 source.

(9) Beach, E. H., Ph. D. Thesis, University of Michigan (1952). Angular distribution studies of $P^{31}(d, p)P^{32}$ reactions.

(10) Bernstein, W., Brewer, H. G., Jr., Rubinson, W., Nucleonics 6, No. 2, 39-45 (1950). A proportional counter x-ray spectrometer.

(11) Bethe, H. A., Bacher, R. F., Revs. Modern Phys. 8, 103 (1936). Nuclear physics. Stationary states of nuclei.

(12) Bilaniuk, O., Ph. D. Thesis, University of Michigan, Department of Physics, in preparation.

(13) Blaser, J. P., Boehm, F., Marmier, P., Scherrer, P., Helv. Phys. Acta 24, 441-64 (1951). Anregungsfunktionen und Wirkungsquerschnitte der (p, n)-Reaktionen (II).

(14) Blatt, J. M., Weisskopf, V. F., "Theoretical Nuclear Physics," Wiley, New York, 1952.

(15) Brown, J., Felber, F., Richards, J., Saxon, D., Rev. Sci. Inst. 19, 818 (1948). On making thin nylon films.

(16) Cacciapuoti, N. B., Nuovo Cimento 14, 213-19 (1938). Determination of the decay constant of P^{32}.

(17) Cassatt, W. A., Jr., Decay scheme and characterization study of radioactive products of deuteron reactions. University of Michigan Ph. D. thesis, September 24, 1954. U. S. Atomic Energy Commission, Rept. AECU-2958, 49 (September, 1954).

(18) Ibid., p. 77.

(19) Cassatt, W. A., Jr., Meinke, W. W., Phys. Rev. 99, 760-1 (1955). Decay scheme of Y^{92}.

(20) Chase, R. L., Higinbotham, W. A., Rev. Sci. Instr. 23, 34-6 (1952). A flexible pulse amplifier with good overload properties.

(21) Chen, J. J. L., Rev. Sci. Inst. 21, 491-2 (1950). Test of rupture strength of thin plastic films.

(22) Cohen, B. L., Phys. Rev. 81, 184-8 (1951). (n, 2n) and (n, p) cross sections.

(23) Compton, A. H., Allison, S. K., "X-Rays in Theory and Experiment," VanNostrand, New York, 1935.

(24) Coryell, C. D., Sugarman, N., "Radiochemical Studies: The Fission Products," McGraw-Hill, New York, 176-83 (1951). Szilard-Chalmers reactions. Principles of enrichment. Article by A. W. Adamson, R. R. Williams, Jr., PAPER 15.

(25) Crandall, W. E., Millburn, G. P., Pyle, R. V., Birnbaum, W., Phys. Rev. 101, 329-37 (1956). $C^{12}(x, xn)C^{11}$ and $Al^{27}(x, x2pn)Na^{24}$ cross sections at high energies.

(26) Curran, S. G., Angus, J., Cockroft, A. L., Phil. Mag. 40 (7), 36-52 (1949). Investigation of soft radiations by proportional counter.

(27) Drabkin, G. M., Orlov, V. I., Rusinov, L. I., Izvest. Akad. Nauk SSSR Ser. Fiz. 19, 324 (1955), Columbia Tech. Transl. p. 294-37. Study of nuclear isomerism of Zn^{69}, Se^{79}, Se^{81}, Nb^{95}, Rh^{103} and Ba^{137}.

(28) Elsasser, W. M., J. phys. radium (7) 4, 549-56 (1933). Sur le principe de Pauli dans les noyaux.

(29) Elsasser, W. M., J. phys. radium (7) 5, 389-97 (1934). Sur le principe de Pauli dans les noyaux. II.

(30) Elsasser, W. M., J. phys. radium (7) 5, 635-39 (1934). Sur le principe de Pauli dans les noyaux. III.

(31) Elsasser, W. M., J. phys. radium (7) 6, 473-76 (1935). Energies de liaison des noyaux lourds.

(32) Elsasser, W. M., Phys. Rev. 51, 55 (1937). The self-consistent field and Bohr's nuclear model.

(33) Fajans, K., Beer, P., Ber. deut. chem. Ges. 46, 3486-97 (1913). Das Verhalten der Radioelemente bei Fällungsreaktionen.

(34) Fajans, K., Erdey-Gruz, T., Z. physik. Chem. 158 (A), 97-151 (1932). Ueber die Adsorption von Ionen, insbesondere der Radioelemente und Farbstoffe an salzartigen Verbindungen.

(35) Fajans, K., Physik. Z. 14, 136-42 (1913), Radium 10, 61-5 (1913). The position of the radio-elements in the periodic table.

(36) Feather, N., Pro. Cambridge Phil. Soc. 34, 599-611 (1938). Further possibilities for the absorption method of investigating the primary beta-particles from radioactive substances.

(37) Fogelström, I., Westermark, T., Nucleonics 14, No. 2, 62-5 (1956). Production of P^{33} by neutron irradiation of sulfur.

(38) Francis, J. E., Bell, P. R., Kelly, G. G., Nucleonics 12, No. 3, 54-6 (1954). Scintillation counting today: spectrometry. Double-line linear amplifier.

(39) Friedlander, G., Perlman, M. L., Scharff-Goldhaber, G., Phys. Rev. 80, 1103-4 (1950). Conversion coefficient of the 35-kev gamma-ray of Te^{125}.

(40) Frisch, O. R., "Progress in Nuclear Physics," Vol. 3, Academic Press, New York, 18-62 (1953). Energy measurements with proportional counters. Article by D. West.

(41) Geiger, H., Physik. Z. 14, 1129 (1913). Demonstration einer einfachen Methode zur Zählung von alpha- und beta-Strahlen.

(42) Geiger, H., Müller, W., Physik. Z. 29, 839-41 (1928). Das Elektronenzählrohr.

(43) Gile, J. D., Garrison, W. M., Hamilton, J. G., J. Chem. Phys. 18, 1685 (1950). Carrier-free radioisotopes from cyclotron targets. Preparation and isolation of $Sc^{44, 46, 48}$ from titanium.

(44) Ghoshal, S. N., Phys. Rev. 73, 417-18 (1948). Excitation curves of (α, n); (α, 2n); (α, 3n) reactions on silver.

(45) Ghoshal, S. N., U. S. Atomic Energy Commission, Rept. UCRL-709 (July, 1950). An experimental verification of the theory of compound nucleus.

(46) Goldhaber, M., Hill, R. D., Revs. Modern Phys. 24, 179-239 (1952). Nuclear isomerism and shell structure.

(47) Hall, K. L., Determination of (d, alpha) reaction cross sections, University of Michigan Ph. D. thesis, September 24, 1954. U. S. Atomic Energy Commission, Rept. AECU-3126 (September 1955).

(48) Ibid., p. 43.

(49) Ibid., p. 48.

(50) Ibid., p. 67.

(51) Ibid., p. 95.

(52) Ibid., p. 112.

(53) Ibid., p. 124.

(54) Ibid., p. 167.

(55) Ibid., p. 176.

(56) Ibid., p. 188.

(57) Hartree, D. R., Cambridge Phil. Soc. 24, 89-132 (1928). The wave mechanics of an atom with a non-coulomb central field. Theory and methods.

(58) Harvey, J. A., Phys. Rev. 81, 353-64 (1951). Neutron binding energies from (d, p) reactions and nuclear shell structure.

(59) Hawkings, R. C., Merritt, W. F., Craven, J. H., Proceedings of a Symposium "Recent Developments and Techniques in the Maintenance of Standards," held at the National Physical Laboratory (May 1951).

(60) Haxel, O., Jenson, J. H. D., Suess, H. E., Z. Physik 128, 295-311 (1950). Modellmaessige Deutung der ausgezeichneten Nukleonenzahlen im Kernbau.

(61) Hicks, H. G., Gilbert, R. S., Stevenson, P. C., Hutchin, W. H., U. S. Atomic Energy Commission, Rept. LRL-65 (December 1953). The qualitative anionic behavior of a number of metals with an ion exchange resin, "Dowex 2".

(62) Higinbotham, W. A., Rankowitz, S., Rev. Sci. Instr. 22, 688-90 (1951). A combined current indicator and integrator.

(63) Hintz, N. M., Ramsey, N. F., Phys. Rev. 88, 19-27 (1952). Excitation functions to 100 Mev.

(64) Hollander, J. M., Perlman, I., Seaborg, G. T., Rev. Mod. Phys. 25, 469-651 (1953). Table of Isotopes.

(65) Hughes, D. J., Harvey, J. A., U. S. Atomic Energy Commission, Rept. BNL-325 (July 1955). Neutron cross sections.

(66) Hughes, D. J., Sherman, D., Phys. Rev. 78, 632-3 (1950). Fast neutron cross sections and nuclear shells.

(67) Hyde, E. K., Florence, M. G., Larsh, A. E., Phys. Rev. 97, 1255-58 (1955). Isomeric state of Y^{88} in the decay of Zr^{88}.

(68) Keister, G. L., Schmidt, F. H., Phys. Rev. 93, 140-5 (1954). The second-forbidden beta spectra of Co^{60} and Sc^{46}.

(69) Kemp, E. L., U. S. Atomic Energy Commission, Rept. LA-1207 (July 1950). Scaler model SC-3.

(70) King, J. S., Ph. D. Thesis, University of Michigan (1953). Angular distributions from the reactions $Cl^{35}(d, p)Cl^{36}$, $Sc^{45}(d, p)Sc^{46}$, and $V^{51}(d, p)V^{52}$ as a test of the shell model.

(71) Kistner, O. C., Schwarzschild, A., Rustad, B. M., Phys. Rev. 105, 1339-41 (1957). Positron spectrum of O^{15}.

(72) Klema, E. D., Hanson, A. O., Phys. Rev. 73, 106-10 (1948). A determination of the $S^{32}(n, p)P^{32}$ cross section for neutrons having energies of 1.6 to 5.8 Mev.

(73) Kortüm, G. F. A., Buchholz-Meisenheimer, H., "Die Theorie der Destillation und Extraktion von Flüssigkeiten," Springer, Berlin, 1952.

(74) Kraus, K. A., Nelson, F., "Proceedings of the International Conference on the Peaceful Uses of Atomic Energy," Vol. 3, 113-25 (1956). Anion exchange studies of the fission products.

(75) Kunin, R., Myers, R. J., "Ion Exchange Resins," Wiley, New York, 1950.

(76) Larkins, J. H., U. S. Atomic Energy Commission, Rept. LA-1238 (May 1951). Thin window proportional beta-chamber.

(77) Lillie, A. B., Conner, J. P., Rev. Sci. Instr. 22, 210-11 (1951). Preparation of thin tritium targets.

(78) Lockett, E. E., Thomas, R. H., Nucleonics 11, No. 3, 14-17 (1953). The half-lives of several radioisotopes.

(79) Lyon, W. S., Kahn, B., Phys. Rev. 99, 728-30 (1955). Decay of Sc^{47}.

(80) Mann, W. B., Seliger, H. H., J. Research Natl. Bur. Standards 50, 197-200 (1953). Refinements in radioactive standardization by 4π beta counting.

(81) Mayer, M. G., Phys. Rev. 74, 235-9 (1948). On closed shells in nuclei.

(82) Mayer, M. G., Phys. Rev. 75, 1969-70 (1949). On closed shells in nuclei.

(83) Mayer, M. G., Phys. Rev. 78, 16-23 (1950). Nuclear configurations in the spin-orbit coupling model. Empirical evidence.

(84) Mayer, M. G., Jensen, J. H. D., "Elementary Theory of Nuclear Shell Structure," Wiley, New York, 1955.

(85) McIsaac, L. D., Voigt, A., U. S. Atomic Energy Commission, Rept. ISC-271 (June 1952). A new technique for the separation of radiophosphorus from sulfur.

(86) McMillan, E. M., Miller, R. D., Phys. Rev. 73, 80-1 (1948). Absolute cross section for the reaction $C^{12}(p, pn)C^{11}$ at high energy.

(87) Meinke, W. W., Ph. D. Thesis, University of California, 46 (April 1954). High energy bombardment products of thorium.

(88) Meinke, W. W., Ph. D. Thesis, University of California, 76 (April, 1954). High energy bombardment products of thorium.

(89) Meinke, W. W., U. S. Atomic Energy Commission, Rept. UCRL-432 (August 1949). Chemical procedure used in bombardment work at Berkeley.

(90) Meinke, W. W., Wick, G. C., Seaborg, G. T., J. Inorg. Nuclear Chem. 3, No. 2, 69-92 (1956). High-energy excitation functions in the heavy region.

(91) Moseley, H. G. J., Fajans, K., Phil. Mag. 22, 629-38 (1911). Radioactive products of short lives.

(92) Mulder, D., Hoeksema, G. W., Sizoo, G. J., Physica 7, 849-59 (1940). Measurements on the period of radioactive phosphorus.

(93) Nachod, F. C., "Ion Exchange: Theory and Application," Academic Press, New York, 1949.

(94) Parkinson, W. C., private communication.

(95) Pate, B. D., Yaffe, L., Can. J. Chem. 33, 15-23 (1955). A new material and techniques for the fabrication and measurement of very thin films for use in 4π counting.

(96) Pate, B. D., Yaffe, L., Can. J. Chem. 33, 929-37 (1955). Disintegration-rate determination by 4π counting. Source-mount absorption correction.

(97) Peacock, W. C., Jones, J. W., U. S. Atomic Energy Commission, Rept. AECD-1812 (March 1948). Decay scheme of Y^{88}.

(98) Perkins, L. R., E. I. Du Pont de Nemours and Co. Polychemical Dept. Research Div., private communication to W. W. Meinke.

(99) Preiswerk, P., Stähelin, P., Helv. Phys. Acta 24, 300 (1951). Term diagrams of several niobium isotopes.

(100) Rankowitz, S., private communication to W. W. Meinke.

(101) Rexroth, V. G., U. S. Atomic Energy Commission, Rept. LA-1239 (May 1951). Model PA-2 pulse amplifier.

(102) Rich, M., Madey, R., U. S. Atomic Energy Commission, Rept. UCRL-2301 (March 1954). Range-energy tables.

(103) Rieman, W. III, Neuss, J. D., Naiman, B., "Quantitative Analysis, a Theoretical Approach," McGraw-Hill, New York, 1951.

(104) Rubinson, W., Bernstein, W., U. S. Atomic Energy Commission, Rept. BNL-132(S-11), 104-110 (July 1951). Emission of Pb x-rays in the decay of Po^{210}.

(105) Rubinson, W., Bernstein, W., U. S. Atomic Energy Commission, Rept. BNL-93(S-8), 98-107 (October 1950). Emission of lead x-rays in the decay of Po^{210}.

(106) Rutherford, E., Geiger, H., Pro. Roy. Soc. (London) 81(A), 141-61 (1908). An electrical method of counting the number of alpha-particles from radio-active substances.

(107) Rybakov, B. V., Zhur. Eksptl'.i Teoret. Fiz. 28, 651-4 (1955). Range of protons in medium and heavy elements.

(108) Schmeling, P., Z. Naturforschung 10A, 79 (1955). Ueber die Halbwertszeit von Y^{90}.

(109) Segrè, E., "Experimental Nuclear Physics," Vol. 1, Wiley, New York, 149 (1953). Geiger-Müller Counters.

(110) Segrè, E., "Experimental Nuclear Physics," Vol. 1, Wiley, New York, 318 (1953). Energy momentum relations.

(111) Siegbahn, K., ed., "Beta- and Gamma-Ray Spectroscopy," Interscience, New York, 24-51 (1955). Interaction of gamma-radiation with matter. Article by C. M. Davisson.

(112) Siegbahn, K., ed., "Beta- and Gamma-Ray Spectroscopy," Interscience, New York, 201-223 (1955). The coincidence method. Article by A. C. G. Mitchell.

(113) Siegbahn, K., ed., "Beta- and Gamma-Ray Spectroscopy," Interscience, New York, 259-60 (1955). Source and window technique. Article by H. Slätis.

(114) Siegbahn, K., ed., "Beta- and Gamma-Ray Spectroscopy," Interscience, New York, 834 (1955). Measurement of disintegration rate. 4π scintillation counter. Article by J. L. Putnam.

(115) Siegbahn, K., ed., "Beta- and Gamma-Ray Spectroscopy," Interscience, New York, 835 (1955). Measurement of disintegration rate. Beta-gamma coincidence method. Article by J. L. Putnam.

(116) Sinclair, W. K., Holloway, A. F., Nature 167, 365 (1951). Half-lives of some radioactive isotopes.

(117) Smith, W. G., Hamilton, J. H., Robinson, R. L., Langer, L. M., Phys. Rev. 104, 1020-25 (1956). Beta decay of Tb^{161}.

(118) Soddy, F., Nature 91, 57-8 (1913), The radio-elements and the periodic law.

(119) Strohmaier, K., Z. Naturforschung 6A, 508-9 (1951). Ein einfaches Verfahren zur Herstellung grossflächiger durchsichtiger Häute aus Aluminiumoxyd mit einer Dicke zwischen 50 und 300 mu.

(120) Sun, K. H., Pecjak, F. A., Nucleonics 14, No. 11, 122-6 (1956). Recoil separation of isotopes.

(121) Szilard, L., Chalmers, T. A., Nature 134, 462 (1934). Chemical separation of the radioactive element from its bombarded isotope in the Fermi effect.

(122) Thompson, W. E., U. S. Atomic Energy Commission, Rept. ORNL-1056 (November 1951). 2. Instrument research and development quarterly progress report for period ending April 20, 1951. Article by Borkowski.

(123) Treybal, R. E., "Liquid Extraction," McGraw-Hill, New York, 1951.

(124) Way, K., King, R. W., McGinnis, C. L., van Lieshout, R., U. S. Atomic Energy Commission, Rept. TID-5300 (June 1955). Nuclear level schemes A = 40 - A = 92.

(125) Weast, R. C., Hodgman, C. D., Wallace, C. W.,"Handbook of Chemistry and Physics," Chemical Rubber Publishing Co., Cleveland, Ohio, 1955.

(126) Willard, H. H., Tang, N. K., Ind. Eng. Chem. Anal. Ed. 9, 357-63 (1937). Quantitative determination of aluminum by precipitation with urea.

(127) Willard, H. H., Tang, N. K., J. Am. Chem. Soc. 59, 1190-6 (1937). A study of the precipitation of aluminum basic sulfate by urea.

(128) Willard, H. H., Diehl, H., "Advanced Quantitative Analysis," Van Nostrand Co., New York, 56, 1950.